UAB
Universitat Autònoma de Barcelona

INTRAOPERATIVE EVALUATION OF PERFUSION OF THE ANTEROLATERAL THIGH PERFORATOR FREE FLAP FOR LOWER EXTREMITY RECONSTRUCTION USING INFRARED DYNAMIC THERMOGRAPHY AND INDOCYANINE GREEN ANGIOGRAPHY

Paúl David Zamora Alarcón

ADVERTIMENT. L'accés als continguts d'aquesta tesi queda condicionat a l'acceptació de les condicions d'ús establertes per la següent llicència Creative Commons:  https://creativecommons.org/licenses/?lang=ca

ADVERTENCIA. El acceso a los contenidos de esta tesis queda condicionado a la aceptación de las condiciones de uso establecidas por la siguiente licencia Creative Commons:  https://creativecommons.org/licenses/?lang=es

WARNING. The access to the contents of this doctoral thesis it is limited to the acceptance of the use conditions set by the following Creative Commons license:  https://creativecommons.org/licenses/?lang=en

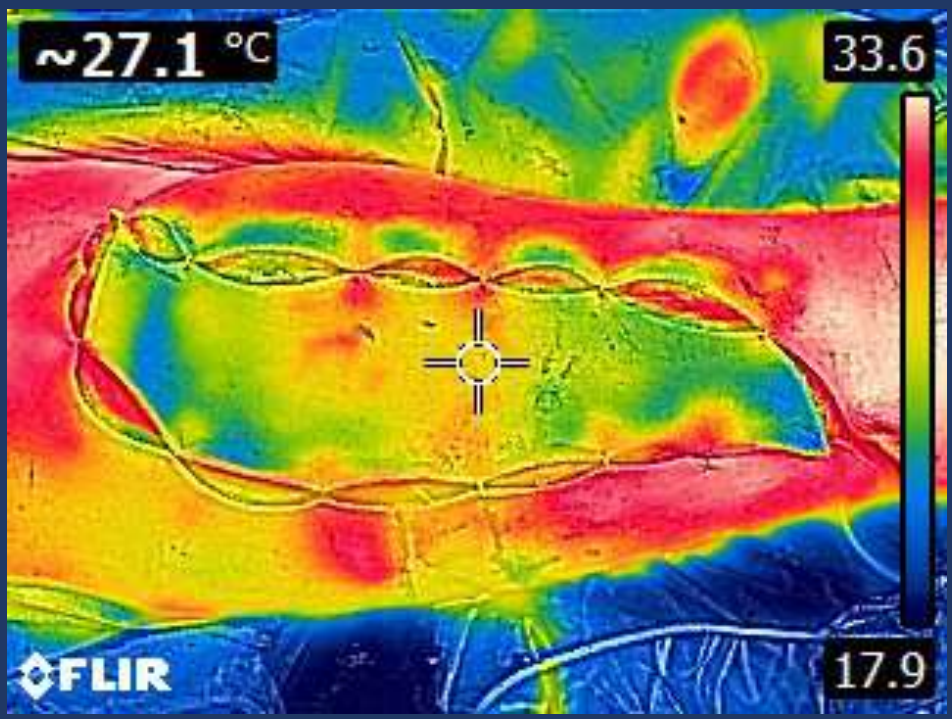
Universitat Autònoma de Barcelona

INTRAOPERATIVE EVALUATION OF PERFUSION OF THE ANTEROLATERAL THIGH PERFORATOR FREE FLAP FOR LOWER EXTREMITY RECONSTRUCTION USING INFRARED DYNAMIC THERMOGRAPHY AND INDOCYANINE GREEN ANGIOGRAPHY

Paúl David Zamora Alarcón

2026

INTRAOPERATIVE EVALUATION OF PERFUSION OF THE ANTEROLATERAL THIGH PERFORATOR FREE FLAP FOR LOWER EXTREMITY RECONSTRUCTION USING INFRARED DYNAMIC THERMOGRAPHY AND INDOCYANINE GREEN ANGIOGRAPHY



Paúl David Zamora Alarcón

"Where anatomy ends, technology begins —
not to replace the surgeon's hands, but to refine their purpose."

2026

Doctoral Program in Surgery and Morphological Sciences

Department of Surgery

Universitat Autònoma de Barcelona

INTRAOPERATIVE EVALUATION OF PERFUSION OF THE ANTEROLATERAL THIGH PERFORATOR FREE FLAP FOR LOWER EXTREMITY RECONSTRUCTION USING INFRARED DYNAMIC THERMOGRAPHY AND INDOCYANINE GREEN ANGIOGRAPHY

Doctoral thesis submitted by Paúl David Zamora Alarcón to obtain the title of doctor

Thesis Supervisors:

Manuel Fernández Garrido MD. PhD.
Jaume Masià Ayala MD. PhD.
Xavier León Vintró MD. PhD

Thesis Tutor:

Xavier León Vintró MD. PhD

Barcelona, 2026

"What we do in life,
echoes in eternity"

Maximus Decimus Meridius

Acknowledgements

To my parents, **Mónica and Gino**, for your unconditional support. Your trust and encouragement have been the foundation that allowed me to move forward confidently, knowing I could grow without fear of making mistakes.

To my brother **Gino Jr.**, always my role model as the eldest brother. Following your path led me to study medicine, and without your influence, I would not be here today.

To my brother **Diego**, your admiration has been a driving force. I strive to be an example for you, although most of the time it is you who inspires me.

To **María José**, my soulmate. I deeply admire your intelligence and strength. You are the engine that drives me to pursue new goals, and with you, every step forward becomes shared growth.

To **Manuel**, my mentor and friend, whose constant support, guidance, and encouragement made this thesis possible. Your trust and insistence on moving forward were invaluable throughout this journey.

To all those who were part of this first chapter of my path as a **plastic surgeon**.

To my attending surgeons during residency — **Carmen, Gemma, Susana, Leyre, and Marilú** — for sharing your knowledge with patience and motivating me each in your own way.

To my co-residents, especially **Elena**, for her patience, friendship, and for growing alongside me; and **Andree**, for our endless conversations that fueled mutual motivation and inspired ideas like this thesis.
To the **residents at Sant Pau**, whose ambition and dedication continue to inspire me.

To the **nurses, assistants, and administrative staff**, for your patience and support; our work as surgeons would not be possible without you.

To **J.P. Hong**, for his boundless energy and contagious passion for microsurgery and supermicrosurgery, which inspired me to keep learning and progressing.

To **Marco Innocenti**, for welcoming me warmly in Bologna and reinforcing my motivation to continue exploring thermography in reconstructive surgery.

To **Xavi,** for his unwavering support, academic generosity, and guidance, which were instrumental during the most demanding moments of this thesis.

To **Jaume**, for the professional experience we shared, which taught me valuable lessons about the path I want to follow — and the one I prefer to avoid.

To all of you, my sincere gratitude for being part of this journey.

Abbreviations

ALT	Anterolateral Thigh Perforator Free Flap
ASIS	Antero Superior Iliac Spine
BMI	Body Mass Index
ChT	Chemotherapy
CT	Computed Tomography
CT-angio	Computed AngioTomography
DIEP	Deep Inferior Epigastric Perforator
E-E	End to End
E-S	End to Side
DIRT	Dynamic infrared thermography
ICG	Indocyanine green
ICG – A	Indocyanine green angiography
LD	Latissimus Dorsi
MDCT	Multidetector Computed Tomography
MRI	Magnetic Resonance Imaging
PRS	Plastic Reconstructive Surgery
RT	Radiotherapy
ROI	Region of interest
TRAM	Transverse Rectus Abdominis

Index

ABSTRACT **10**

RESUMEN **12**

1: INTRODUCTION **16**

1.1 Brief resume 16
1.2 Soft tissue reconstruction of the lower limb: Clinical relevance and challenges 18
1.3 Flaps evolution 20
1.4 The Anterolateral Thigh Flap (ALT) 30
1.5 Flap Perfusion Assesment 34
1.6 Study rationale and justification 43

2: HYPOTHESIS **46**

3: OBJECTIVES **48**

4: MATERIALS AND METHODS **50**

4.1 Study Design 50
4.2 Setting and Participants 58
4.3 Inclusion and Exlusion Criteria 59
4.4 Variables 60
4.5 Surgical Technique and ALT Flap Elevation 87
4.6 Imaging Protocols 100
4.7 Standardization of Image Acquisition 101
4.8 Image Analysis and Framework 102
4.9 Software and Analytical Workflow 104
4.10 Statistical Analysis 109
4.11 Ethical Considerations 114

5: RESULTS **116**

5.1 Study population and baseline surgical characteristics 116
5.2 T1 Indocyanine Green Angiography Perfusion Assessment as Reference Standard 123
5.3 Standardization of Dynamic Infrared Thermography Based on the T1 ICG Reference Profile 128
5.4 T1 comparison between ICG-A and standardized DIRT 134
5.5 Temporal evolution of flap perfusion assessed by standardized thermography (T1–T2–T3) 141
5.6 Focused analysis of distal flap territories (zones 1a and 4b) 148
5.7 Intra-flap thermographic perfusion patterns and zonal temperature distribution (quantitative analysis) 154
5.8 Compositional concordance between ICG-A and thermography at T1 157
5.9 Diagnostic performance of thermography based on compositional discrepancy 164

6: DISCUSSION **168**

6.1 Summary and global interpretation of the main findings 168
6.2 Agreement between DIRT and ICG-A: what does "agreement" really mean? 173
6.3 Spatial heterogeneity of perfusion within the ALT flap 175
6.4 Temporal intraoperative changes and the role of venous drainage (T1–T2–T3) 177
6.5 Subjectivity of ICG-A and the need for objective fluorescence quantification 180
6.6 Strengths and weaknesses of dynamic infrared thermography 182
6.7 Methodological limitations of the study 186
6.8 What we would do differently if the study were repeated 188
6.9 Clinical implications 190
6.10 Final synthesis 192
6.11 Achievement of the Study Objectives 194

7: CONCLUSIONS.....201

8: FUTURE LINES 203

9: BIBLIOGRAPHY.....206

Abstract

Introduction

Accurate intraoperative assessment of flap perfusion is essential in lower-limb free flap reconstruction, where vascular compromise may result in partial or total flap loss. Indocyanine green angiography (ICG-A) is widely used for this purpose but presents limitations related to availability, subjectivity of interpretation, and physiological dependency. Dynamic infrared thermography (DIRT) is a non-invasive, contrast-free technique that may provide complementary information on cutaneous perfusion, although its role in lower-limb reconstruction remains insufficiently defined.

Objectives

The primary objective of this study was to assess the agreement between dynamic infrared thermography and indocyanine green angiography in the intraoperative evaluation of perfusion of anterolateral thigh (ALT) free flaps in lower-extremity reconstruction. Secondary objectives included analysis of spatial perfusion behavior within the flap and evaluation of intraoperative temporal changes associated with venous drainage.

Methods

A prospective, observational, unicentric study was conducted in patients undergoing ALT free flap reconstruction of lower-limb defects. Perfusion was assessed intraoperatively at three timepoints: before pedicle division (T1), after arterial and single venous anastomosis (T2), and after addition of a second venous anastomosis (T3). ICG-A was performed at T1, while DIRT was applied at all timepoints using a standardized cooling–rewarming protocol. Images were analyzed using a 1 cm^2 region-of-interest grid, longitudinal zonal and subzonal segmentation, and patient-specific thermographic standardization. Statistical analysis included correlation analysis, Bland–Altman plots, compositional data analysis, and receiver operating characteristic (ROC) analysis.

Results

Twenty five ALT free flaps were analyzed. DIRT showed moderate to strong agreement with ICG-A for global perfusion assessment at baseline. Spatial analysis demonstrated consistent proximal-to-distal thermal gradients, with flap extremities behaving as watershed zones. Temporal analysis revealed non-linear thermal changes across T1–T3, particularly related to venous outflow modifications. ROC analyses demonstrated meaningful discrimination of non-viable zones defined by ICG-A.

Conclusions

Dynamic infrared thermography demonstrates clinically relevant agreement with indocyanine green angiography in the intraoperative assessment of ALT free flap perfusion. Although it cannot replace ICG-A, DIRT provides complementary physiological information and may serve as a useful adjunct or screening tool, particularly in settings where ICG-A is unavailable.

Resumen

Introducción

La evaluación intraoperatoria precisa de la perfusión es un aspecto clave en la reconstrucción microquirúrgica de la extremidad inferior, donde los compromisos vasculares pueden conducir a necrosis parcial o total del colgajo. La angiografía con verde de indocianina (ICG-A) es una herramienta ampliamente utilizada, pero presenta limitaciones relacionadas con su disponibilidad, la subjetividad en la interpretación y su dependencia de condiciones fisiológicas. La termografía dinámica infrarroja (DIRT) es una técnica no invasiva y sin contraste que puede aportar información complementaria sobre la perfusión cutánea, aunque su papel en la reconstrucción de la extremidad inferior no está bien definido.

Objetivos

El objetivo principal de este estudio fue evaluar el grado de concordancia entre la termografía dinámica infrarroja y la angiografía con verde de indocianina en la valoración intraoperatoria de la perfusión de colgajos libres anterolaterales de muslo (ALT) en reconstrucción de extremidad inferior. Como objetivos secundarios, se analizó el comportamiento espacial de la perfusión dentro del colgajo y los cambios intraoperatorios asociados al drenaje venoso.

Métodos

Se realizó un estudio prospectivo, observacional y unicéntrico en pacientes sometidos a reconstrucción de defectos de extremidad inferior mediante colgajo ALT libre. La perfusión se evaluó intraoperatoriamente en tres tiempos: antes de la desconexión del colgajo (T1), tras la anastomosis arterial y de una vena (T2) y tras la adición de una segunda vena (T3). La ICG-A se realizó en T1, mientras que la DIRT se aplicó en los tres tiempos mediante un protocolo estandarizado de enfriamiento y recalentamiento. El análisis se llevó a cabo mediante una cuadrícula de regiones de interés de 1 cm^2, segmentación zonal y subzonal longitudinal, y estandarización termográfica específica para cada paciente. El análisis estadístico incluyó correlaciones, gráficos de Bland–Altman, análisis composicional y curvas ROC.

Resultados

Se analizaron 25 colgajos ALT libres. La DIRT mostró una concordancia moderada a alta con la ICG-A en la valoración global de la perfusión basal. El análisis espacial evidenció gradientes térmicos proximodistales consistentes, con las extremidades del colgajo comportándose como territorios de transición. El análisis temporal mostró cambios térmicos no lineales entre T1, T2 y T3, especialmente relacionados con modificaciones del drenaje venoso. Los análisis ROC demostraron una capacidad discriminativa relevante para identificar zonas no viables definidas por ICG-A.

Conclusiones

La termografía dinámica infrarroja muestra una concordancia clínicamente relevante con la angiografía con verde de indocianina en la evaluación intraoperatoria de la perfusión de colgajos ALT. Aunque no puede sustituir a la ICG-A, la DIRT aporta información fisiológica complementaria y puede considerarse una herramienta de apoyo o cribado, especialmente en entornos donde la ICG-A no está disponible.

"Technology is the extension of the surgeon's eyes and hands — allowing us to see what was once invisible and operate with the precision of thought"

Dr. Robert Acland

1

Introduction

1: Introduction

1.1 Brief resume

Reconstructive microsurgery of the lower limb represents one of the most demanding areas of plastic and reconstructive surgery. Traumatic injuries, oncologic resections, and chronic wounds frequently result in extensive soft tissue defects with exposed bone, hardware, or tendons, where local tissues are insufficient for coverage. In these scenarios, free perforator flaps have become the cornerstone for limb salvage, offering reliable vascularized tissue with minimal donor-site morbidity. Among them, the anterolateral thigh (ALT) flap has emerged as a true workhorse for lower-limb reconstruction due to its versatility, long pedicle, and ability to provide large fasciocutaneous paddles.

Despite these advances, partial flap necrosis remains a significant concern. In the lower limb, even a 1 cm^2 area of necrosis can lead to exposure of bone or titanium plates, increasing the risk of infection and osteomyelitis and potentially resulting in limb loss. Therefore, precise intraoperative assessment of flap perfusion is critical to guide flap design, trimming, and inset, aiming to minimize complications and improve outcomes.

Traditionally, perfusion has been evaluated clinically, relying on subjective parameters such as color, capillary refill, dermal bleeding, and turgor. However, the subjectivity and interobserver variability of these signs have prompted the development of objective imaging techniques. Among these, Indocyanine Green Angiography (ICG-A) has become the current gold standard, allowing real-time visualization of surface perfusion. In parallel, Dynamic Infrared Thermography (DIRT) has emerged as a non-invasive, repeatable method capable of assessing the functional dynamics of cutaneous blood flow.

The present thesis focuses on the comparative evaluation of ICG-A and DIRT for intraoperative perfusion assessment of ALT free flaps in lower-limb reconstruction, aiming to determine whether thermography can reliably identify well-perfused and at-

risk areas, complementing or even replacing fluorescence angiography in certain contexts.

The following sections will provide the theoretical framework necessary to understand the clinical and scientific basis of this study. We will begin with the principles and challenges of soft tissue reconstruction in the lower limb, review the historical evolution of flap surgery with emphasis on perforator-based reconstruction, and focus on the ALT flap as a workhorse in extremity salvage. Finally, we will analyze the current methods for flap perfusion assessment, highlighting the rationale and justification for this comparative study between ICG-A and DIRT.

-

1.2 Soft tissue reconstruction of the lower limb: Clinical relevance and challenges

Soft tissue reconstruction of the lower limb represents one of the most demanding scenarios in reconstructive microsurgery. Unlike other anatomical regions where partial flap compromise can often be managed conservatively, the **exposure of critical structures such as bone, tendons, vessels, nerves, or orthopedic hardware** in the leg can quickly lead to deep infection or osteomyelitis, which may compromise limb salvage.

Even a **1 cm² area of distal flap necrosis** may necessitate additional surgery, prolonged hospitalization, and, in some cases, result in amputation. The limited local tissue coverage of the lower leg, combined with the frequent presence of hardware following fracture fixation or tumor resection, explains why this region has historically been considered a **high-risk zone** for reconstructive failure (1)(2)

The typical etiologies requiring free flap coverage in the lower limb include **high-energy trauma**, **Gustilo IIIB and IIIC open fractures**, **post-oncologic resections of soft tissue sarcomas**, and **chronic wounds or osteomyelitis** following previous surgeries. In these cases, the **availability of local flaps is often insufficient** to achieve robust coverage, due to the limited arc of rotation, lack of bulk, and vulnerability to distal necrosis. Furthermore, **infection risk in the lower limb is amplified** by poor vascularity, particularly in patients with diabetes mellitus or peripheral vascular disease, where arterial inflow and venous drainage may already be compromised (3).

The modern era of **microsurgical free flaps** has dramatically improved the outcomes of lower-limb salvage, with success rates in contemporary series exceeding 95% (4). However, this high survival rate **does not eliminate the problem of partial necrosis**, which in the leg may be just as consequential as total flap failure. Unlike in breast or trunk reconstruction, where small skin losses can be treated with secondary healing or skin grafting, the **loss of even minimal tissue in the lower limb can expose plates or screws**, leading to **infection, flap dehiscence, or delayed union of the underlying fracture** (5,6). For this reason, **precise intraoperative assessment of flap perfusion** is

paramount in this anatomical region, guiding surgeons in the identification and preservation of the most reliable tissue.

1.3 Flaps evolution

I. Historical evolution of flap surgery

The evolution of flap surgery illustrates the journey from empirical local tissue rearrangements to highly precise **perforator-based microsurgical reconstruction**. Understanding this trajectory is essential to appreciate how modern strategies for lower-limb salvage were developed, as well as to contextualize the role of **objective perfusion assessment** in current practice.

The **earliest references to flap reconstruction** date back to **ancient India**, where **Sushruta (~600 BCE)** described the **forehead flap for nasal reconstruction**, as recorded in the *Sushruta Samhita* (7). These early procedures relied purely on **random blood supply** from the subdermal plexus and empirical observation of survival patterns.



Figure 1.1. *Portrait of Sushruta, an ancient Indian surgeon traditionally considered a founding figure of reconstructive surgery. His treatise, the Sushruta Samhita (circa 6th century BCE), includes early descriptions of skin flaps, grafting techniques, and surgical principles that remain conceptually relevant in modern reconstructive surgery.*

In Europe, the Renaissance marked a second milestone: **Gaspare Tagliacozzi (1597)** published *De Curtorum Chirurgia per Insitionem*, where he described the **tubed arm flap for nasal reconstruction**, emphasizing the importance of **maintaining vascular continuity** between donor and recipient sites (8). Despite these advances, flap survival was inconsistent, and the procedures required **long immobilization periods**.



Figure 1.2. *Illustration from Gaspare Tagliacozzi's De Curtorum Chirurgia per Insitionem (1597), depicting the classic pedicled arm flap used for nasal reconstruction, a foundational milestone in the development of reconstructive plastic surgery.*

The **19th century** brought a fundamental shift with the **recognition of axial flaps**—tissues perfused by a **known, named artery and vein**. Surgeons such as **Johann Friedrich Dieffenbach** and **Carl Ferdinand von Graefe** contributed to early clinical applications of axial flaps, paving the way for more **predictable outcomes** (9).

The **World Wars of the 20th century** accelerated reconstructive innovation, as **Sir Harold Gillies** and **Filatov** developed **tubed pedicle flaps** to address massive facial and limb injuries (10). These innovations, although still pedicled and staged, laid the foundation for microsurgery by demonstrating the feasibility of **long-distance tissue transfer**.

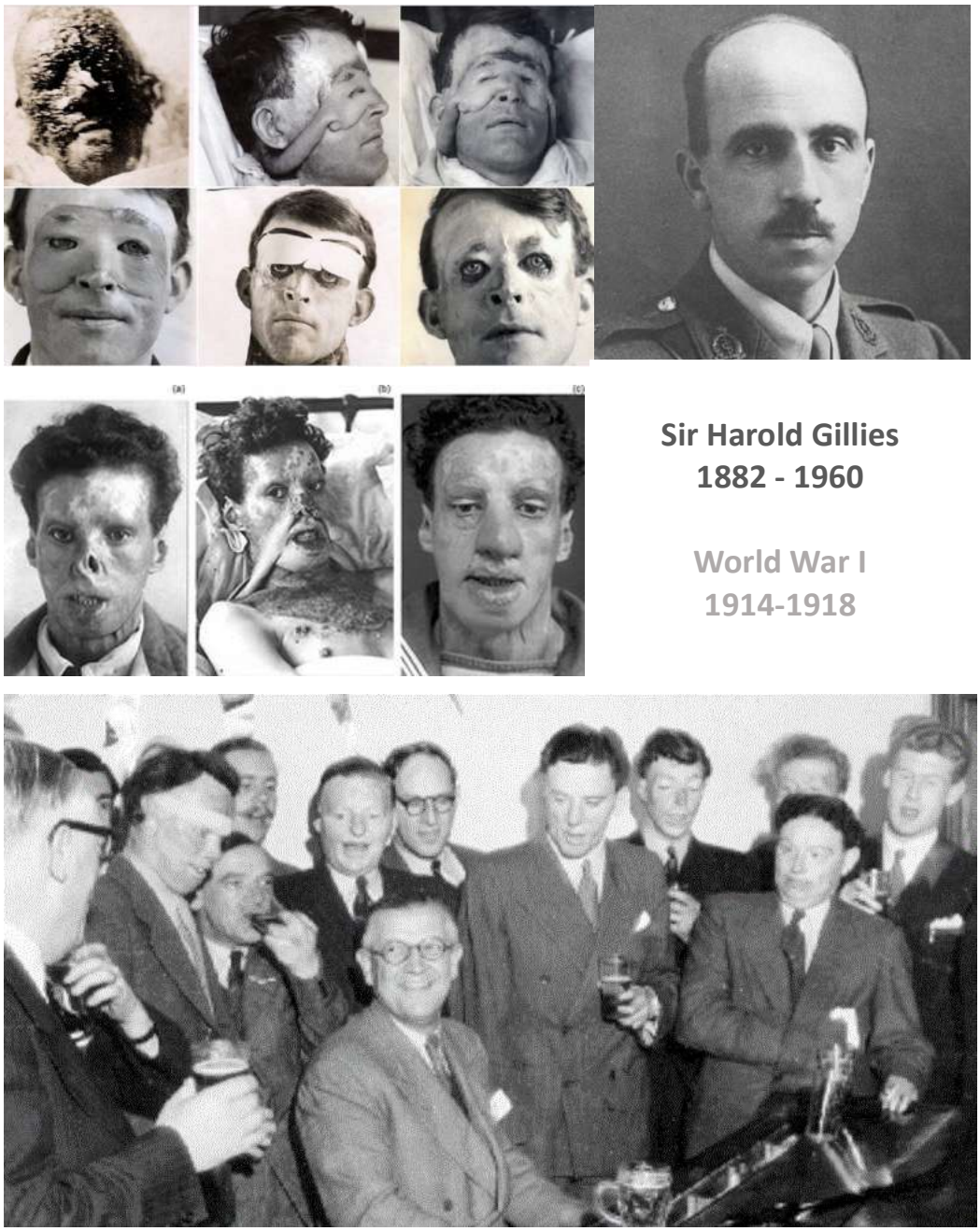


Figure 1.3. *Origins of modern reconstructive plastic surgery during World War I. Examples of bipalpebral and nasal reconstruction using tubed pedicle flaps (upper left), portrait of Sir Harold Gillies (right), and photograph of the Guinea Pig Club(lower), an association of patients treated by Gillies.*

The **microsurgical era** began in the **1970s**, with the advent of the **operating microscope, microvascular instruments, and reliable suture materials**. Experimental work by **Fujino and McCraw** clarified **myocutaneous vascular territories**, while **Taylor and Palmer (1987)** provided a **three-dimensional vascular map of the body**, introducing the **angiosome concept**(11) (12). This knowledge not only improved flap safety but also facilitated the **design of free flaps** that could be **completely detached and reanastomosed to distant vessels**, revolutionizing reconstructive surgery.

The 1980s and 1990s marked the evolution toward perforator-based flaps. **Song et al. (1984)** first described the free anterolateral thigh (ALT) flap as a septocutaneous fasciocutaneous flap (13). Later, **Koshima and Soeda (1989)** pioneered the true perforator flap concept, demonstrating that skin and subcutaneous tissue could be harvested on a single perforator while preserving the underlying muscle, thus minimizing donor-site morbidity (14). These advances consolidated perforator flaps as the gold standard for lower-limb salvage, combining reliable perfusion with functional preservation.

II. Angiosome, Perforasome and Choke Vessels: Anatomical basis and functional considerations in flap perfusion

The anatomical foundation for modern flap design was profoundly transformed by the work of Taylor and Palmer in 1987 (15). Through meticulous *in vivo* and cadaveric injection studies using lead oxide–gelatin and India ink, they demonstrated that the human body can be divided into approximately 374 **angiosomes**—*three-dimensional vascular territories each supplied by a single source artery and its venae comitantes*. These territories extend from the skin through subcutaneous fat, fascia, muscle, and bone, forming reproducible anatomical units. By dissecting and radiographically documenting these injections, Taylor mapped the territories supplied by major arteries, describing their boundaries and the vessels linking them.

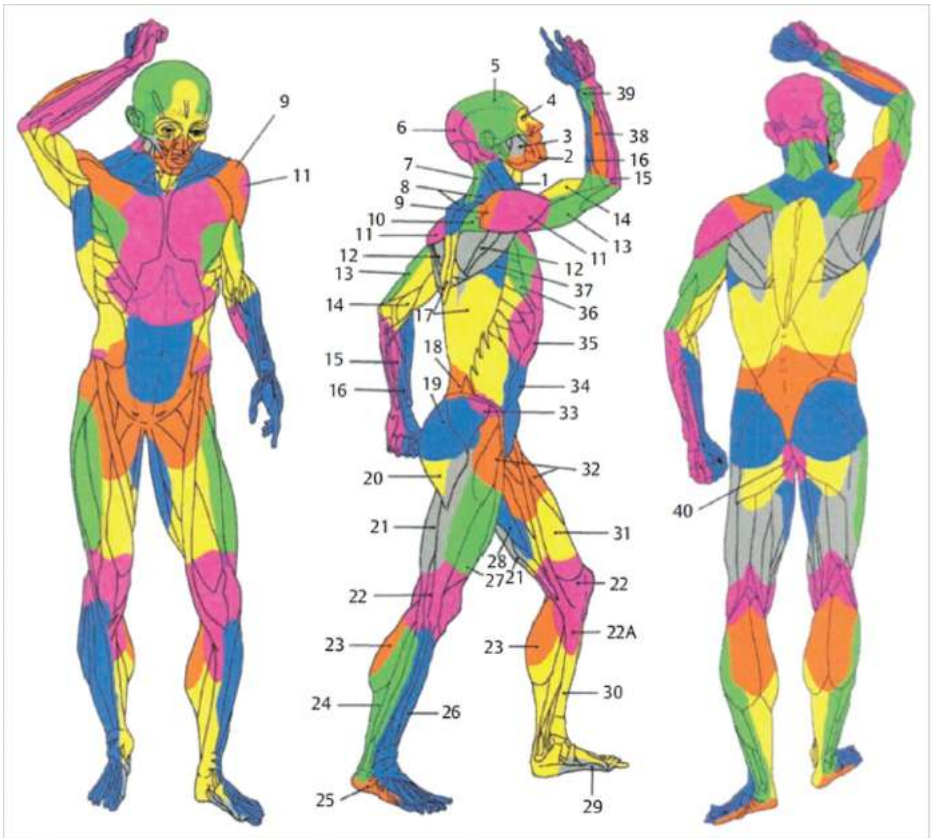


Figure 1.4. *Angiosome concept as described by Taylor and Palmer. Schematic representation of the three-dimensional vascular territories of the body, illustrating the distribution of angiosomes supplied by source arteries and their interconnections, which form the anatomical basis for modern perforator flap surgery and flap perfusion assessment.*
Adapted from Taylor and Palmer (15)

A pivotal finding was that adjacent angiosomes are interconnected via two distinct types of anastomoses:

- **True anastomoses**, in which vessel calibre remains constant across the connection, allowing free, bidirectional flow.
- **Choke anastomoses** (or *choke vessels*), in which the connecting artery exhibits a reduced calibre—often one-third to one-half of the source vessel diameter—restricting baseline flow (15),(16).

Taylor and Palmer's atlas not only provided a vascular "map" of the body but also offered a rational basis for predicting flap viability, enabling the safe extension of flaps into adjacent angiosomes under certain conditions.

From Angiosome to Perforasome: Refining the Microvascular Map

While the angiosome describes the macro-territory of a source artery, it does not directly reflect the more localized and clinically relevant territory supplied by an individual perforator.

This refinement was introduced by Saint-Cyr et al. in 2009 (17) with the perforasome theory. Using a combination of cadaveric and clinical studies, they employed static three-dimensional (3D) CT angiography, dynamic four-dimensional (4D) CT angiography, and intraoperative clinical observations to define the **perforasome** *as the cutaneous vascular territory nourished by a single musculocutaneous or septocutaneous perforator.*

Saint-Cyr's studies demonstrated:

- Each perforator supplies a central zone of robust perfusion.
- Peripheral extension into adjacent perforasomes depends on interperforator connections, which may be true or choke anastomoses.
- Flow across choke vessels can be delayed by several seconds to minutes, producing distinct filling patterns on angiography.

- Perforator location (central vs. eccentric) significantly affects territory symmetry and distal perfusion.

Unlike an angiosome, which may contain multiple perforators and extend through deep tissues, the perforasome represents the smallest, functionally independent vascular unit relevant for perforator flap surgery. This microvascular focus is particularly critical in the design and survival of flaps where perfusion at the distal edges depends on the recruitment of adjacent perforasomes.

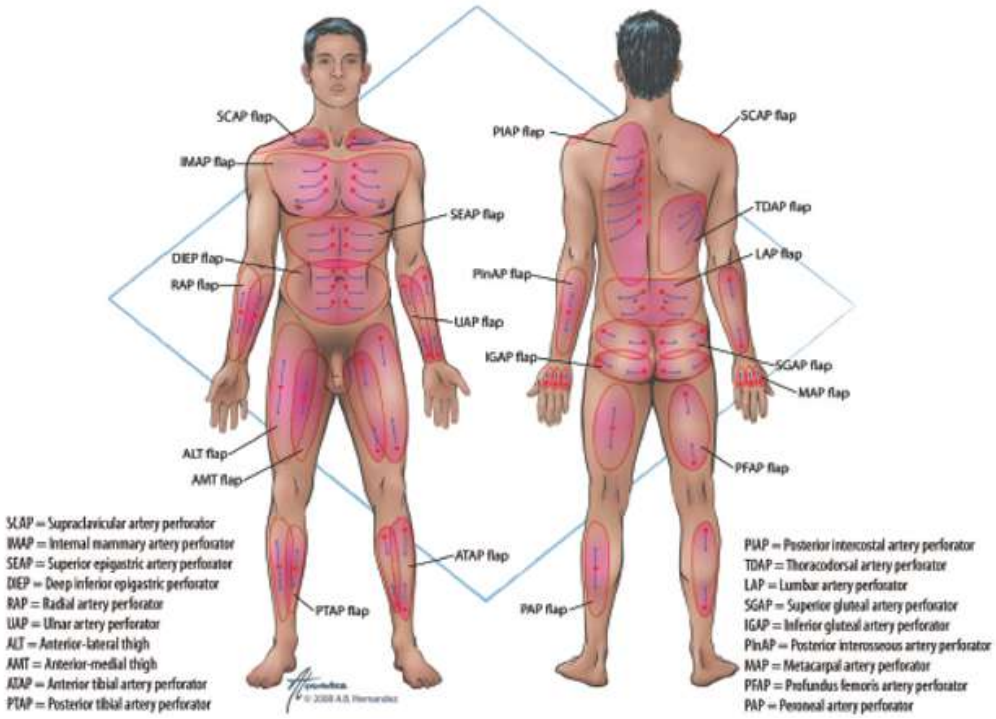


Figure 1.5. *Perforasome concept as described by Saint-Cyr. Schematic illustration of perforator-based vascular territories (perforasomes) and their linking vessels, highlighting the anatomical basis for perforator flap design and perfusion beyond the dominant perforator.*
Adapted from Saint-Cyr et al.(17)

Choke Vessels: Structure, Function, and Variability

Choke vessels occupy a pivotal role in both the angiosome and perforasome frameworks. Anatomically, they are narrow-calibre arteries bridging adjacent territories, typically with a well-developed muscular media. Physiologically, they act as flow regulators: at baseline, their constricted lumen limits blood transfer; under conditions of sustained demand, they can dilate and remodel into true anastomoses. This conversion process

can be accelerated by surgical delay, trauma, or ischemic preconditioning, often beginning within 48–72 hours and becoming functionally complete by 5–7 days (16),(18).

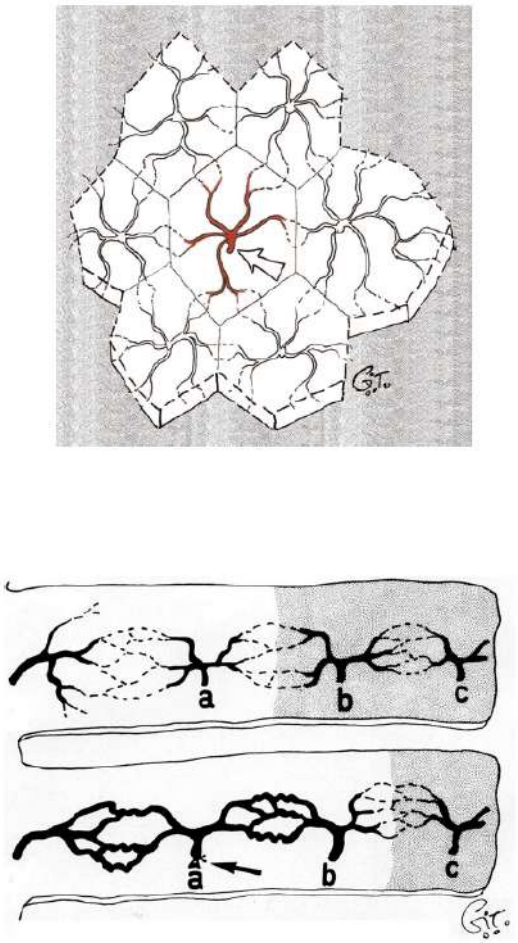


Figure 1.6. *Choke vessel concept in perforator flap perfusion.*
Upper image: *schematic representation of a dominant ("true") perforator supplying a central perforasome, surrounded by adjacent perforasomes connected through small-caliber interperforator vessels (choke vessels), depicted as a hexagonal territorial network.*
Lower image: *linear schematic illustrating the functional behavior of choke vessels between adjacent vascular territories, showing an initial state with closed or functionally restricted choke vessels, limiting perfusion to the neighboring perforasome, and a subsequent state after dilation and remodeling, allowing opening of choke vessels and recruitment of the adjacent territory.*
Adapted from Taylor et al. (16)

Factors influencing choke vessel behaviour:

- **Systemic hemodynamics:** hypotension or hypovolemia reduces driving pressure, limiting choke recruitment.

- **Sympathetic tone:** perioperative stress, hypothermia, or pharmacologic vasoconstrictors can cause additional narrowing.
- **Venous outflow:** congestion may impede forward flow through choke zones.
- **Tissue characteristics:** edema, fibrosis, or radiotherapy can stiffen perivascular tissues, increasing resistance.
- **Patient comorbidities:** diabetes mellitus, peripheral vascular disease, and smoking impair endothelial reactivity and collateral recruitment.
- **Intraoperative handling:** excessive traction, cautery, or compression along choke territories can precipitate vasospasm.

Experimental thermographic studies by Taylor et al. (19) have shown that choke zones often correspond to areas of delayed rewarming after a cooling challenge, reflecting slower filling via restricted channels. In large flaps, necrosis frequently develops at or beyond the second choke zone from the dominant perforator—particularly in designs with elongated geometry or eccentric perforator location.

Functional Relevance in Flap Surgery

The functional angiosome concept, advanced by Taylor in 2017 (20), integrates the anatomical map with the *real-time physiological capacity* of interterritorial connections. In practice, the perfusion territory captured by a perforator at surgery is the sum of:

1. Its primary perforasome (robust, immediate flow).
2. Adjacent perforasomes accessible via true anastomoses (full, synchronous filling).
3. Adjacent perforasomes accessed via choke vessels (delayed, potentially insufficient flow).

The distinction is critical in lower-limb reconstruction. Even minimal distal necrosis can expose bone or orthopedic hardware, leading to infection or amputation. Therefore, relying solely on preoperative anatomical predictions may be inadequate, especially in:

- Large or narrow flaps spanning multiple perforasomes.

- Patients with vascular comorbidities.
- Flaps based on eccentric perforators.
- Acute trauma where vasospasm is common.

In such contexts, **intraoperative assessment of flap perfusion** becomes critical to determine whether the distal extent is functionally viable or at risk. While anatomical mapping offers a framework for design, only real-time evaluation can confirm the effective capture of adjacent territories through choke zones.

In summary, the progression from the angiosome to the perforasome theory, enriched by the understanding of choke vessel physiology, has provided reconstructive surgeons with a detailed anatomical and functional map for flap design. Yet, these maps represent potential territories; the actual territory perfused in each patient is modulated by hemodynamic conditions, vessel reactivity, and the microvascular architecture of choke zones. This variability explains why, even with careful anatomical planning, distal ischemia remains a risk—particularly in large fasciocutaneous flaps for the lower limb.

These principles are especially relevant when considering the anterolateral thigh (ALT) flap, whose potential skin paddle often traverses multiple perforasomes. Understanding its vascular basis in the context of angiosomes, perforasomes, and choke vessels is essential before addressing the clinical strategies for assessing its perfusion, which will be explored in subsequent sections.

1.4 The Anterolateral Thigh Flap (ALT)

I. The Anterolateral Thigh (ALT) Flap as a Workhorse in Lower-Limb Reconstruction

The anterolateral thigh (ALT) flap has emerged as the workhorse perforator flap for lower-limb reconstruction, thanks to its anatomical reliability, versatility, and low donor-site morbidity. First described by Song et al. in 1984 as the "free thigh flap," it was initially conceptualized as a septocutaneous flap based on the descending branch of the lateral circumflex femoral artery (LCFA) (13). Subsequent studies by Koshima et al. (1989) and Kimata et al. (1998) expanded its description, demonstrating the frequent presence of musculocutaneous perforators coursing through the vastus lateralis muscle and highlighting the anatomical variability of its pedicle (21)(22).

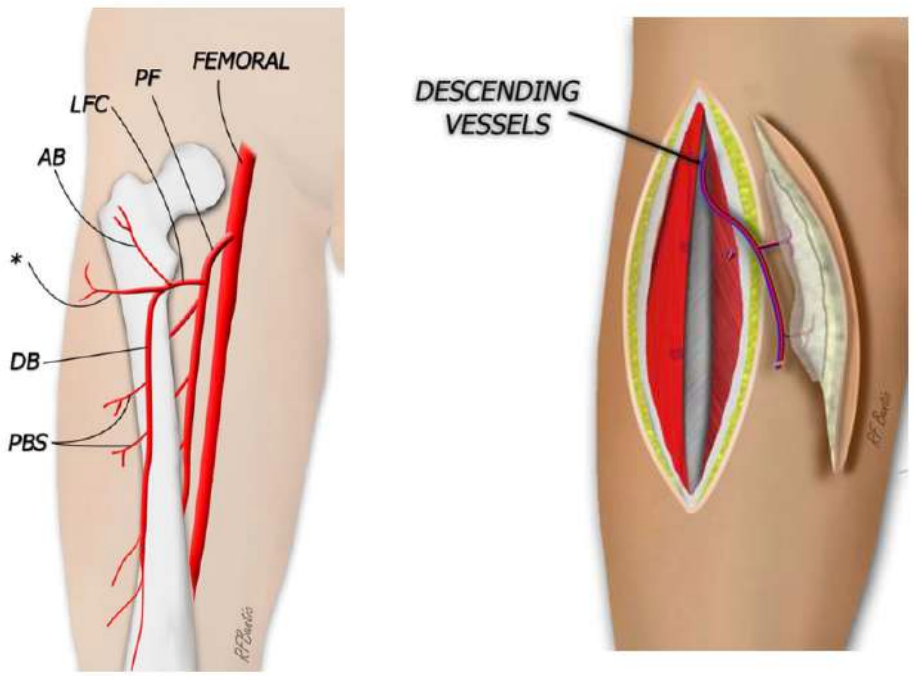


Figure 1.7. *Anatomical basis of the anterolateral thigh (ALT) flap.*
Left image: *Schematic representation of the lateral femoral circumflex artery (LFC) system, giving the descending branch (DB) as the main source of perforator branches (PBS) supplying the anterolateral (ALT) thigh skin territory*
Right image: *Dissected ALT flap with its vascular pedicle and dominant perforator, illustrating the typical appearance prior to pedicle division at the donor site.*
Adapted from Wei FC, microsurgeon.org (23)

The **ALT flap offers multiple advantages** for limb salvage:

- A **long vascular pedicle** (often 8–12 cm) with a consistent caliber suitable for microsurgical anastomosis.
- A **large, customizable skin paddle**, adaptable for **single or double-perforator designs** and chimeric flaps.
- **Thickness variability**, ranging from subfascial to superthin or ultrathin harvest, ideal for covering the **tibia or foot dorsum** without excessive bulk.
- **Low donor-site morbidity**, with primary closure feasible in many cases or split-thickness skin grafting if necessary.

Anatomical and clinical studies confirm that the ALT flap can reliably cover tibial plates, exposed bone, or multi-planar defects, making it indispensable in trauma and oncologic reconstruction (24–32). Despite this reliability, partial necrosis remains a concern, particularly in the distal third of the flap, where perfusion relies on linking choke vessels between perforasomes. This risk reinforces the need for intraoperative perfusion assessment, which directly motivates the exploration of ICG angiography and dynamic infrared thermography in this thesis.

II. Clinical relevance of perfusion and complications in ALT free flaps

Despite the remarkable evolution of reconstructive microsurgery, flap perfusion remains the key determinant of surgical success, especially in lower-limb reconstruction. The anterolateral thigh (ALT) flap, while highly reliable, is not exempt from the risk of partial or total necrosis, and the consequences in the leg are disproportionately severe compared to other anatomical regions.

The **global survival rate of ALT free flaps** in contemporary series ranges from **91% to 98%** (27,30,32–35) , which is comparable to other major perforator flaps. However, **partial flap loss or marginal necrosis** occurs in **3–10% of cases** (36) . In breast or trunk reconstruction, such small losses may be managed conservatively or with simple skin grafting. In contrast, even a minor area of necrosis in the lower limb may expose bone, tendon, vascular grafts, plates, or endoprostheses, creating a high risk of deep infection or osteomyelitis(6). This complication often necessitates reoperation, sometimes with a second free flap, and in extreme cases, amputation becomes unavoidable.



Figure 1.8. *Clinical example of distal perfusion failure in an anterolateral thigh (ALT) flap.*
Left image: *intraoperative view after flap inset, showing an apparently well-perfused skin paddle based on a single dominant perforator.*
Right image: *One week postoperative appearance demonstrating distal skin necrosis, consistent with insufficient perfusion of the distal perforasome, likely due to limited perforasome reach and lack of effective recruitment through choke vessel dilation.*

The mechanisms underlying **partial flap necrosis** in ALT flaps are multifactorial:

- **Anatomical variability** of perforators, particularly when the flap relies on a **single musculocutaneous perforator** with limited choke vessel recruitment.
- **Hemodynamic factors**, such as intraoperative hypotension, vasospasm, or compromised venous drainage.
- **Patient comorbidities**, including **diabetes mellitus, peripheral vascular disease, smoking, or prior trauma**, which reduce microvascular reserve.
- **Flap design choices**, where **excessively long or wide skin paddles** may exceed the functional perforasome territory.

While **clinical monitoring** (color, capillary refill, turgor, bleeding at the flap edge) remains the **traditional first-line method**, it is **subjective and operator-dependent**, with **limited predictive power for partial necrosis** (37). Surgeons often face a **gray zone**: areas that appear marginally perfused may either survive or progress to necrosis. These **borderline zones** are the critical target for **objective intraoperative assessment technologies**.

In the context of lower-limb reconstruction, the stakes of misjudging perfusion are high. A 1 cm^2 necrotic zone over a tibial plate can convert a 95% technically successful free flap into a functional failure, requiring additional surgery and delaying rehabilitation. This reality justifies the integration of imaging techniques capable of mapping real-time perfusion, which forms the central focus of this thesis.

1.5 Flap Perfusion Assesment

I. Indocyanine Green Angiography (ICG-A) for flap perfusion assessment

The intraoperative evaluation of flap perfusion has evolved significantly over the last two decades, moving from purely clinical observation to the use of real-time imaging technologies. Among these, indocyanine green angiography (ICG-A) has become the current gold standard for assessing microvascular perfusion in free flaps, including the anterolateral thigh (ALT) flap for lower-limb reconstruction.

Indocyanine green (ICG) is a water-soluble tricarbocyanine dye that binds strongly to plasma proteins, remaining intravascular after intravenous injection (38). Its optical properties allow it to fluoresce in the near-infrared (NIR) spectrum, with an excitation wavelength around 805 nm and an emission peak near 835 nm. This makes ICG highly suitable for intraoperative angiography, as NIR light can penetrate several millimeters into tissue without causing radiation damage.

ICG was developed in the 1950s and was initially used for cardiac output and hepatic function studies due to its exclusive intravascular distribution and rapid clearance by the liver (39). Its first applications in ophthalmology were described by Flower et al. (1972) for choroidal and retinal angiography (40,41).

Plastic and reconstructive surgery incorporated ICG decades later, particularly for intraoperative evaluation of flap perfusion and mastectomy skin viability, where it demonstrated a capacity to visualize areas of low perfusion that might progress to necrosis if not excised or adjusted(42–51).

Principles of ICG-A and intraoperative acquisition

ICG-A in free flap surgery relies on intravenous injection of a small bolus of ICG, typically 0.1–0.3 mg/kg, followed by real-time visualization with a near-infrared camera system.

After injection, ICG rapidly circulates through the arterial inflow, capillary bed, and venous drainage of the flap. The NIR camera captures a fluorescence sequence that can be analyzed in three main phases:

1. **Arterial inflow phase** – Bright fluorescence appears first at the site of the arterial pedicle and propagates distally along the flap.
2. **Capillary or plateau phase** – Homogeneous perfusion produces uniform fluorescence intensity, ideally within 45–60 seconds.
3. **Venous outflow phase** – Fluorescence diminishes progressively; delayed washout may suggest **venous congestion**.

These sequences allow surgeons to identify hypoperfused zones that might otherwise appear normal under white light. Quantitative analysis is possible through software-based intensity mapping, though in clinical practice, most intraoperative decisions are based on semi-quantitative interpretation of the perfusion pattern (52–58).



Figure 1.9. *Indocyanine green angiography (ICG-A) system and contrast agent.*
Left image: *ICG imaging console, comparable in size to an ultrasound unit, designed for intraoperative use and requiring a dedicated cart.*
Right image: *vial of indocyanine green used for fluorescence angiography.*



Figure 1.10. *Intraoperative application of indocyanine green angiography in an anterolateral thigh (ALT) flap.*
Left image: *dissected ALT flap at the donor site prior to pedicle division.*
Right image: *corresponding intraoperative ICG angiography image demonstrating flap perfusion.*

Clinical applications and advantages

The integration of ICG-A into reconstructive microsurgery has several key advantages:

- **Real-time perfusion mapping** with immediate feedback to the surgical team.
- **Early detection of marginal zones** at risk for necrosis, enabling **intraoperative trimming or flap reorientation**.
- **Assessment of venous congestion** and differentiation from arterial insufficiency.
- **Reduced subjectivity** compared to purely clinical observation.
- **Non-ionizing and safe**, with a low incidence of adverse reactions (<0.1%) (38,59).

For lower-limb reconstruction, ICG-A has been particularly valuable because partial necrosis carries high morbidity. By detecting borderline perfusion areas before flap inset, surgeons can reduce the incidence of distal necrosis, especially in large or long ALT flaps where choke vessel recruitment may be limited in the early postoperative period.(60,61)

Limitations of ICG-A

Despite its benefits, ICG-A has **limitations that must be acknowledged**:

- **Cost and availability** – Dedicated infrared cameras (e.g., Fluobeam®, SPY Elite®) represent a significant financial investment, limiting universal access.
- **Subjectivity in interpretation** – While the visualization is immediate, the threshold for "safe" fluorescence is not strictly standardized across devices or institutions.
- **Surface penetration** – NIR light penetrates only a few millimeters, providing primarily surface perfusion information, which may not fully reflect deep flap vascularity.
- **Dynamic changes post-anastomosis** – Perfusion can evolve over hours, so a single intraoperative snapshot may miss delayed congestion or arterial spasm.
- **ICG pharmacokinetics** – Rapid hepatic clearance allows repeated dosing, but in patients with liver dysfunction, background fluorescence may limit image clarity.

Perfusion patterns and interpretation in ALT flaps

In clinical practice, ICG-A generates **fluorescence maps** that can be interpreted to guide flap inset and trimming. Several **perfusion zones** are typically described in the literature:

- **Well-perfused zones** – Bright, homogeneous fluorescence appears early (<45 s).
- **Borderline zones** – Delayed or heterogeneous fluorescence; these areas require **careful intraoperative judgment**.
- **Hypoperfused or non-perfused zones** – Absence of fluorescence or extreme delay; these should generally be **resected or revised**.

In lower-limb ALT flaps, perfusion frequently decreases toward the distal edge of the flap, corresponding to the limits of the dominant perforasome. Identifying and managing these marginal territories intraoperatively is the primary rationale for ICG-A in limb salvage.

II. Dynamic Infrared Thermography (DIRT) in free flap perfusion assessment

Dynamic Infrared Thermography (DIRT) has emerged as a valuable tool for functional assessment of perfusion in free and pedicled flaps, offering a non-invasive, repeatable, and real-time evaluation of cutaneous blood flow. Its relevance is particularly evident in lower-limb reconstruction with large fasciocutaneous flaps, such as the anterolateral thigh (ALT) flap, where early detection of marginal ischemia can be decisive for flap survival and limb salvage (62–72).

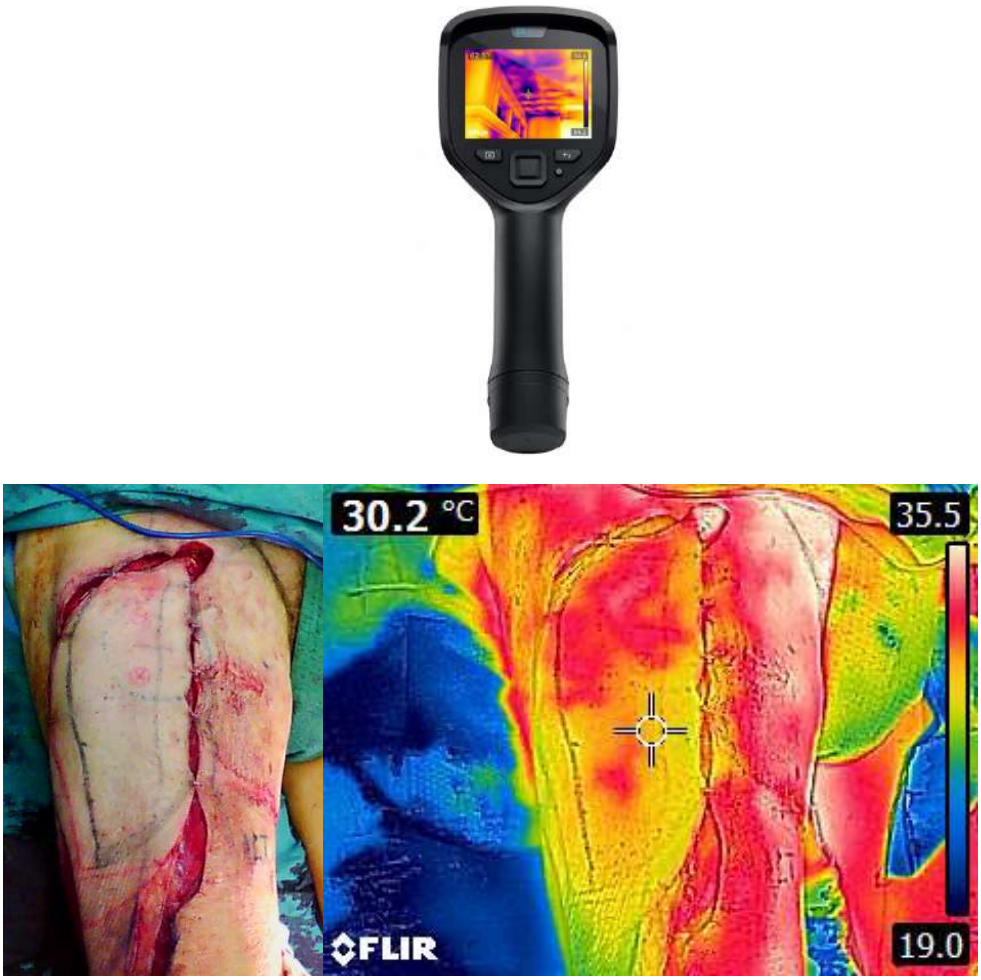


Figure 1.11. *Infrared thermography system and intraoperative application.*
Upper image: *portable infrared thermal camera (FLIR One E6 Pro) used for intraoperative thermal imaging, compact in size but not pocket-based.*
Lower images: left*, dissected anterolateral thigh (ALT) flap at the donor site prior to pedicle division****; right****, corresponding static thermal image illustrating the appearance of flap surface temperature distribution.*

Principles and Physiological Basis

DIRT is based on the thermal behavior of skin and subcutaneous tissue as a surrogate for microvascular perfusion. The technique relies on the principle that well-perfused tissue rewarmes faster after a standardized cooling challenge, due to the continuous supply of warm blood through arterial inflow and capillary circulation. Conversely, areas with delayed or heterogeneous thermal recovery indicate borderline perfusion or venous congestion, which may precede clinical manifestations such as pallor, cyanosis, or turgor changes (64,73).

In practice, dynamic infrared thermography (DIRT) consists of cooling the flap surface for a short, standardized period and then observing the rewarming process with an infrared camera. Temperature recovery reflects tissue perfusion: **well-perfused areas rewarm rapidly and uniformly**, achieving homogeneous temperature rise within seconds. **Borderline or doubtful perfusion** shows a slower and heterogeneous rewarming pattern, often with irregular or delayed temperature increase. **Hypoperfused zones** remain cool for longer periods, displaying minimal or absent temperature recovery during the observation window. Thus, instead of relying solely on anatomical assumptions, DIRT provides a *real-time functional map of perfusion*, allowing surgeons to identify viable tissue, areas at risk, and regions that may progress to necrosis.

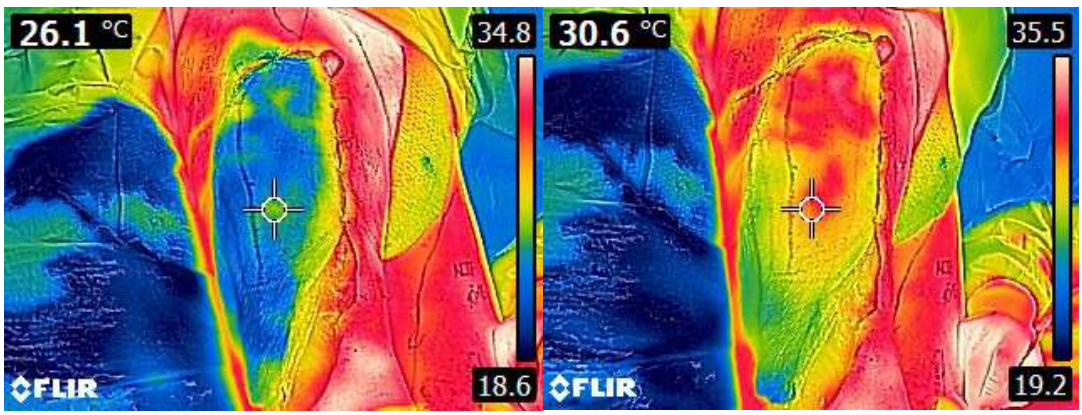


Figure 1.12. *Dynamic infrared thermography (DIRT) assessment of flap perfusion.* ***Left image:*** *thermal image obtained immediately after 1 minute controlled cooling, showing a low baseline surface temperature of approximately 20 °C.*
Right image: *thermal image acquired 10 minutes after rewarming, illustrating differential temperature recovery, with well-perfused areas showing higher rewarming and hypoperfused or doubtful zones remaining cooler..*

Historical Development

The foundations of DIRT in reconstructive surgery were laid more than three decades ago. Wilson and collaborators (62) were the first to demonstrate that dynamic thermography outperformed static imaging in detecting ischemic regions in experimental flaps. Their work established that surface temperature alone could be misleading, as baseline uniformity often masks subtle perfusion deficits. By introducing time as a functional variable, dynamic imaging revealed delayed thermal recovery as a predictor of ischemia and impending necrosis, providing the physiologic rationale that underpins current applications.

Subsequent advances were driven by the clinical and experimental studies of De Weerd and colleagues (63–65), who validated DIRT as a predictive intraoperative tool for free flap perfusion. Their investigations demonstrated that early hot spots correlated with the location of dominant perforators, while delayed or heterogeneous thermal recovery predicted distal flap necrosis. Importantly, these thermal changes were observed hours before clinical signs appeared, emphasizing the potential of DIRT for early risk detection. De Weerd also highlighted its value for functional perforasome mapping, complementing anatomical knowledge obtained from Doppler ultrasound or computed tomography angiography.(74)

As clinical experience expanded, systematic analyses and protocol standardization strengthened the role of DIRT. John et al. conducted a systematic review on the clinical applications of dynamic infrared thermography in reconstructive microsurgery and found that DIRT reliably identifies perfusion heterogeneity within free flaps. By highlighting poorly perfused or delayed-rewarming areas, DIRT allows intraoperative decision-making such as preventive trimming of at-risk zones before flap inset. Their review reported that this strategy reduces the incidence of partial flap necrosis and supports the value of thermography as a functional tool rather than purely clinical assessment (75).

DIRT has also proven useful in pedicled perforator flaps. Sjöberg and collaborators (70) applied the technique to thoracodorsal artery perforator (TDAP) flaps, showing that it

can map individual perforasomes and detect early venous congestion. By identifying delayed rewarming or patchy thermal patterns, the surgical team could intervene early, optimizing flap safety and reducing postoperative complications.

An important step toward wider clinical adoption came with the standardization efforts of Thiessen et al. (66), who defined key technical parameters to ensure reproducibility. They emphasized the need to control ambient temperature, duration and method of cooling, camera distance and angle, and timing of image acquisition. This standardization is essential for multicenter studies and for integrating DIRT into evidence-based reconstructive protocols**.**

Clinical Relevance in ALT Flaps and Lower-Limb Reconstruction

The functional insights provided by DIRT are particularly relevant for large fasciocutaneous flaps such as the anterolateral thigh (ALT) flap, which is the workhorse of lower-limb reconstruction. Distal portions of these flaps often rely on choke vessel recruitment between adjacent perforasomes, a process that may be incomplete in the immediate postoperative period. Identifying these borderline territories intraoperatively is critical, as even 1 cm^2 of necrosis in the lower limb can expose bone, plates, or prosthetic material, leading to infection, osteomyelitis, and potential limb loss (30,33,34,36,76–79).

Dynamic Infrared Thermography (DIRT) allows surgeons to visualize flap perfusion dynamically, complementing the anatomical information obtained with Indocyanine Green Angiography (ICG-A). While ICG-A offers a high-resolution static image of perfusion, DIRT adds a functional and temporal dimension, showing real-time changes in temperature that reflect blood inflow. Areas that rewarm rapidly indicate better perfusion, whereas delayed or heterogeneous rewarming may suggest marginal perfusion or early venous congestion. Because it is completely non-invasive, dye-free, and repeatable, DIRT presents an attractive option to monitor perfusion intraoperatively and in the early postoperative period.

Although initial experimental work by Wilson and later clinical application by de Weerd and others introduced DIRT as a feasible adjunct in perforator flap surgery, current evidence remains limited. Some studies report that first hotspots during thermal rewarming identify perforators; however, perforator detection is not the primary clinical challenge during ALT free flap surgery. What truly influences flap survival is not the location of a perforator but the perfusion capacity of its vascular territory. For this reason, the present study focuses on perfusion assessment, not perforator mapping. To date, DIRT has not been validated as equivalent to ICG-A for evaluating the perfused surface area of free flaps—particularly in lower-limb reconstruction, where even small areas of necrosis can jeopardize limb salvage. Available literature positions DIRT as a potentially complementary and cost-effective tool, but further comparative studies are required to determine its accuracy, reproducibility, and real impact on flap outcomes.

1.6 Study rationale and justification

Lower-limb reconstruction remains one of the most demanding areas in reconstructive microsurgery, where even minimal partial flap loss can translate into major functional failure, prolonged hospitalization, and risk of osteomyelitis or amputation. Among the available options, the anterolateral thigh (ALT) flap has established itself as the workhorse for these complex defects due to its long pedicle, reliable perforators, and low donor-site morbidity. Nevertheless, its success still depends critically on precise intraoperative assessment of perfusion, especially in distal or borderline territories where choke vessel recruitment is uncertain (19,20,80).

Traditional clinical assessment—based on color, turgor, capillary refill, and bleeding—is subjective and often insufficient to reliably identify borderline perfusion zones. The current gold standard, indocyanine green angiography (ICG-A), provides real-time perfusion mapping but has significant limitations, including cost, need for intravenous contrast, limited tissue penetration, and potential for incomplete temporal assessment (60,61). In contrast, Dynamic Infrared Thermography (DIRT) emerges as a non-invasive, repeatable, and cost-effective technique, capable of mapping functional perfusion dynamically, with the potential to identify high-risk areas early and reduce flap-related complications (64,65).

Despite growing interest, direct comparative studies between ICG-A and DIRT in ALT flaps for lower-limb reconstruction remain scarce. Establishing how these two modalities correlate and whether DIRT can serve as a reliable alternative or complement to ICG-A represents a clinically relevant question with potential to optimize limb salvage protocols, reduce costs, and improve patient outcomes.

The present thesis is designed to fill this knowledge gap by performing a prospective intraoperative comparison of ICG-A and DIRT for ALT flap perfusion assessment in lower-limb reconstruction. Through this approach, we aim to:

1. **Characterize perfusion patterns** obtained by each technique in clinically relevant intraoperative stages.
2. **Identify concordance and discrepancies** between fluorescence-based and thermal imaging modalities.
3. **Evaluate the potential of DIRT** as a **reliable, non-invasive alternative** for real-time flap monitoring.

By integrating anatomical knowledge, technological advances, and clinical relevance, this work contributes to the evidence-based refinement of lower-limb reconstructive strategies, reinforcing the concept that objective perfusion assessment is essential to maximize flap survival and functional outcomes.

2

Hypothesis

2: Hypothesis

- Dynamic infrared thermography (DIRT) is a reliable and cost-effective alternative to indocyanine green angiography (ICG-A) for the intraoperative assessment of perfusion in free anterolateral thigh (ALT) perforator flaps used in lower extremity reconstruction.



Objectives

3: Objectives

I. Main Objective

- To assess whether dynamic infrared thermography (DIRT) provides comparable intraoperative assessment of flap perfusion to indocyanine green angiography (ICG-A) in anterolateral thigh flap (ALT) reconstruction of the lower extremity.

II. Secondary Objectives

- To evaluate the spatial agreement and discrepancies between dynamic infrared thermography and indocyanine green angiography in the classification of well-perfused, doubtful, and non-perfused regions of the ALT flap.
- To characterize thermographic temperature distribution across different intraoperative timepoints (T1, T2, and T3), with particular attention to spatial heterogeneity and distal territories.
- To explore thermographic changes associated with venous outflow configuration, comparing single- and dual-vein drainage over time.
- To explore the relationship between thermographic temperature distribution and angiographic perfusion categories, assessing its potential relevance for intraoperative interpretation.

4

Material and Methods

4: Materials and Methods

4.1 Study Design

This study is a **prospective observational intraoperative imaging comparison** designed to evaluate the agreement between **Dynamic Infrared Thermography (DIRT)** and **Indocyanine Green Angiography (ICG-A)** for perfusion assessment of free **anterolateral thigh (ALT) perforator flaps** used in lower-limb reconstruction.

I. Intraoperative timepoints and imaging strategy

For the purposes of intraoperative perfusion assessment, three standardized timepoints were defined: **T1, T2, and T3**. These timepoints were selected to capture physiologically distinct stages of flap perfusion during lower limb reconstruction and to allow both cross-modal and longitudinal analysis.

T1 — In situ (native donor-site perfusion)

Before pedicle division, the ALT flap remains attached to its donor site and perfused by its native vascular supply (typically one dominant perforator artery and two venae comitantes).

This timepoint represents the most physiological condition for perfusion assessment and was therefore selected as the **reference baseline** for the study. At T1, **both indocyanine green angiography (ICG-A) and dynamic infrared thermography (DIRT)** were performed.

T2 — After anastomosis of one artery and one vein

Following pedicle division and transfer to the recipient site, perfusion is re-established through one arterial inflow and one venous outflow. This configuration is intrinsically more vulnerable to **venous congestion**, particularly in lower-limb reconstructions where high hydrostatic pressure, dependent positioning, and pre-existing vascular disease are

common. At this timepoint, flap perfusion is influenced by transient ischemia–reperfusion phenomena and partial venous drainage. **Only dynamic infrared thermography** was performed at T2.

T3 — After completion of the second venous anastomosis

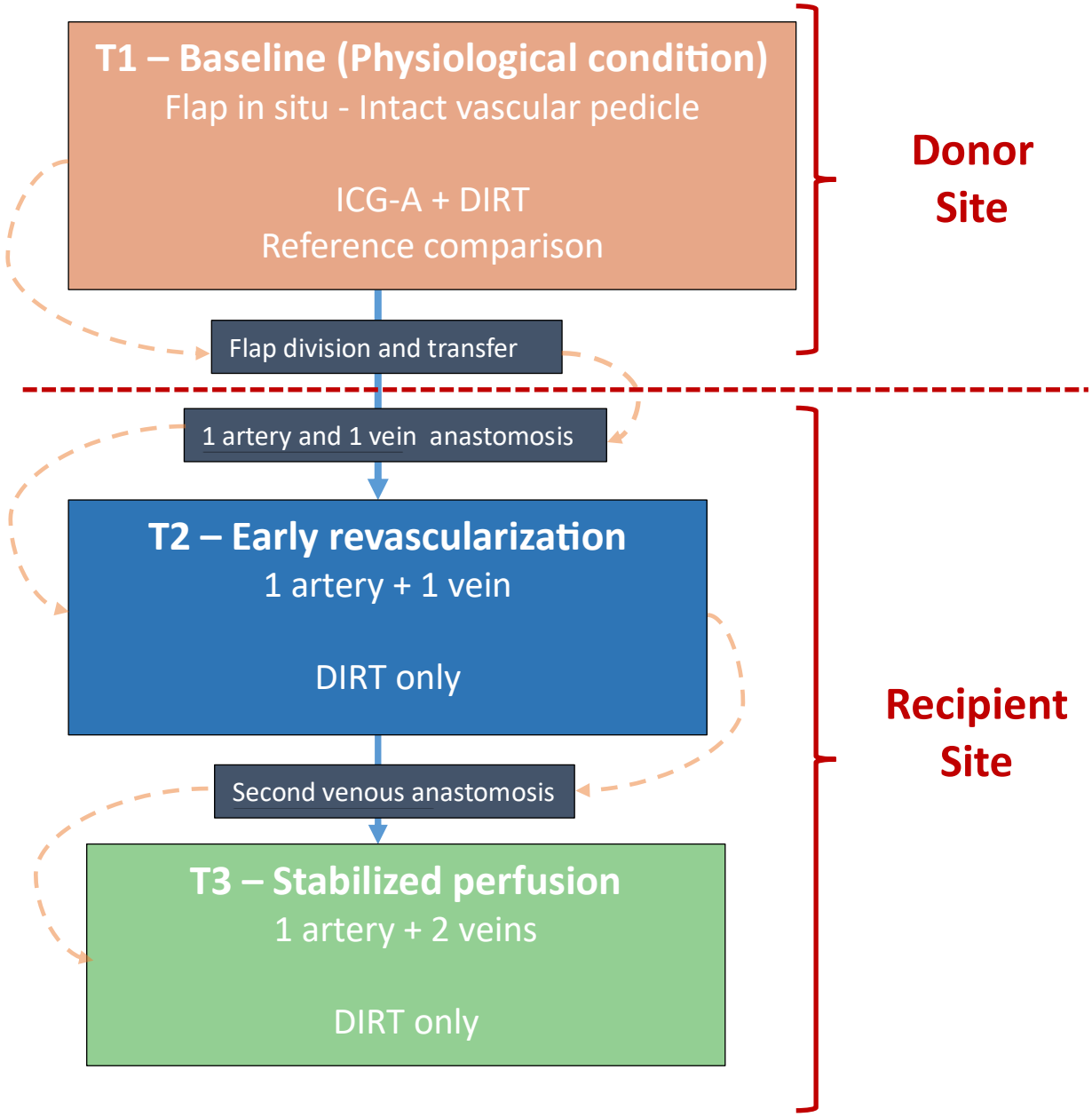
Once a second venous anastomosis is performed—restoring a two-vein drainage pattern analogous to the flap's native physiology—the perfusion environment changes substantially. As at T2, **only dynamic infrared thermography** was performed.

Dual venous outflow is believed to:

- Reduce venous congestion
- Improve washout kinetics
- Diminish peripheral thermal asymmetry
- Stabilize perfusion in borderline territories.

Indocyanine green angiography was intentionally restricted to T1 in order to minimize repeated dye administration and because T1 provides the most controlled and physiologically relevant conditions for cross-modal comparison. In addition, image acquisition at the donor site (anterolateral thigh) prior to flap transfer allows optimal positioning, minimal motion artifacts, and consistent illumination and exposure conditions.

Figure 4.1. *Intraoperative imaging workflow and defined timepoints*



Accordingly, **T1 constitutes the sole timepoint used for direct comparison between ICG-A and standardized thermography**, whereas T2 and T3 are used exclusively for **longitudinal intra-flap perfusion analysis using thermography**.

Rationale for selection of T1 as the reference timepoint

T1 was selected as the reference timepoint for several methodological reasons. First, perfusion at T1 reflects intact physiological circulation without the confounding effects of ischemia–reperfusion injury or altered venous drainage. Second, thermographic and angiographic image acquisition at the donor site allows higher reproducibility and spatial accuracy compared with post-transfer measurements. Finally, comparison at T1 enables assessment of whether thermography can reproduce the **spatial and regional perfusion patterns** identified by ICG-A under physiological conditions, which is central to the study objective.

Control of systemic and environmental conditions for intraoperative perfusion assessment

To ensure that perfusion measurements were physiologically comparable across all three intraoperative stages (T1–T2–T3), both environmental and systemic conditions were kept within strict predefined ranges. Operating-room temperature was maintained between 20–22 °C, and patient core temperature was stabilized between 36–37 °C using warmed IV fluids and active warming as needed. Hemodynamic parameters—including arterial pressure, heart rate, and oxygen saturation—were individually optimized according to each patient's preoperative baseline, with mean arterial pressure maintained within a normotensive range using norepinephrine when required. Hemoglobin levels were kept above 9 g/dL, with transfusion administered if necessary.

These measures ensured that any observed changes in perfusion patterns were attributable to the vascular condition of the flap rather than systemic instability. Thus, T1 captures perfusion under stable physiological baseline conditions, while T2 and T3 were conducted under hemodynamic and thermal parameters deliberately matched to those recorded at T1, allowing meaningful inter-stage and inter-patient comparisons.

II. Sample Size and Power Considerations

The main quantitative endpoint for sample size planning was the **agreement between DIRT and ICG-A** in terms of perfused area per flap, expressed as the correlation between temperature-based and fluorescence-based perfusion measures (percentage of well-perfused area or equivalent zonal indices).

Because no prior studies were available specifically for DIRT vs ICG-A in ALT flaps for lower-limb reconstruction, the calculation was based on conservative assumptions for a **correlation / agreement study**:

- Expected true correlation between DIRT and ICG-A: **$\rho \approx 0.80$** (strong but not perfect agreement, consistent with the hypothesis that DIRT provides a clinically acceptable level of agreement while not being identical to ICG-A).
- Clinically acceptable lower bound of the 95% confidence interval: **$\rho \geq 0.50$** (values below this threshold would be considered insufficient for a clinically useful alternative imaging modality).
- Two-sided $\alpha = 0.05$.

Using Fisher's z-transformation for correlation estimates, a sample of **n = 20 flaps** provides a standard error of approximately $1/\sqrt{(n-3)}$, which yields a 95% confidence interval around an expected correlation of 0.80 with a lower bound close to **0.55**. This satisfies the pre-specified requirement that the lower limit of the confidence interval remains above 0.50, thus offering adequate **precision** to judge whether DIRT behaves as a potentially acceptable alternative or complementary tool to ICG-A.

In addition, each flap is evaluated at **three intraoperative timepoints** (T1 in situ, T2 after 1 artery + 1 vein, T3 after addition of a second vein), and each image is analysed at multiple spatial levels (1 cm^2 ROIs, zones 1–4, and subzones 1a/1b and 4a/4b). Although the formal sample size is based on the number of flaps (patients), these repeated measurements substantially increase the amount of paired DIRT–ICG data available for secondary analyses (zonal gradients, ROC curves for temperature thresholds, venous

congestion patterns), improving the descriptive and exploratory power of the study without exposing additional patients to risk.

From a **practical standpoint**, the centre performs approximately 10–20 ALT free flaps for lower-limb reconstruction per year, but not all cases fulfill the inclusion criteria. Therefore, a target of **20 consecutive eligible patients** over roughly two years was considered feasible and ethically justifiable, while still consistent with methodological recommendations for method-comparison and agreement studies (typically requiring ≥ 15–20 subjects).

Given the exploratory nature of this thesis and the limited prior evidence, the sample size is thus best interpreted as **pragmatic but analytically grounded**, providing a reasonable balance between statistical precision, feasibility, and ethical considerations.

Sample size justification (correlation-based, Fisher's z transformation)

Because an important analytic focus of the study is to evaluate the **strength of association between regional and global perfusion metrics derived from standardized dynamic infrared thermography and those obtained from indocyanine green angiography at baseline (T1)**, sample size estimation was additionally informed by correlation-based considerations.

Given the absence of validated effect sizes for intraoperative thermographic perfusion assessment, a **correlation-based approach using Fisher's z-transformation** was adopted to estimate the minimum number of flaps required to ensure a sufficiently narrow confidence interval around the expected correlation coefficient at baseline.

1. **Fisher's z-transform of the expected correlation**

$$z_\rho = \tfrac{1}{2} \ln\left(\frac{1+\rho}{1-\rho}\right)$$

2. **Fisher's z-transform of the minimally acceptable (lower bound) correlation**

$$z_{\rho_L} = \frac{1}{2} \ln\left(\frac{1+\rho_L}{1-\rho_L}\right)$$

3. **Half-width in the z-scale**

$$w = z_\rho - z_{\rho_L}$$

4. **Relation between half-width and sample size (95 % CI, $Z_{0.975}$=1.96)**
   For a correlation estimated in a sample of size n, the standard error in the z-scale is:

$$SE_z = \frac{1}{\sqrt{n-3}}$$

and the 95 % confidence interval is:

$$z_\rho \pm Z_{0.975}\, SE_z$$

Imposing that the lower limit of the 95 % CI does not fall below $z_{\rho L}$ gives:

$$z_\rho - Z_{0.975} \frac{1}{\sqrt{n-3}} = z_{\rho_L}$$

Rearranging, the final expression for sample size estimation is:

$$n = 3 + \left(\frac{Z_{0.975}}{z_\rho - z_{\rho_L}}\right)^2$$

Applying this to our study

- Expected correlation between DIRT and ICG-A: ρ=0.80
- Minimal acceptable lower bound: ρL=0.55

- Confidence level: 95 % → Z0.975=1.96

1. **Fisher's z for ρ=0.80:**

$$z_\rho = \tfrac{1}{2}\ln\left(\frac{1+0.80}{1-0.80}\right) = \tfrac{1}{2}\ln(9) \approx 1.10$$

2. **Fisher's z for ρL=0.55:**

$$z_{\rho_L} = \tfrac{1}{2}\ln\left(\frac{1+0.55}{1-0.55}\right) \approx \tfrac{1}{2}\ln(3.44) \approx 0.62$$

3. **Half-width in z-scale:**

$$w = z_\rho - z_{\rho_L} \approx 1.10 - 0.62 = 0.48$$

4. **Sample size:**

$$n = 3 + \left(\frac{1.96}{0.48}\right)^2 \approx 3 + (4.08)^2 \approx 3 + 16.6 \approx 19.6$$

Rounded to the nearest integer, this yields:

$$n \approx 20 \text{ flaps}$$

Therefore, a minimum of 20 free ALT flaps was considered adequate to ensure that the 95 % confidence interval for the DIRT–ICG correlation would not fall below 0.55, assuming a true underlying correlation of approximately 0.80.

4.2 Setting and Participants

The study was conducted at the Plastic and Reconstructive Surgery Department of Hospital de la Santa Creu i Sant Pau (Barcelona, Spain), between January 2020 and December 2021.

Recruitment Setting

- Consecutive patients undergoing ALT free flap reconstruction for **soft-tissue defects of the lower limb** (inguinal region, thigh, knee, leg, foot).
- All surgeries performed by the same microsurgical team with standardized operative protocols.

Data source

Clinical data were extracted from:

- Electronic Health Records (SAP/ETC system).
- Anesthesia records.
- Operative notes.
- Nursing intraoperative flowsheets.

All imaging files (ICG-A and DIRT) were collected intraoperatively and archived in a structured digital repository.

4.3 Inclusion and Exlusion Criteria

I. Inclusion Criteria

- Patients aged 18 years or older.
- Patients undergoing reconstruction of lower extremity soft tissue defects using ALT free flaps.
- ALT flap elevation based on one or two perforators from the descending branch of the lateral circumflex femoral artery.
- Intraoperative availability of both ICG and DIRT imaging systems.
- Informed consent for participation in the study.

II. Exclusion Criteria

- Patients with known allergy to ICG or iodine.
- Severe peripheral vascular disease in donor or recipient sites.
- Intraoperative conversion to another type of flap.
- Flap failure requiring intraoperative abandonment of reconstruction.
- Intraoperative re-exploration for microvascular compromise (arterial or venous thrombosis).
- Technical limitations precluding valid image acquisition.
- Previous surgery or scarring at the ALT donor site.

4.4 Variables

Variables are grouped into **independent** (clinical and surgical covariates) and **dependent** (imaging-based outcomes). All variables were extracted manually from SAP records and entered into an Excel database. Missing data were not retrospectively imputed or estimated.

I. Independent Variables

a. Patient Demographics and Baseline Status

- **Age (years):** Integer 0–100 (no months/days). Value recorded as age at index surgery (date of surgery), as documented in EHR.
- **Sex:** Categorical (Male / Female), as documented in EHR.
- **BMI (kg/m²):**
    - Weight in kilograms (integer, no decimal; scale reading closest to surgery, typically pre-op holding).
    - Height in centimeters (convert to meters with two decimals for BMI).
    - BMI = weight (kg) / [height (m)]², recorded with non-decimal.
    - If height/weight missing on surgery day, use the closest preoperative measurement (≤30 days).
- **Smoking Status**

  Primary Variable: Smoking Status (Yes/No)

  This variable captures long-term vascular exposure, not only short-term smoking behavior.
    - **"Smoker" (Yes)** was defined as any patient who:
        - was actively smoking at the time of surgical indication **or,**
        - had a significant history of habitual smoking (≥1 cigarette/day) and had quit less than 12 months before surgery.

Rationale:

Although perioperative guidelines often consider ≥30 days abstinence as beneficial for wound complications, arteriolar and endothelial damage induced by chronic tobacco use persists for months to years. Therefore, former smokers with only short-term cessation (<12 months) were classified as "smokers" for the purpose of vascular risk stratification.

- **"Non-smoker" (No)** included:
  - patients who had never smoked,
  - former smokers with sustained abstinence ≥12 months,
  - or individuals with only minimal or sporadic lifetime exposure (e.g., <100 cigarettes total), consistent with epidemiological definitions of "never smoker".

Justification:

This definition reflects the microvascular physiology relevant to flap perfusion, where chronic smoking—not short-term abstinence—is the main determinant of endothelial dysfunction, arterial stiffness, reduced capillary density, and impaired thermal recovery patterns.

Secondary Variable: Smoking Intensity (Packs per Day)

For patients classified as active smokers, daily cigarette consumption was further categorized into an ordinal variable:

Table 4.1. Smoking Intensity categories definition

Category	Definition
< 1 pack/day	≤ 19 cigarettes per day
1–2 packs/day	20–40 cigarettes per day
> 2 packs/day	≥ 41 cigarettes per day

These thresholds mirror standard *pack-per-day* (PPD) subdivisions widely used in vascular surgery, anesthesiology, and wound-healing research due to their association with vasoconstriction, endothelial dysfunction, reduced oxygen delivery, and impaired microcirculation—all factors known to compromise flap perfusion.

- **Comorbidities**

  Comorbidities were collected as **binary variables (Yes/No)** based on objective diagnostic criteria. Given their direct impact on microvascular perfusion, three comorbidities were specifically evaluated:

  - **Diabetes Mellitus (DM)**

    Recorded as ***Yes*** when the patient had one of the following:

    - Documented medical diagnosis of DM 1 or 2
    - Laboratory confirmation within 6 months before surgery (one criteria):
      - HbA1c ≥ 6.5%
      - Fasting glucose ≥ 126 mg/dL
      - Random glucose ≥ 200 mg/dL with symptoms.

    Otherwise, recorded as ***No*****.**

  - **Peripheral Arterial Disease (PAD)**

    Recorded as ***Yes*** if any of the following were present:

    - Documented diagnosis of PAD,
    - ABI < 0.9, or
    - Imaging evidence of ≥50% arterial stenosis (Doppler, CTA, MRA).

    If none were present, PAD was recorded as ***No*****.**

    *Rutherford classification was not applied to PAD, as it corresponds to symptomatic staging rather than diagnosis.

- **Critical Limb Ischemia (CLI)**

  CLI represents the advanced stage of PAD and was recorded as ***Yes*** whe the patient met clinical or hemodynamic criteria consistent with Rutherford categories 4–6*:

  - Ischemic rest pain >2 weeks
  - Ischemic ulcers
  - Gangrene
  - ABI ≤ 0.4
  - Toe pressure < 30 mmHg
  - $TcPO_2$ < 30 mmHg.

  If these criteria were absent, CLI was recorded as ***No*.**

  Justification: CLI is a strong predictor of perfusion-related complications.

  ***Brief explanation – Rutherford Classification:**

  The Rutherford classification is the standard system for staging lower-limb ischemia, ranging from category 0 (asymptomatic) to category 6 (major tissue loss). Categories 4–6 define Critical Limb Ischemia (CLI), indicating severely compromised perfusion requiring urgent revascularization and representing the group at highest risk for tissue necrosis. This classification is endorsed by the European Society for Vascular Surgery (ESVS) and the Society for Vascular Surgery (SVS) as the diagnostic framework for chronic limb-threatening ischemia.(81,82)

b. Cancer and Treatment Related Variables

- **Prior Radiotherapy (RT)**
  - **Binary variable:** Yes/No

  Considered present when the patient had completed radiotherapy ≥ 4 weeks before surgery, acknowledging that preoperative RT may induce chronic microvascular changes that could influence flap perfusion, especially in lower-limb reconstruction.

- **Neoadjuvant Chemotherapy**
    - **Binary variable:** Yes/No

      Registered when systemic chemotherapy was administered before the reconstructive procedure, given its potential systemic effects on tissue perfusion and wound healing.

c. Etiology of the Defect

Categorical variable classified into four clinically meaningful groups. Etiology was recorded because the underlying cause of the defect may influence the vascular status of the recipient site and therefore impact flap perfusion.

- **Tumoral**

  Includes defects resulting from oncologic resections, predominantly soft-tissue sarcomas.

- **Traumatic**

  Defects caused by high-energy trauma, including open fractures, crush injuries, degloving injuries, road-traffic accidents, and other mechanisms resulting in soft-tissue loss.

-

  This category also includes secondary complications derived from orthopedic trauma surgery, such as:
    - Exposure of osteosynthesis material (plates, locking nails, screws),
    - Exposure of joint prostheses,
    - Osteomyelitis,
    - Non-union or malunion requiring coverage.

- **Diabetic Foot–related Defects**

  Ulcers, infections, or necrosis associated with diabetes mellitus. These patients typically have:
    - Peripheral neuropathy.
    - Microvascular disease.
    - Impaired wound healing.

- Increased risk of infection.

These factors can compromise local perfusion and influence both flap survival and postoperative outcomes, justifying their classification as a standalone etiologic group**.**

- **Other Causes**

  Defects secondary to conditions not encompassed by the three previous groups. This group captures the remaining indications for lower-limb soft-tissue reconstruction where etiology does not fit the more specific categories above.

d. Defect Location (Recipient Site)

- Inguinal region
- Thigh
- Knee
- Leg
- Foot

Rationale for Inclusion

Lower-limb perfusion shows a well-recognized proximal-to-distal decline in arterial inflow, venous return, and microvascular density. As a result, the anatomical location of the defect may modulate:

- Inflow dynamics after arterial anastomosis
- Venous drainage adequacy
- Speed and completeness of fluorescence filling on ICG-A
- DIRT rewarming patterns, particularly in areas prone to marginal perfusion or venous congestion
- Risk of partial flap necrosis, especially in distal segments (leg and foot).

  Including this variable allows the study to determine whether perfusion agreement between DIRT and ICG-A is location-dependent.

Technical Considerations Relevant to Perfusion Imaging

In addition to vascular biology, the geometry of the recipient defect affects how reliably each modality can be interpreted across the three intraoperative stages (T1: in situ, T2: 1 vein, T3: 2 veins):

Inguinal Region & Thigh (Proximal Sites)

- Typically flat, single-plane defects, which simplifies flap inset and minimizes folding or torsion.
- Lower tension after inset, reducing risk of peripheral hypoperfusion.
- Both ICG-A and DIRT are easier to interpret, with homogeneous illumination and thermal behavior.

Knee

- Defects may involve one, two, or even three anatomical surfaces, meaning that flap inset frequently requires folding, bending, or contouring. These maneuvers can influence:
  - Venous outflow
  - Peripheral temperature recovery
  - Symmetry of ICG filling patterns
- Such three-dimensional configurations add interpretative complexity to both imaging modalities during T2 and T3, as thermal distributions may be affected by mechanical angulation rather than intrinsic vascular compromise.

Leg

- Usually, flat defects unless circumferential.
  - However, vascular reserve is lower, increasing sensitivity to marginal inflow or venous congestion.
  - Perfusion patterns may display greater heterogeneity across zones 1–4, making zone-based analysis particularly relevant.

Foot

- Perfusion varies markedly depending on sub-region: dorsal foot, plantar surface, heel, lateral or medial malleolus.
- When multiple surfaces are involved (e.g., crossing the ankle), geometry becomes three-dimensional, complicating image capture and analysis.
- The distal vascular bed is naturally more compromised, which may accentuate differences between DIRT and ICG-A in borderline zones.

Purpose Within the Study

Including defect location as an independent variable enables:

- Evaluating whether distal sites show greater doubtful or hypoperfused areas.
- Interpreting whether venous congestion patterns in T2 vs. T3 are affected by the anatomical region.
- Understanding the impact of flap geometry (single- vs. multi-surface inset) on thermal imaging.

e. Intraoperative Hemodynamic and Environmental Data Collection

To control for potential confounding factors affecting flap perfusion, a structured set of hemodynamic and environmental parameters was recorded systematically throughout the procedure. These variables were extracted from the anesthetic chart in the electronic clinical record (SAP® system, Hospital de la Santa Creu i Sant Pau) and transcribed into the study database.

- **Baseline Physiological Parameters (Preoperative / Start of Surgery)**

At the beginning of the procedure, prior to flap elevation, the following baseline values were recorded:

- **Systolic/diastolic arterial pressure (mmHg)**
- **Heart rate (beats per minute)**
- **Peripheral oxygen saturation (SpO_2) (%)**

These values served as reference to verify that patients started surgery under stable physiological conditions.

- **Hemodynamic and Environmental Parameters Recorded During the Three Intraoperative Timepoints (T1, T2, T3)**

  For each of the predefined assessment stages:

  i. T1: flap in situ (before pedicle division)
  ii. T2: after anastomosis of 1 artery + 1 vein
  iii. T3: after completion of the second venous anastomosis

  the following variables were collected:

  - **Hemodynamic Parameters**
    - Arterial blood pressure (mmHg)
    - Heart rate (bpm)
    - Peripheral oxygen saturation (SpO_2) (%)

    These were monitored to ensure that observed perfusion differences were not attributable to systemic instability.
  - **Thermal Conditions**
    - Operating-room ambient temperature (°C)
    - Patient core temperature (°C)

    Both factors may influence thermal recovery patterns in DIRT and were therefore recorded at each stage.
  - **Blood Transfusions**
    - Packed red blood cells administered (Yes/No)
    - Number of units transfused (integer value)

    Acute correction of anemia could theoretically alter perfusion dynamics.
  - **Vasoactive Medications**
    - Use of vasoactive drugs (Yes/No)
    - Type of drug administered, selected among:
      - Ephedrine
      - Norepinephrine
      - Phenylephrine

Vasoactive agents were documented because they can influence arterial inflow, venous tone, and thermographic signals.

Purpose of Collecting Hemodynamic Variables

These data allow:

- Verification that the patient remained hemodynamically stable across all imaging stages.
- Assessment of whether fluctuations in perfusion patterns could be attributed to systemic rather than flap-specific factors.
- Adjustment or sensitivity analyses, if required, to exclude confounding influences when comparing DIRT and ICG-A.

f. Flap Design and Surgical Details

- **Flap design and Anatomy**
  - **Flap skin paddle size (cm):**
    - Length (long axis of skin island), in centimeters (no decimal).
    - Width (short axis), in centimeters (no decimal).
    - Surface area (cm^2) calculated as length × width; if markedly ellipsoid, also record ellipse estimate ($\pi \cdot a \cdot b/4$) for sensitivity analysis.
  - **Perforator count**: Integer (total number of cutaneous perforators included in the flap).
  - **Perforator type (dominant perforator):** Categorical (septocutaneous / musculocutaneous) per intraoperative finding.
  - **Dissection plane:** Categorical (subfascial / suprafascial / super-thin / ultra-thin / pure skin perforator) per operative note**.**
  - **Pedicle length (cm):** From perforator origin to arterial anastomosis end. No decimal.
  - **Pedicle vessel diameter (mm):** If measured; arterial and venous ends (one decimal), otherwise NA.

- **Ischemia time (minutes)**
    - **Definition:** Time elapsed from pedicle division in the donor site (anterolateral thigh) until reperfusion at the recipient site, defined as the moment when arterial anastomosis is released, and blood flow is reestablished.
    - **Measurement:** Recorded in whole minutes using OR timestamps documented in the surgical report and confirmed by the surgical team.
    - **Important note:** The connection of the second vein does not contribute to ischemia time, since reperfusion is already established once the artery is unclamped.
    - **Units:** minutes (integer).
    - **Source of data:** Intraoperative documentation (SAP–Operating Room/ Anesthetic Record).
    - **Format:** Continuous quantitative variable.

g. Recipient Vessels (arteries and veins)

The recipient vessels used for microvascular anastomosis were recorded as a categorical, structured variable, distinguishing between arterial and venous inflow/outflow sources. All data were extracted from the operative reports registered in the institutional electronic health system (SAP®, Hospital de la Santa Creu i Sant Pau).

- **Arterial Recipient Vessels**

Arteries were classified into five main categories, based on their anatomical origin and frequency of use:

    - **Anterior Tibial Artery (ATA)**
        - Selected when defects were located in the leg, dorsum of the foot, or anterior ankle.

- **Posterior Tibial Artery (PTA)**
    - Frequently used for medial leg, heel, and plantar reconstructions.
    - Offers strong caliber match with ALT pedicles.
- **Peroneal Artery**
    - Typically accessed in lateral leg or deep posterior compartments.
- **Dorsalis Pedis Artery ("Pedia")**
    - Used in distal foot and dorsal defects.
- **"Other" Arterial Variants**
    - Recorded when less conventional vessels were used, including:

a. Superficial Inferior Epigastric Artery (SIEA)
b. Descending Genicular Artery / Saphenous descending artery
c. Popliteal artery
d. Deep Inferior Epigastric Artery (DIEA)
e. Medial plantar artery

- **Venous Recipient Vessels**

  Venous outflow was recorded as a separate categorical variable. Given the importance of venous drainage—and the fact that the study explicitly analyzes perfusion differences between *1 vein vs. 2 veins*—the venous classification was described as follows:

  - **Deep Venous System (Venae Comitantes)**
    - Paired venae comitantes accompanying ATA, PTA, peroneal, or dorsalis pedis arteries.
  - **Superficial Venous System**
    - Great saphenous vein (GSV)
    - Short saphenous vein (SSV)

  These veins were chosen when:

    - Deep veins were unsuitable,

- Additional drainage was required,
- Venous congestion risk was high.

- **Combined Outflow (“Both”)**

  Cases where:

  - One deep vein **plus**
  - One superficial vein

  were anastomosed to provide dual venous drainage.

This category is clinically relevant because in lower-limb free flaps dual venous anastomosis may reduce the risk of venous congestion—part of the rationale for T2 vs. T3 comparisons.

How the Variable Was Recorded

For each case, the recipient vessel field included:

Table 4.2. Recipient vessels

Component	Description	Data Type
Recipient artery	Anterior tibial (ATA), Posterior tibial (PTA), Peroneal, Dorsalis pedis, Other (specify)	Categorical + free text
Recipient veins	Deep venous system / Superficial system / Both / Other (specify)	Categorical + free text
Specific vessel names	Recorded exactly as written in the operative note	Free text

- **Anastomosis Type**

  Arterial Anastomosis

  Arterial anastomoses were classified into three categories:

  - **End-to-end (T–T)**

    Direct connection between the flap artery and a transected recipient artery.

    Rationale:

    - Preferred when the vessel is expendable.
    - Offers laminar flow and familiar handling characteristics.
    - Low turbulence and straightforward monitoring.

  - **End-to-side (T–L)**

    The flap artery is connected to a longitudinal arteriotomy on the side of the recipient artery to preserve distal perfusion.

    Rationale:

    - Maintains downstream arterial flow—important in lower limb reconstruction.
    - Frequently supported in the literature, though some microsurgeons consider it more sensitive to turbulence and external compression compared to T–T.

  - **Flow-through**

    Used when the anatomical branching pattern of the ALT pedicle allowed the flap artery to serve as an interposition graft, restoring arterial continuity while simultaneously perfusing the flap.

    Rationale (surgeon-driven decision):

    - The senior surgeon preferred flow-through whenever anatomically feasible.
    - Based on extensive experience in trauma and sarcoma cases—situations with compromised or previously treated vascular beds.

- Considered a more anatomical and physiological reconstruction:

a. Two end-to-end anastomoses instead of one end-to-side
b. Reduced turbulence
c. Greater tolerance to external compression
d. Preservation of distal run-off for possible future reconstructions (e.g., sarcoma recurrences)
e. Potentially more stable inflow dynamics in irradiated or chemotherapy-altered tissues.

- **Data type:**
  - Categorical (T–T / T–L / Flow-through), with optional free-text specification.

Venous Anastomoses

All venous anastomoses were performed end-to-end, and each flap vein was documented independently (first vein and second vein).

Why two veins instead of one?

While many microsurgical units achieve excellent results with a single venous anastomosis, this surgical team systematically performed two for lower limb reconstruction.

Rationale:

- The lower limb is uniquely susceptible to venous congestion.
- Many included patients had risk factors such as:
  - Trauma-associated venous injury,
  - Post-chemotherapy endothelial fragility,
  - Sequelae of radiotherapy,
  - Peripheral vascular disease.

- A single venous thrombosis can be catastrophic:
  - Exposure of osteosynthesis hardware,
  - Osteomyelitis,

        - Delayed adjuvant therapy in sarcoma patients,
        - Limb-threatening complications.
    - Although not yet strongly supported by evidence, the team's empirical experience is that two veins may:
        - Reduce postoperative edema,
        - Improve drainage dynamics,
        - Facilitate earlier dangling,
        - Provide "physiological redundancy" in a high-risk anatomical region.
    - This philosophy is primarily caution-based, considering the high functional cost of flap failure in the lower limb.
    - **Data type:**
        - Categorical (First vein: T–T / Second vein: T–T)
        - Number of veins used (1 or 2)

Table 4.3. Independent Variables

Variable	Definition / How Obtained	Data Type	Source / Tool
Age (years)	Age at the date of surgery, recorded in whole years (0–100).	Continuous (integer)	EHR (SAP)
Body Mass Index (BMI)	Weight (kg) and height (cm) recorded ≤30 days pre-op. BMI = kg/m² (one decimal).	Continuous	EHR + manual calculation
Smoking Status (Yes/No)	"Yes" = active smoking within 90 days before surgery. "No" = never-smoker or ≥1 year abstinent.	Binary categorical	Clinical interview / EHR
Smoking Intensity (packs/day)	Categorized as <1 pack/day, 1–2 packs/day, >2 packs/day.	Ordinal categorical	Clinical interview
Diabetes Mellitus (DM)	Yes if documented diagnosis OR HbA1c ≥ 6.5% OR fasting glucose ≥126 mg/dL within 6 months.	Binary	EHR (SAP labs)
Peripheral Arterial Disease (PAD)	Yes if ABI <0.9 OR ≥50% stenosis on imaging OR diagnosis registered.	Binary	Vascular studies + EHR
Critical Limb Ischemia (CLI)	Yes if Rutherford 4–6 (pain, ulcer, gangrene), ABI ≤0.4, toe pressure <30 mmHg.	Binary	Vascular studies + EHR
Prior Radiotherapy	Radiotherapy completed ≥4 weeks pre-op.	Binary	Oncology records
Neoadjuvant Chemotherapy	Systemic chemotherapy administered before reconstruction.	Binary	Oncology records

Defect Etiology	Tumoral / Traumatic / Diabetic foot / Other.	Categorical	Operative report + EHR
Defect Location	Inguinal / Thigh / Knee / Leg / Foot.	Categorical	EHR + operative note
Baseline Hemodynamics	SBP/DBP (mmHg), HR (bpm), SpO_2 (%) at start of surgery.	Continuous	Anesthesia chart
Intraoperative Hemodynamics (T1–T3)	ABP, HR, SpO_2 at each perfusion imaging stage.	Continuous	Anesthesia chart
Ambient Temperature	OR temperature (°C) recorded at each timepoint.	Continuous	OR monitoring
Patient Core Temperature	Rectal or esophageal temperature (°C) per anesthesia monitor.	Continuous	Anesthesia monitor
Blood Transfusions	PRBC administered (Yes/No) and number of units.	Binary + integer	Anesthesia record
Vasoactive Drugs	Yes/No; if Yes: norepinephrine / phenylephrine / ephedrine; peak dose and whether running during imaging.	Categorical + free text	Anesthesia chart
Flap Size	Length and width measured in cm; area = L×W (cm^2).	Continuous	Operative note
Perforator Count	Number of perforators included in the flap.	Integer	Operative note
Perforator Type	Septocutaneous / Musculocutaneous.	Categorical	Operative findings
Dissection Plane	Subfascial / Suprafascial / Super-thin / Ultra-thin.	Categorical	Operative note

Pedicle Length	Length in cm (no decimals).	Continuous	Operative note
Recipient Artery	ATA / PTA / Peroneal / Dorsalis pedis / Other (free text).	Categorical + free text	Operative note
Recipient Veins	Deep / Superficial / Both / Other (free text).	Categorical + free text	Operative note
Anastomosis Type (Artery)	End-to-end / End-to-side / Flow-through.	Categorical	Operative note
Anastomosis Type (Vein)	End-to-end (first and second vein).	Categorical	Operative note
Ischemia Time	Minutes from pedicle division to reperfusion.	Continuous	OR timestamps

II. Dependent Variables

The dependent variables comprised all perfusion-related outcomes derived from intraoperative imaging using dynamic infrared thermography (DIRT) and indocyanine green angiography (ICG-A). Variables were defined to capture perfusion at the primary acquisition level (ROI/cm²) and at progressively aggregated anatomical levels (zones and subzones), allowing both high spatial resolution analysis and physiologically meaningful regional interpretation. All dependent variables were extracted from standardized image analyses performed intraoperatively, as detailed below.

a. Primary thermographic variables (ROI/cm² level - DIRT)

Dynamic infrared thermography was analyzed using a standardized grid of **1 cm² regions of interest (ROI/cm²)** applied to the entire flap surface. Each ROI represented the smallest unit of thermographic acquisition and constituted the basis for all subsequent derived variables.

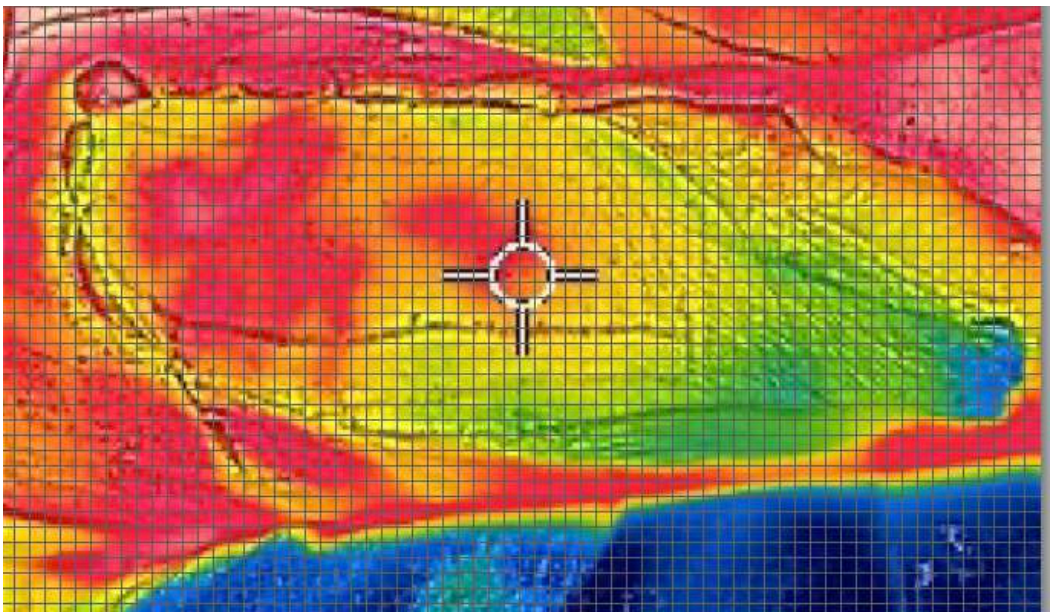


Figure 4.2. ***Dynamic infrared thermography (DIRT) raw image with 1 cm² region-of-interest (ROI) grid.***

Raw intraoperative dynamic infrared thermography image of an anterolateral thigh (ALT) flap during the rewarming phase, displayed with a superimposed 1 cm² grid used for systematic ROI-based data acquisition. This image illustrates the spatial complexity and high density of temperature data collected across the entire flap surface.

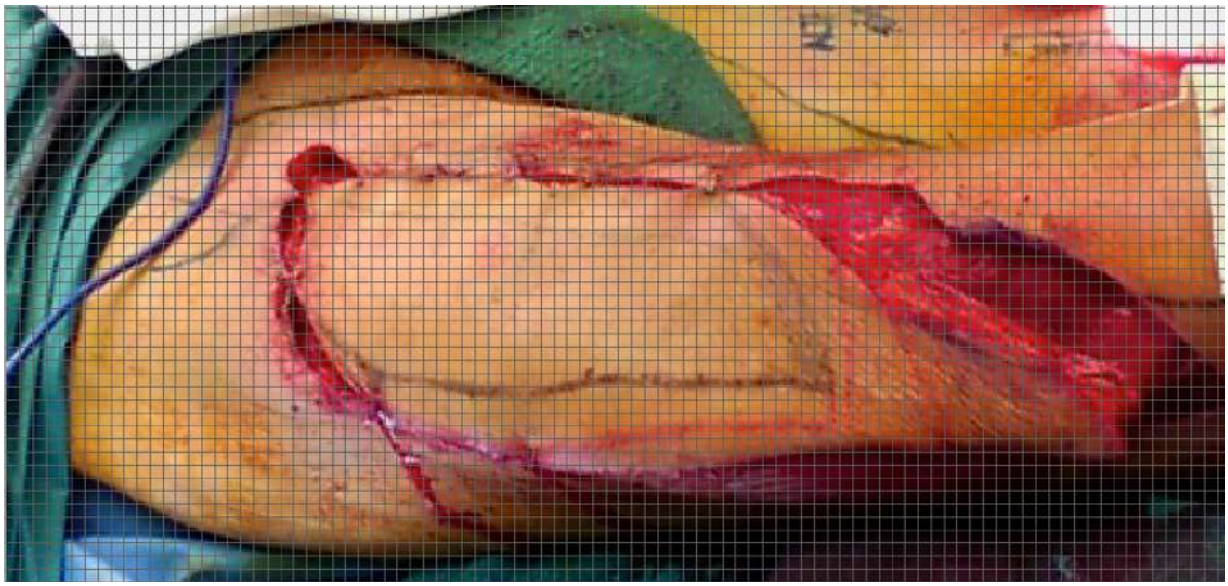


Figure 4.3. ***Clinical reference image of the flap with corresponding 1 cm² ROI grid.*** *Intraoperative clinical photograph of the anterolateral thigh (ALT) flap with a superimposed 1 cm² grid, displayed to provide anatomical orientation and facilitate spatial correlation with the corresponding dynamic infrared thermography image. This reference image allows visual interpretation of flap geometry and surface anatomy prior to thermographic image processing and quantitative analysis.*

For each ROI, the following primary thermographic variables were recorded:

- **Absolute temperature (°C)** - Mean temperature value of each ROI

From ROI-level temperature values, the following **derived continuous variables** were calculated at the flap and zonal levels:

- **Mean flap temperature (°C)**
- **Mean zonal and subzonal temperature (°C)**
- **Temperature standard deviation (SD)** within each flap, reflecting intra-flap thermal heterogeneity
- **Minimum and maximum flap temperatures (°C)**

Data type: Continuous.

b. Thermographic perfusion standardization (DIRT)

Given the substantial interindividual variability in absolute temperature values observed intraoperatively, fixed absolute temperature thresholds (e.g., <25 °C, 25–30 °C, >30 °C) previously described in experimental or postoperative settings were deemed inappropriate for intraoperative flap assessment in this cohort.

Instead, thermographic perfusion was **standardized de novo** using a **patient-specific, distribution-based approach**, anchored to the physiological perfusion profile identified by ICG-A at T1.

For each patient and timepoint, ROI-level temperatures were normalized using the **mean flap temperature ($\bar{T}$)** and **standard deviation (SD)**, and each ROI was classified into one of three ordinal thermographic perfusion categories:

- **2 = well perfused**
- **1 = doubtful perfusion**
- **0 = non-perfused**

Table 4.4. Thermographic perfusion categories after standartization

Thermographic category	Temperature criterion	Expected proportion (%)
Well perfused	$T \geq (\bar{T} - 1\ SD)$	≈ 68%
Doubtful perfusion	$(\bar{T} - 2\ SD) \leq T < (\bar{T} - 1\ SD)$	≈ 27%
Non-perfused	$T < (\bar{T} - 2\ SD)$	≈ 5%

This transformation yielded ordinal thermographic perfusion scores for each ROI/cm² and enabled calculation of:

- **Percentage of well-perfused surface (%)**
- **Percentage of doubtful perfusion (%)**
- **Percentage of non-perfused surface (%)**

at flap, zonal, and subzonal levels.

- **Data type:** Ordinal (0–1–2) and derived percentages (%).

c. ICG-A perfusion variables (reference standard at T1)

Indocyanine green angiography was performed exclusively at **T1**, under physiological baseline conditions, and served as the **reference standard** for perfusion assessment.

Using the same 1 cm² region-of-interest (ROI) grid applied to thermographic images, each ROI was assigned an ordinal ICG-A perfusion score based on fluorescence intensity:

- **0 = non-perfused** (absent fluorescence)
- **1 = intermediate perfusion** (gray zone)
- **2 = well-perfused** (bright fluorescence)



Figure 4.4. ***Indocyanine green angiography (ICG-A) raw image with 1 cm² region-of-interest (ROI) grid.***

Raw intraoperative indocyanine green angiography image of an anterolateral thigh (ALT) flap displayed with a superimposed 1 cm² grid for systematic ROI-based perfusion data acquisition. This ICG-A image illustrates the spatial complexity and high density of perfusion information collected across the flap surface.

From these ROI-level scores, the following variables were derived:

- **Zonal and subzonal ICG perfusion scores (mean and percentage distribution)**
- **Global flap perfusion profile (% well-perfused, doubtful, non-perfused)**

The quantitative perfusion distribution obtained with ICG-A at T1 was used to define the **physiological reference perfusion pattern**, which subsequently informed thermographic standardization and comparative analyses.

Data type: Ordinal (0–1–2) and derived percentages (%).

d. Zonal and subzonal perfusion variables (DIRT and ICG-A)

To assess spatial perfusion gradients, the flap was longitudinally divided into four anatomical zones of equal length, centered around the dominant perforator (zones 1–4).

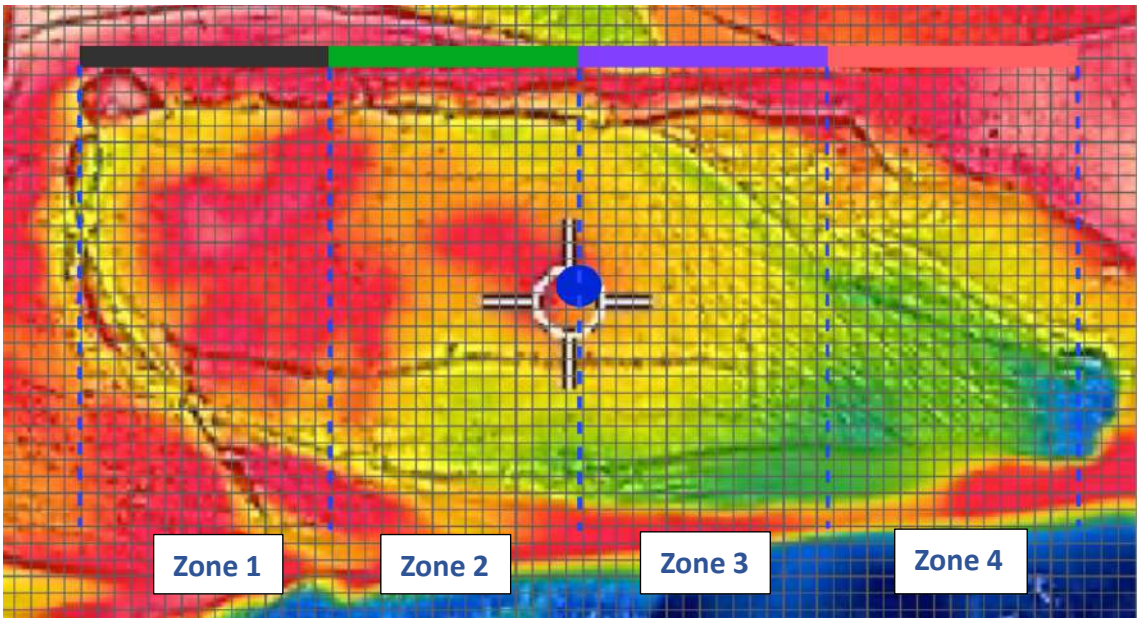


Figure 4.5. ***Schematic longitudinal division of the flap into four analytical zones.***
Schematic representation of the anterolateral thigh (ALT) flap showing longitudinal division into four zones (zones 1–4) based on the main axis of the thigh. The longitudinal axis follows the long axis of the lower limb, and total flap length was divided into four equal segments. The central blue point indicates the typical location of the dominant perforator. This zonal subdivision was used for systematic perfusion analysis across the flap surface.

For each zone, ROI-level data were aggregated to derive:

- Mean thermographic temperature (°C)
- Mean standardized thermographic perfusion category (0–2)
- Percentage distribution of perfusion categories
- Mean ICG-A perfusion score (T1 only)

To further refine analysis of marginal territories, the most peripheral zones were subdivided into subzones:

- **Zone 1a / 1b** (proximal end, relative to the perforator)
- **Zone 4a / 4b** (distal end, highest risk of hypoperfusion)

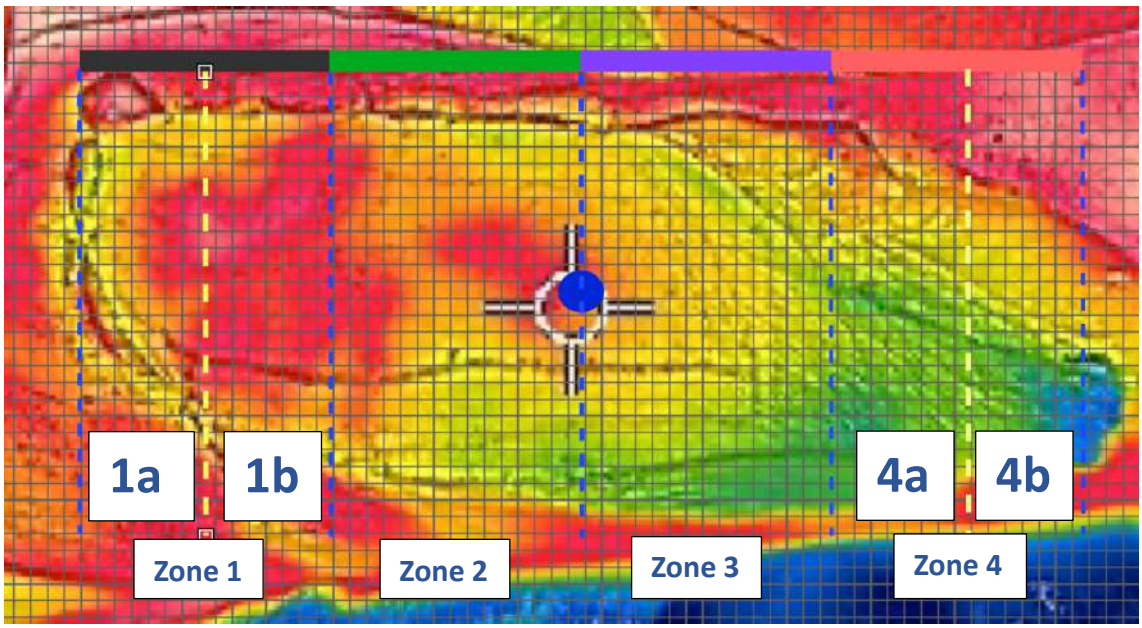


Figure 4.6. ***Subzonal longitudinal division of distal flap regions.***
Schematic representation of the anterolateral thigh (ALT) flap illustrating additional subzonal division of the distal regions. A dashed yellow line subdivides zone 1 and zone 4 into two subzones (1a/1b and 4a/4b, respectively). This secondary longitudinal subdivision was introduced to enhance spatial resolution in the distal flap areas, which are theoretically more susceptible to hypoperfusion and represent regions of primary interest for perfusion analysis in this study.

This subzonal approach enabled detailed evaluation of perfusion heterogeneity and detection of subtle marginal ischemia not apparent at the whole-flap or zonal level.

Data type: Mixed continuous (temperature), ordinal (0–2), and percentage (%)

e. Concordance and association variables between DIRT and ICG-A

Concordance between imaging modalities was assessed **exclusively at T1**, the only timepoint at which both ICG-A and thermography were performed. It was evaluated using **aggregated ROI/cm² data**, allowing physiologically meaningful comparison at multiple anatomical scales:

- **Zonal and subzonal agreement** in perfusion classification
- **Correlation between thermographic and ICG-derived regional and global perfusion metrics**
- Association between distal hypoperfusion and global perfusion status

Concordance analysis focused on **regional perfusion distributions and spatial gradients**, consistent with the study's objective of assessing physiological equivalence rather than exact numerical identity between modalities.

Data type: Correlation coefficients, ordinal agreement, and derived percentages.

Summary of dependent variables

In summary, dependent variables were structured hierarchically, with ROI/cm² serving as the primary acquisition unit, from which continuous thermographic measures, standardized categorical perfusion scores, and aggregated zonal and subzonal variables were derived. ICG-A variables at T1 provided the physiological reference framework for thermographic standardization and comparative analysis, enabling robust assessment of spatial perfusion patterns and modality concordance.

Table 4.5. Dependent Variables

Variable	Definition / How Obtained	Data Type
Mean ROI Temperature	Mean temperature per 1 cm² ROI from DIRT grid.	Continuous
Min/Max Temperature	Lowest and highest ROI temperature	Continuous
Mean flap temperature (°C)	Average of all ROI/cm² temperature values across the entire flap surface.	Continuous
Mean zonal / subzonal temperature (°C)	Average ROI/cm² temperature calculated for each anatomical zone (1–4) and subzone (1a/1b, 4a/4b).	Continuous
Thermal heterogeneity (SD)	Standard deviation of ROI/cm² temperatures within the flap, representing intra-flap thermal dispersion.	Continuous
Temperature Perfusion Score (Standardized)	2 = well perfused ($T \geq \bar{T} - 1$ SD) 1 = doubtful perfusion ($\bar{T} - 2$ SD $\leq T < \bar{T} - 1$ SD) 0 = non-perfused ($T < \bar{T} - 2$ SD)	Ordinal categorical (0–1–2)
Thermographic perfusion distribution (%)	Percentage of ROI/cm² classified as well perfused, doubtful, or non-perfused at flap, zonal, and subzonal levels.	Percentage (%)
ICG Perfusion Score (ROI)	0 = black (no perfusion), 1 = gray (doubtful), 2 = white (good perfusion).	Ordinal categorical
ICG-A perfusion distribution (%)	% distribution of well-perfused, doubtful, and non-perfused ROI/cm² at flap, zonal, and subzonal levels (T1)	Percentage (%)
Zonal Perfusion (1–4)	Aggregated thermographic and ICG-A perfusion metrics calculated for each anatomical zone, allowing assessment of central-to-peripheral gradients.	Continuous + ordinal
Subzone Perfusion (1a/1b, 4a/4b)	Distal/proximal extensions analyzed separately to detect marginal hypoperfusion	Continuous + ordinal
DIRT–ICG concordance metrics (T1)	Correlation and agreement between regional and global perfusion metrics derived from standardized thermography and ICG-A at baseline.	Correlation coefficients / % agreement

4.5 Surgical Technique and ALT Flap Elevation

The surgical technique for anterolateral thigh (ALT) flap elevation was conducted following a standardized protocol to minimize interprocedural variability and ensure homogeneity in the perfusion assessments performed with ICG-A and DIRT. All procedures were performed by the same microsurgical team, using preoperative imaging, intraoperative navigation, and structured steps for flap design, elevation, pedicle dissection, and recipient-site preparation.

I. Preoperative Planning and Perforator Localization

a. CT Angiography–Based Perforator Mapping

All ALT flaps were planned using preoperative multidetector computed tomographic angiography (MDCT), routinely performed from the umbilicus to the feet. Perforator mapping was not delegated to radiology; instead, the surgical team directly reviewed the axial, coronal, sagittal, and 3D reconstructions to identify suitable perforators.

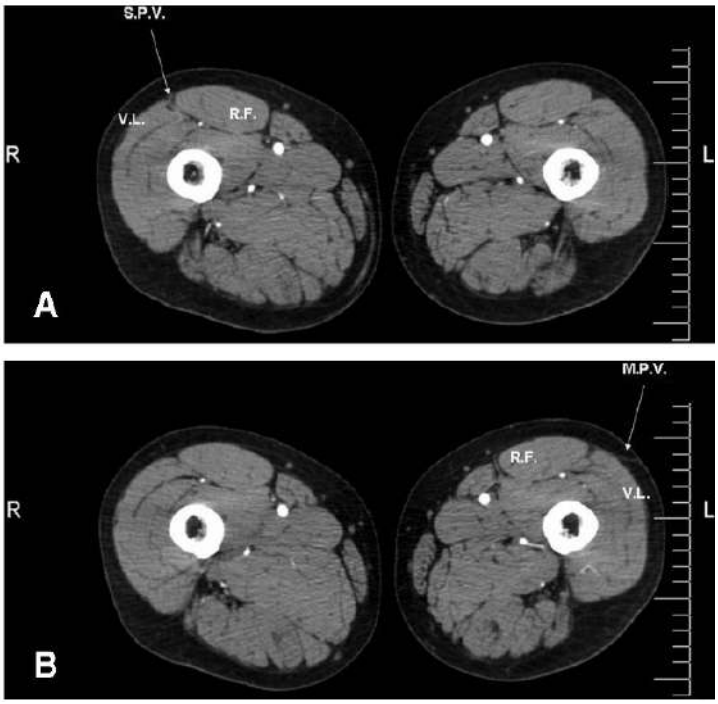


Figure 4.7. ***Preoperative perforator mapping of the anterolateral thigh (ALT) flap using multidetector computed tomography angiography (MDCT-A).***

(A) Right thigh showing a septocutaneous perforator vessel (SPV) arising between the vastus lateralis (VL) and rectus femoris (RF) muscles (arrow).

(B) Left thigh demonstrating a musculocutaneous perforator vessel (MPV) coursing through the vastus lateralis muscle.

Following established anatomical landmarks, the line between the **anterior superior iliac spine (ASIS)** and the **superolateral patellar border** was used to identify the intermuscular septum between the rectus femoris and vastus lateralis. For each perforator, the horizontal (x-axis) and vertical (y-axis) coordinates corresponding to fascial penetration were measured and documented. These coordinates were transferred to the patient's skin intraoperatively.

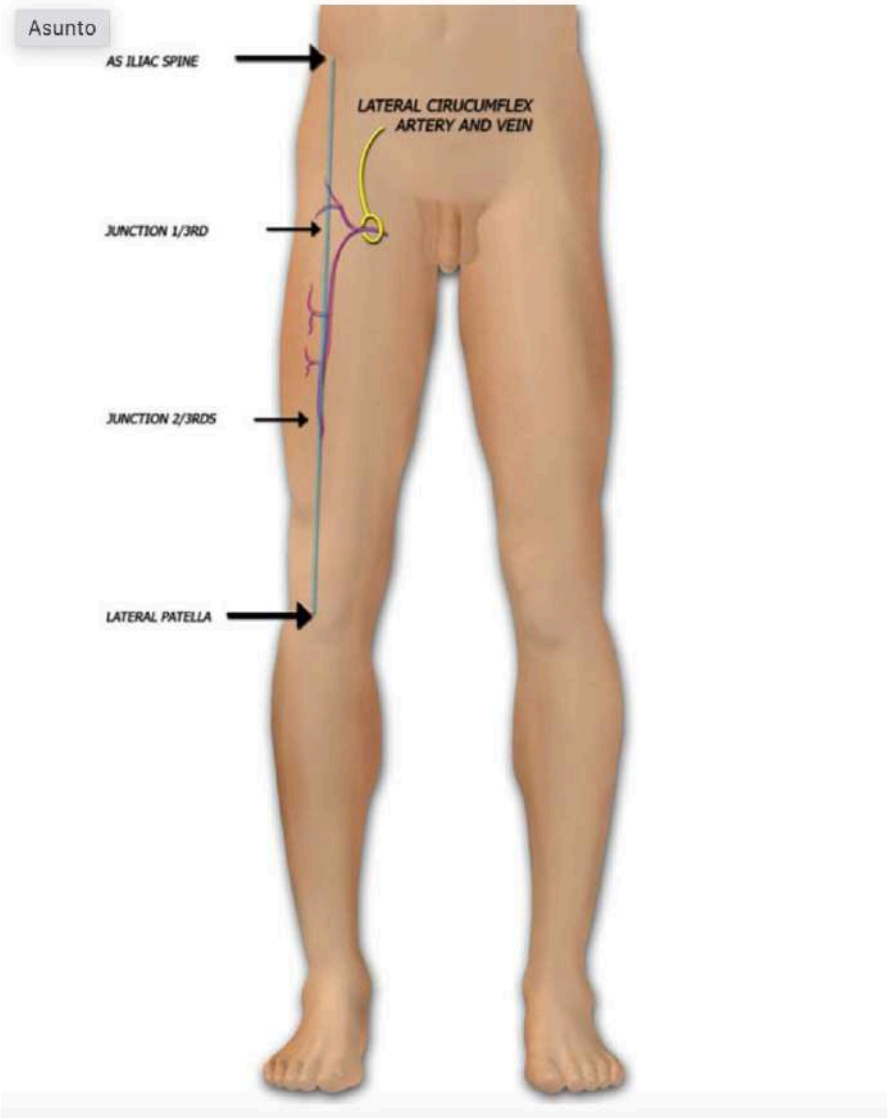


Figure 4.8. ***Schematic surface landmarks for planning of the anterolateral thigh (ALT) flap.***
Schematic illustration showing surface landmarks used for ALT flap planning, including the anterior superior iliac spine (ASIS), lateral patella, and the line connecting both landmarks, corresponding to the projected intermuscular septum between the rectus femoris and vastus lateralis muscles.

b. Handheld Doppler and Color Doppler Ultrasound

After marking the projected coordinates on the thigh, perforators were confirmed using handheld Doppler. When plane selection required precision—especially for *superthin* or *ultrathin* flaps—high-resolution color ultrasound was used to trace the perforator from its intramuscular or septocutaneous course up to:

1. **Deep fascia perforation**, and
2. **Superficial fascia perforation**.

Both points were marked on the skin.

To simplify flap design while maximizing perfusion reliability:

- A **3-cm diameter circle** was drawn around the deep fascial perforator point.
- If the superficial perforation point fell outside this circle, the radius was expanded directionally to ensure at least 1.5 cm of clearance beyond both perforation points.

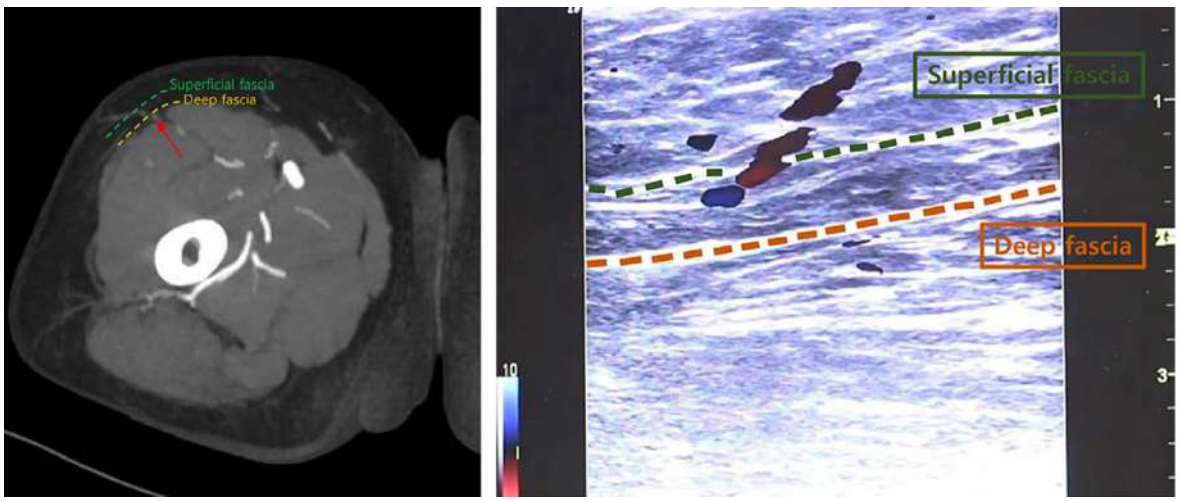


Figure 4.9. ***Multimodal imaging of ALT perforator course through the fascial planes.***
Left image: *axial multidetector computed tomography angiography (MDCT-A) of the thigh demonstrating an ALT perforator traversing the deep fascia and continuing through the superficial fascia toward the skin.*
Right image: *corresponding intraoperative ultrasound image illustrating the same perforator course, with clear visualization of its passage through the deep and superficial fascial layers. Ultrasound assessment was used to evaluate perforator trajectory and fascial penetration, particularly relevant during flap thinning procedures*

II. Flap Design and Skin Island Planning

The recipient-site defect was measured after orthopedic or ablative surgery. The ALT flap was then designed **2 cm longer and 2 cm wider** than the defect to allow for tension-free inset.

The skin paddle followed a **vertical, fusiform "huso" configuration**, centered over the dominant perforator whenever anatomy permitted. This ensured predictable axial perfusion and consistent alignment for later zonal and grid-based analyses.

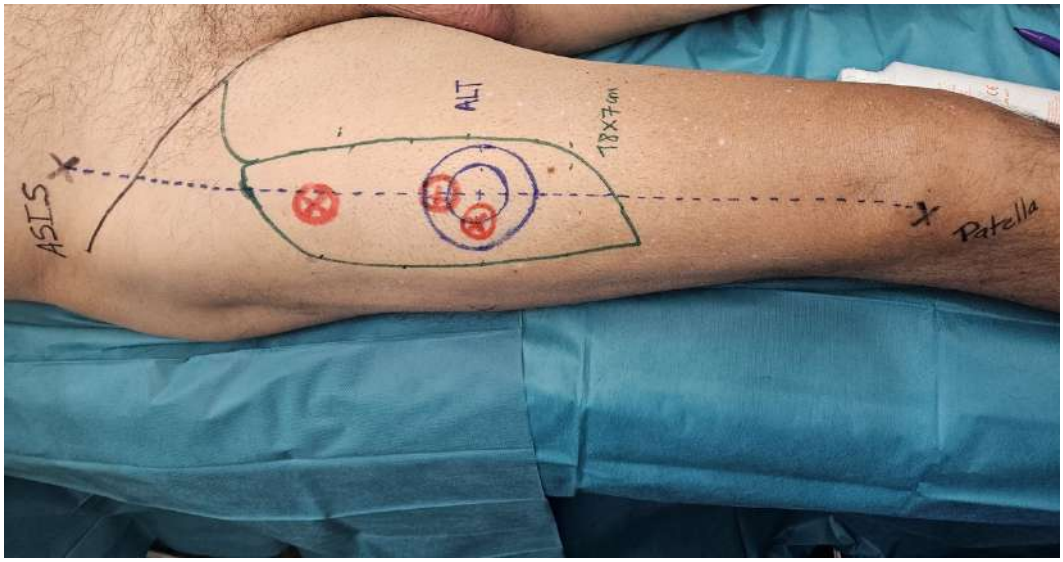


Figure 4.10. ***Clinical marking of the anterolateral thigh (ALT) flap.***
Intraoperative photograph demonstrating ALT flap surface marking following anatomical landmarks. The ASIS–patella line is drawn, the midpoint is identified, and a 3-cm radius circle is marked. Perforator locations (red circles with central cross) are plotted according to preoperative imaging coordinates and subsequently confirmed intraoperatively with handheld doppler and color ultrasound. Final flap design is tailored to the size and requirements of the defect to be reconstructed.

III. Initial Elevation Technique and Pedicle Dissection

After marking, the skin incision was made with a cold scalpel, followed by elevation using monopolar electrocautery (35 W, cut mode; 35 W coagulation for hemostasis). The flap was elevated **from medial to lateral**, reaching the perforator early and allowing controlled retrograde dissection.

Once the perforator was visualized, it was dissected retrograde to its origin. In most cases, the dominant vessel followed the **descending branch of the lateral circumflex femoral artery (LCFA-DB)**.

The dissection continued proximally to maximize pedicle length and diameter, often exposing the:

- LCFA descending branch
- Circumflex femoral system
- Branching points of the transverse or ascending branches

Flow-Through Consideration

When anatomy provided a suitable branch, the pedicle was preserved to allow **flow-through arterial reconstruction**.

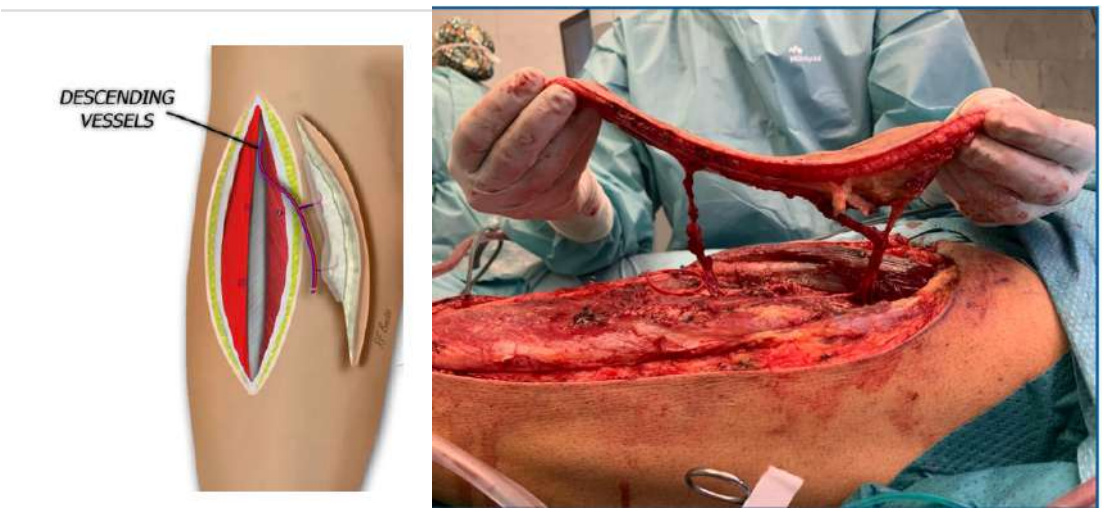


Figure 4.11. ***Anterolateral thigh (ALT) flap dissected attached at donor site***
Left image: *schematic representation of an ALT flap showing the dissected skin paddle and vascular pedicle at the donor site.*
Right image: *intraoperative photograph of an ALT flap at the donor site with two identified perforators, including a single perforator and a convergent "Y-shaped" configuration, in which two perforators join before entering the main pedicle.*

IV. Plane of Elevation and Thickness Selection

Plane selection (subfascial, suprafascial, superthin, ultrathin) was individualized according to:

- Recipient-site contour requirements
- Donor-site adiposity
- Patient comorbidities (e.g., smoking, vasculopathy, diabetes)

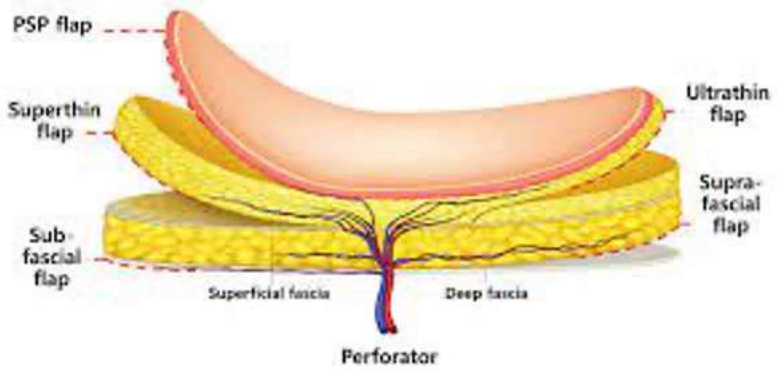


Figure 4.12. ***Schematic representation of different elevation planes in the anterolateral thigh (ALT) flap.***
Diagram illustrating the various planes of ALT flap elevation, including subfascial, suprafascial, superthin, ultrathin, and pure-skin-perforator flap designs. The relationship between the perforator vessel, deep fascia, superficial fascia, and overlying skin and subcutaneous tissue is depicted, highlighting the anatomical basis for flap thinning and plane selection.

a. Principles Guiding Plane Selection

- **Subfascial elevation** was preferred in high-risk patients—heavy smokers, vascular disease, uncontrolled diabetes—to preserve maximal vascular reliability.
- **Suprafascial plane** was chosen when moderate thinning was beneficial for contouring.
- **Superthin / ultrathin flaps** were reserved for selected patients with favorable comorbidity profiles and defects requiring minimal bulk (e.g., ankle or dorsum of foot).

b. Preservation of the "Hot Zone"

When superthin or ultrathin elevation was indicated, a **3-cm radius centered on the perforator** was always delineated as the **hot zone**.

This region represents the *primary vascular hub* of the ALT flap, where the perforator exits the deep fascia and forms its earliest branching network.

Because this microvascular tree is highly sensitive to:

- Thermal injury
- Traction
- Excessive manipulation

no thinning was performed within the hot zone.

Thus:

- In **superthin/ultrathin** dissections, the remainder of the skin paddle was thinned above the superficial fascia, but the hot zone was preserved **subfascially or suprafascially** to protect early perforator branches and ensure reliable perfusion to peripheral zones.
- In **subfascial or suprafascial flaps**, no additional thinning was required; therefore, a hot zone did not need to be explicitly marked, as the perforator anatomy was inherently safeguarded by the chosen plane.

c. Skin island thinning elevation (superthin / ultrathin harvest)

When the flap was intentionally thinned (superthin or ultrathin technique), the elevation of the skin island was performed with special attention to minimizing thermal injury and mechanical stress on the superficial vascular plexuses:

- **Dissection was carried out above the superficial fascia using monopolar electrocautery in cutting mode (25 W)**. This setting reduces lateral thermal spread compared with coagulation mode, thereby protecting the subdermal and subcutaneous plexuses that supply distal flap territories.
- **Selective hemostasis was performed with bipolar cautery**, avoiding unnecessary coagulation points that could compromise microcirculation in the thinning plane.

- **Gentle handling of the skin island was strictly maintained**. Throughout elevation and thinning, the flap was supported with broad, atraumatic contact (e.g., using fingers or large forceps pads), avoiding focal pressure points that could distort microvascular flow or bruise the delicate dermal plexus.

These technical refinements were particularly important because **perfusion of distal flap zones depends heavily on the integrity of the superficial vascular plexuses**, especially once the deep fascia is not included. Preserving these networks is essential to avoid compromising the distal "tips" of the flap, where ischemia risk is highest.

V. Recipient Site Preparation and Vessel Selection

Preparation of the recipient site followed a structured, reproducible approach aimed at ensuring optimal vascular conditions for microvascular anastomosis. In most cases—particularly defects of the *leg, ankle, and foot*—recipient vessel dissection was performed under tourniquet control, as this facilitated identification of anatomical landmarks, reduced venous oozing, and improved visualization of the vascular pedicles. Tourniquet use was avoided only when the ALT flap was harvested from the ipsilateral limb, or in select cases where limb perfusion could not be safely interrupted. Total ischemia time was kept below 120 minutes in all cases.

a. Preoperative Localization

Recipient vessels were planned preoperatively using a combination of:

- Multidetector CT angiography (MDCT) to evaluate the condition and suitability of potential recipient vessels. The study team assessed the **patency**, **course**, and **approximate height** at which the anterior tibial, posterior tibial, peroneal, or dorsalis pedis arteries could be safely found during dissection. The MDCT provided essential information in cases of **trauma**, **sarcoma**, or **peripheral vasculopathy**, helping to identify segments where vessels remained intact and free from injury, fibrosis, or anatomical distortion.

- Handheld Doppler, used for bedside confirmation of pulsatility and approximate surface projection.
- Color Doppler ultrasonography, performed intraoperatively to verify vessel patency, caliber, and precise depth.

This step was particularly valuable in patients with peripheral arterial disease, post-traumatic vascular alterations, or sarcoma resections, where vessels may be occluded, displaced, or encased in fibrotic tissue.

b. Vessel Exposure

Dissection proceeded using loupe magnification and fine bipolar coagulation to avoid thermal injury. The vessels were mobilized with adequate length for tension-free anastomosis, while preserving adjacent branches whenever possible. Special attention was given to preventing kinking of the artery or veins once the flap was inset.

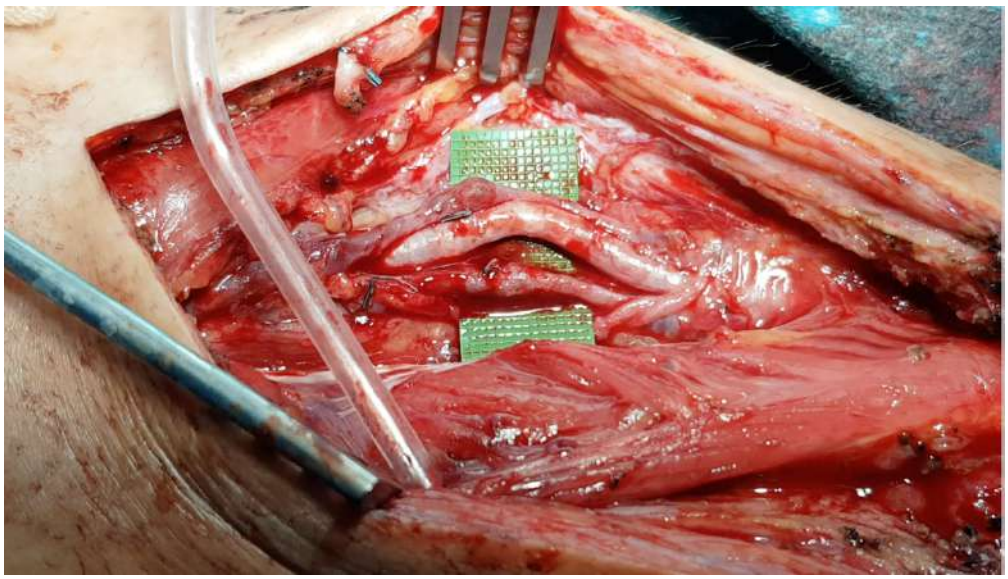


Figure 4.13. ***Intraoperative appearance of recipient vessels prior to microvascular anastomosis.***

Intraoperative view of the dissected recipient vessels, showing the artery centrally located with a lighter appearance and two accompanying veins positioned laterally with a darker coloration. A green background is placed beneath the vessels to enhance contrast and facilitate visual identification during subsequent microvascular anastomosis.

c. “Tips and Tricks” routinely applied

To standardize recipient site preparation and minimize complications:

- Pre-incision ultrasonography was used to confirm patency before committing to a recipient site.
- Two venous options (deep system and superficial system) were identified whenever feasible, to allow intraoperative choice based on caliber and flow characteristics.
- In cases with hardware (plates, nails) or after sarcoma resections, dissection proceeded from healthy tissue toward scarred tissue, reducing the risk of vessel damage.
- When the MDCT suggested poor vessel quality at the expected site, the team extended the dissection proximally or distally to locate a suitable segment.
- Once exposed, vessels were irrigated and wrapped in moist gauze while the flap team completed pedicle preparation.

d. Tourniquet Release and Final Assessment

Before performing the anastomoses, the tourniquet was released and vessel quality reassessed, ensuring:

- good arterial pulsatility,
- adequate venous outflow,
- absence of segmental spasm,
- and sufficient length for flap positioning without torsion.

Only after confirming satisfactory vascular conditions was the flap transferred and the first microvascular anastomosis performed.

VI. Anastomoses and Inset

a. Arterial Anastomosis

Three configurations were used:

- **End-to-end (T–T)**
- **End-to-side (T–L)**
- **Flow-through** (when anatomically feasible)

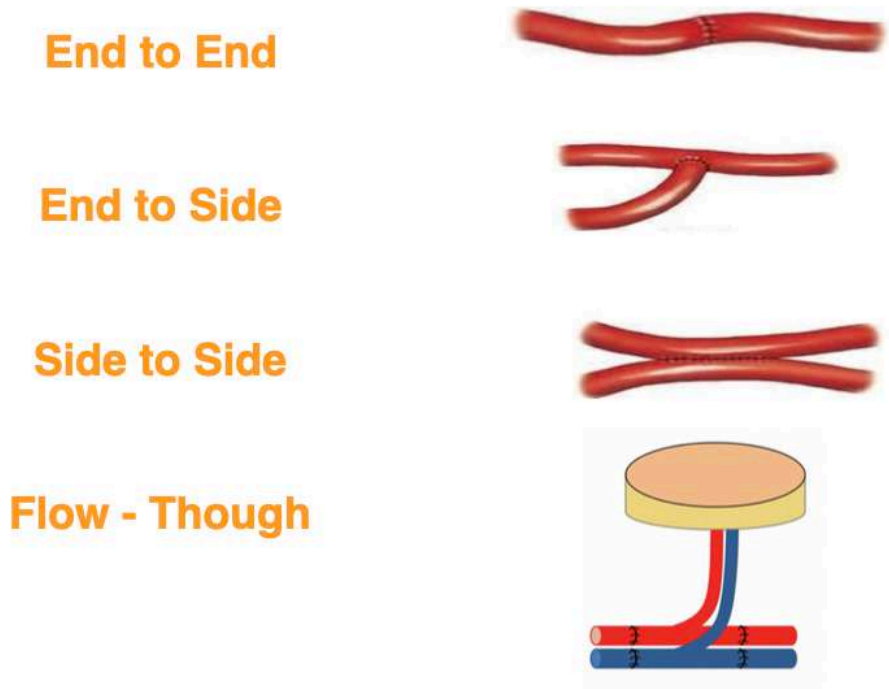


Figure 4.14. ***Schematic representation of microvascular anastomosis techniques.***
Diagram illustrating different microvascular anastomosis configurations, including end-to-end, end-to-side, side-to-side, and flow-through techniques. In the present study, end-to-end, end-to-side, and flow-through anastomoses were used, whereas the side-to-side configuration is shown for illustrative purposes only.

b. Venous Anastomoses

All veins were anastomosed **end-to-end**, with most cases receiving **two venous anastomoses** to reduce the risk of congestion in a limb known for poor venous reserve.

VII. Donor and Recipient Site Closure

Donor Site

- Hemostasis with monopolar coagulation
- Placement of **two No. 12 suction drains**, secured with 2/0 silk
- Layered closure using Vicryl 2/0, Vicryl 3/0, and Monocryl 3/0



Figure 4.15. ***Donor-site closure after anterolateral thigh (ALT) flap harvest.***
Intraoperative view of the donor site demonstrating primary closure without the need for skin grafting. A suction drain is placed prior to definitive closure. This image illustrates that, despite harvesting a large skin paddle, direct closure of the donor site is achievable in the majority of cases.

Recipient Site

- Flap inset ensuring no torsion or kinking of pedicle
- Penrose drains placed strategically
- Application of postoperative NIRS monitoring (INVOS™ — not part of study metrics but standard protocol)
- Protective dressings (Linitul, Betadine gel, gauze, Velban, crepe), avoiding pressure on flap edges



Figure 4.16. ***Recipient-site reconstruction with an anterolateral thigh (ALT) flap.***
Left image: *soft-tissue defect in the distal third of the left leg with exposed bone prior to reconstruction.*
Right image: *immediate postoperative view following ALT flap transfer, showing the flap inset and adapted to the defect after microvascular anastomosis, with Penrose drains in place.*

VIII. Postoperative Management

Standard postoperative management—extremity elevation for 7–10 days and progressive dangling protocol—ensured homogeneous care across the cohort.

4.6 Imaging Protocols

I. Indocyanine Green Angiography (ICG-A)

ICG-A was performed using the Fluobeam® 800 imaging system (Fluoptics, Grenoble, France). A single vial of indocyanine green (ICG) (25 mg) was diluted in 10 mL of sterile saline and administered intravenously as a 2.5 mL bolus at T1 timepoint. Image acquisition began immediately after injection and continued until the entire flap was adequately filled with fluorescence, typically lasting around 1 minute to allow for complete perfusion. The imaging camera was held perpendicular to the flap surface at a standardized distance of 20 cm, under ambient operating room lighting. Once maximal fluorescence was achieved, a still image capturing the entire skin paddle was obtained for subsequent analysis (T1 only).

II. Dynamic Infrared Thermography (DIRT)

DIRT was performed using the FLIR E6 Pro camera (Teledyne FLIR Systems, USA), which includes its own integrated display and recording system. Ambient operating room temperature was maintained between 21 °C and 22 °C, and patient core temperature was kept within the normal physiological range of 35.5 °C to 37.0 °C. A standardized cold challenge was applied by placing a sterile gauze soaked in saline at 20 °C on the flap surface for 1 minute. Immediately after gauze removal, a thermal image was acquired to verify that the entire skin paddle had cooled uniformly at 20 °C; this initial image was used solely to confirm effective cooling and was not included in the perfusion analysis. Ten minutes after the cold challenge, a second thermographic image was taken to assess perfusion recovery. Only this delayed image was used for subsequent evaluation. All thermal recordings were performed at a fixed distance of 20 cm and perpendicular to the flap surface. The entire procedure was repeated at each of the three predefined intraoperative timepoints (T1, T2 and T3).

4.7 Standardization of Image Acquisition

Flap images were digitally aligned and corrected for size and orientation to ensure spatial comparability across modalities and timepoints. The anatomical borders of the cutaneous island were manually traced and verified by the operating surgeon based on intraoperative markings and suture references.

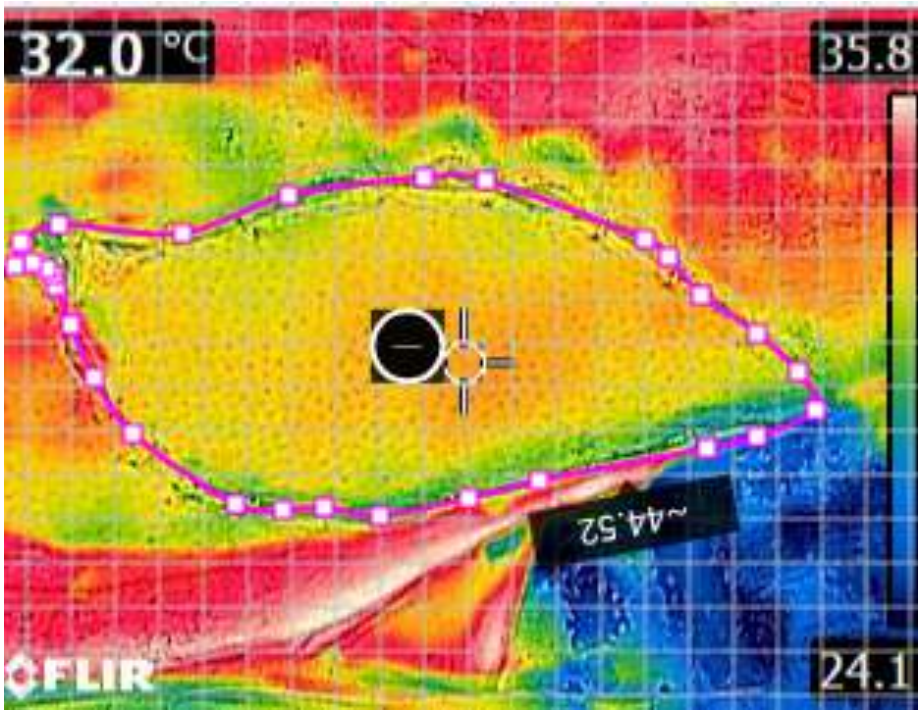


Figure 4.17. ***Standardization of flap image alignment***
Example of a thermographic image imported into a digital measurement environment illustrating manual alignment, scaling, and orientation correction. The cutaneous island borders were manually delineated ensuring spatial consistency across imaging modalities and timepoints. Delineation was performed based on intraoperative markings and verified by the operating surgeon.

4.8 Image Analysis and Framework

I. ROI Grid Analysis 1 cm² Grid Resolution

To increase objectivity and spatial reproducibility, each flap image was overlaid with a grid of 1 cm² squares, generating a matrix of contiguous regions of interest (ROIs). The grid was applied equally to both ICG-A and DIRT images. For each ROI:

- **Thermographic data** were extracted at the pixel level using FLIR Tools®, yielding a representative temperature value used for subsequent intra-flap standardization and spatial analysis.
- **ICG-A data** were classified according to fluorescence intensity using an ordinal perfusion score:
    - 0 = non-perfused (absent fluorescence - black),
    - 1 = intermediate (gray zone)
    - 2 = well-perfused (bright fluorescence - white).

ROI-level values constituted the primary spatial units for all subsequent zonal, subzonal, and compositional analyses.

II. Zonal Perfusion Analysis (Zonas 1-4)

In addition to the 1 cm² grid segmentation, the flap was longitudinally divided into **four perfusion zones of equal length**, using the perforator as the mid-point reference:

- **Zone 1** – proximal extreme
- **Zone 2** – proximal-central (perforator-adjacent territory)
- **Zone 3** – distal-central (perforator-adjacent territory)
- **Zone 4** – distal extreme

This zonal model reflects perforasome theory and the progressive decline in perfusion away from the dominant perforator. While historically only the distal extreme (Zone 4) has been described as highest risk for ischemia—especially in fasciocutaneous/subfascial

ALT flaps—clinical experience with **thin, suprafascial, and pure perforator flaps** shows that both extremes (proximal and distal) behave as watershed territories.

For each zone, ROI-level data were aggregated to describe the spatial distribution of thermographic and angiographic perfusion categories and to enable zone-based comparative analyses.

III. Subzone Analysis (1a–1b and 4a–4b)

To increase sensitivity for detecting small ischemic segments—which can lead to flap failure in lower-limb reconstruction—even when overall perfusion appears acceptable, **both flap extremities** were further subdivided:

- **Zone 1a (proximal-tip) / Zone 1b (proximal-mid)**
- **Zone 4a (distal-mid) / Zone 4b (distal tip)**

Subzones were analysed independently based on the distribution and proportion of ROI-level thermographic values and ICG-A perfusion categories.

This refinement acknowledges that in contemporary perforator-based ALT thinning, ischemia may occur at either extremity, particularly when suprafascial dissection reduces choke-vessel connectivity. In this context, loss of even a single 1 cm^2 unit in zones 1a or 4b may expose critical structures and constitute a clinically relevant perfusion deficit.

4.9 Software and Analytical Workflow

Digital image analysis in this study was performed using **FLIR Tools® (Teledyne FLIR Systems, USA)** and a basic 2D graphic editor (**Microsoft Paint**). Each software fulfilled a specific, well-defined role within the analytical workflow, enabling objective thermographic data extraction, standardized spatial segmentation, and reproducible comparison between imaging modalities.

This workflow supported perfusion assessment at the **ROI/cm² level**, as well as at **zonal and subzonal anatomical levels**, and formed the basis for all quantitative analyses presented in the Results section.

I. FLIR Tools® (Teledyne FLIR Systems, USA)

FLIR Tools® is a dedicated thermographic analysis platform that allows extraction of **true numerical temperature values** from radiometric thermal images. Its use ensured that all thermographic measurements were objective, reproducible, and independent of subjective visual interpretation of color scales.

Workflow and Functionality

1. Importing Thermal Images

DIRT images acquired at each intraoperative stage (T1, T2, T3) were exported from the FLIR E6 Pro camera and imported into FLIR Tools® in their native radiometric format (.jpg with embedded temperature metadata). This format preserves pixel-by-pixel temperature data.

2. Application of the 1 cm² ROI Grid

Although the grid was conceptualized externally, the thermal measurements per ROI were extracted using FLIR Tools® as follows:

- A 1 cm² grid was superimposed manually over the flap image.
- Each ROI was drawn to correspond exactly to one cell of the predefined grid used in the study.

- FLIR Tools® automatically calculated:
    - Mean temperature (°C)
    - Minimum and maximum temperature (°C)

3. ROI-level temperature extraction

For each ROI, FLIR Tools® provided temperature values by sampling all pixels within that region. This allowed:

- Objective quantification of perfusion
- Avoidance of color-scale misinterpretation
- Standardization across timepoints and patients

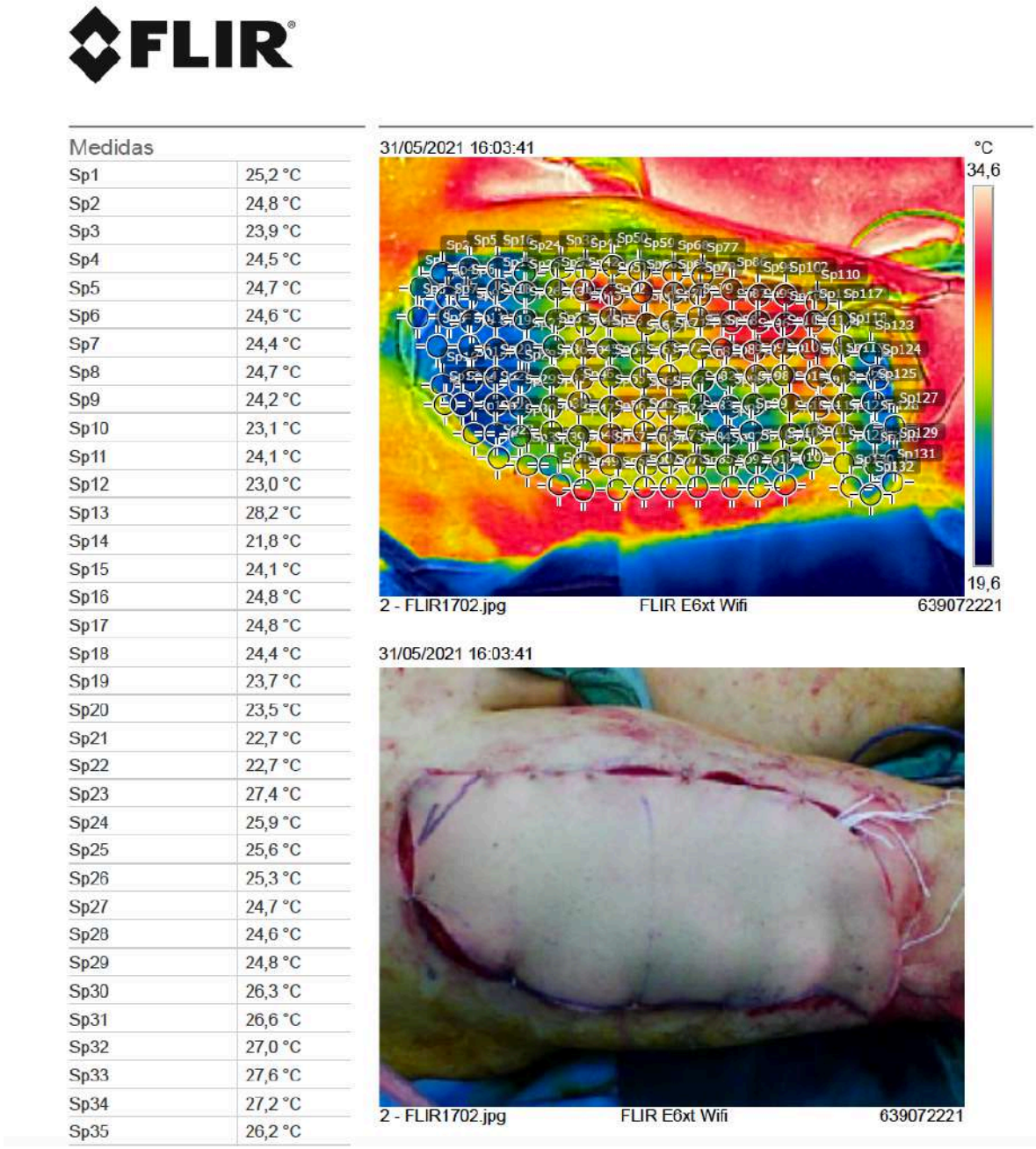
DIRT temperature data for each ROI were exported and entered into the Excel database used for statistical analysis.

4. Derivation of thermographic perfusion metrics

From ROI-level temperature values, the following variables were derived:

- Mean flap temperature
- Mean zonal and subzonal temperatures
- Temperature standard deviation (SD) as a measure of intra-flap thermal heterogeneity
- Minimum and maximum flap temperatures

In addition, ROI-level temperatures were subsequently normalized using patient-specific mean temperature and standard deviation to generate **standardized thermographic perfusion categories (0–1–2)**, as described in Section X (Thermographic standardization).



Medidas	
Sp1	25,2 °C
Sp2	24,8 °C
Sp3	23,9 °C
Sp4	24,5 °C
Sp5	24,7 °C
Sp6	24,6 °C
Sp7	24,4 °C
Sp8	24,7 °C
Sp9	24,2 °C
Sp10	23,1 °C
Sp11	24,1 °C
Sp12	23,0 °C
Sp13	28,2 °C
Sp14	21,8 °C
Sp15	24,1 °C
Sp16	24,8 °C
Sp17	24,8 °C
Sp18	24,4 °C
Sp19	23,7 °C
Sp20	23,5 °C
Sp21	22,7 °C
Sp22	22,7 °C
Sp23	27,4 °C
Sp24	25,9 °C
Sp25	25,6 °C
Sp26	25,3 °C
Sp27	24,7 °C
Sp28	24,6 °C
Sp29	24,8 °C
Sp30	26,3 °C
Sp31	26,6 °C
Sp32	27,0 °C
Sp33	27,6 °C
Sp34	27,2 °C
Sp35	26,2 °C

Figure 4.18. ***Example of thermographic measurement report with ROI-based temperature sampling.***

Representative output generated by the FLIR analysis software after ROI-based temperature acquisition. The thermographic image displays multiple measurement spots (Sp), each corresponding to a predefined 1 cm² region of interest across the flap surface, with the associated temperature values listed in the measurement panel. A corresponding clinical image of the flap is included for anatomical reference. For illustrative purposes, only a subset of spot measurements is shown, as the complete dataset cannot be fully displayed within a single image.

II. Microsoft Paint (image preparation and spatial referencing)

Microsoft Paint was used as a 2D graphic editor to support image preparation and spatial consistency between thermographic and indocyanine green angiography (ICG-A) images. Its use was limited to basic preprocessing tasks and did not involve quantitative measurement.

Workflow and Functionality

1. Image Alignment

Images from DIRT and ICG-A were:

- Scaled to identical pixel dimensions
- Aligned according to anatomical skin markings and the flap's geometric axis
- Adjusted in rotation to correct minor intraoperative angulation differences

This step ensured that ROI grids, zones, and subzones corresponded spatially between modalities and across timepoints.

2. Image preparation for grid-based analysis

Paint was used to:

- Crop both DIRT and ICG-A images to include only the flap surface.
- Standardize image borders
- Facilitate visual reference during manual placement of the standardized 1 cm^2 ROI grid.

The same ROI grid geometry was applied to both modalities. For ICG-A images, each ROI was manually positioned using the prepared reference images and assigned a perfusion score (0–1–2) based on fluorescence intensity. This ensured spatial correspondence between thermographic and angiographic analyses and enabled direct zonal and subzonal comparison at T1.

Table 4.6. Software used and analytical workflow

Software	Primary function	Output generated
FLIR Tools® (Teledyne FLIR Systems, USA)	Extraction of ROI/cm² temperature values.	Numerical temperature values per ROI; zonal, subzonal, and global.
Microsoft Paint	Image cropping, orientation, and spatial standardization of both DIRT and ICG-A images; visual reference for manual placement of the standardized 1 cm² ROI grid in both modalities.	Spatially aligned reference images enabling consistent ROI, zonal, and subzonal analysis across modalities

4.10 Statistical Analysis

All statistical analyses were performed using **SPSS Statistics v28 (IBM Corp., Armonk, NY, USA)** and **Microsoft Excel (Microsoft Corp., Redmond, WA, USA)**. Excel was used for data organization, calculation of derived variables, and aggregation of ROI/cm²-level measurements into zonal, subzonal, and global perfusion metrics. SPSS was used for descriptive and inferential statistical analyses.

I. Descriptive statistics

Continuous variables were summarized as mean ± standard deviation (SD) or median with interquartile range (IQR), as appropriate, together with minimum and maximum values. Categorical variables were expressed as absolute frequencies and percentages. Descriptive analyses were performed separately for each intraoperative timepoint (T1, T2, and T3) and at the patient and zonal levels, accounting for missing data when present.

II. Categorical perfusion pattern analysis

Perfusion patterns derived from indocyanine green angiography (ICG-A) at T1 and from standardized thermography were qualitatively classified into normal perfusion, arterial failure, venous congestion, and mixed patterns. This classification was used for descriptive and exploratory purposes to support the interpretation of thermographic behavior across intraoperative timepoints.

The relationship between ICG-A and thermographic perfusion patterns was explored using cross-tabulation in cases with complete data for both modalities, without formal hypothesis testing. Analyses were restricted to descriptive comparisons and were not intended to establish statistical agreement or diagnostic performance.

III. Temperature analysis according to ICG-A perfusion category

To explore the relationship between thermographic behavior and angiographic perfusion status, ROI-level thermographic temperature values were compared across

ICG-A perfusion categories (0 = non-perfused, 1 = doubtful, 2 = well perfused) defined at baseline (T1).

This exploratory analysis was performed at each intraoperative timepoint (T1, T2, and T3), using the baseline ICG-A classification as a reference framework to examine the temporal evolution of thermographic temperature behavior. Comparisons were conducted using one-way analysis of variance (ANOVA), treating ICG-A perfusion category as a grouping variable and thermographic temperature as a continuous outcome. When appropriate, post hoc pairwise comparisons were adjusted using the Bonferroni correction.

IV. Zonal temperature distribution analysis

Mean thermographic temperatures were compared across anatomical flap zones (1a, 1b, 2, 3, 4a, and 4b) using **one-way ANOVA** to assess the presence of spatial temperature gradients along the flap. Post hoc pairwise comparisons were adjusted using the Bonferroni correction when appropriate. Analyses were performed independently for each intraoperative timepoint (T1, T2 and T3).

V. Agreement and comparative analyses between modalities

Agreement between ICG-A and standardized thermography at baseline (T1) was initially explored using **correlation analyses** and **Bland–Altman plots** for global perfusion metrics, with particular emphasis on non-perfused surface area as the most clinically relevant parameter. These analyses an overall assessment of global agreement but where not intended to capture spatial or compositional discrepancies.

Because flap perfusion variables (well perfused, doubtful, and non-perfused tissue) represent **compositional data**, i.e., proportions that sum to approximately 100% within each flap zone, conventional marginal correlation analyses were avoided due to the risk of spurious associations related to the closure effect.

Therefore, **compositional data analysis methods** were applied to evaluate concordance between indocyanine green angiography (ICG-A) and thermography. Each flap zone was analysed independently (zones 1a, 1b, 2, 3, 4a, and 4b). For each zone and patient, the perfusion compositions obtained with both techniques (well perfused, doubtful, non-perfused) were transformed using the **centered log-ratio (clr) transformation**, expressing each component as the logarithm of its ratio to the geometric mean of the composition. This transformation allows representation of compositional data in an unconstrained Euclidean space.

Compositional concordance between ICG-A and thermography was quantified on a zone-by-zone basis using the **Aitchison distance**, which measures the discrepancy between two complete compositions. Lower values indicate higher compositional agreement between techniques. Results were summarized using descriptive statistics of compositional distances by zone and graphically represented to facilitate clinical interpretation. All analyses were performed at the patient level, excluding observations with incomplete data for either technique.

Temporal and paired comparisons

To assess intraoperative perfusion changes over time, repeated measurements obtained from the same flap across different timepoints were analysed using paired statistical tests. When comparing more than two related intraoperative stages (T1, T2, and T3), the Friedman test was used as a non-parametric alternative to repeated-measures ANOVA. When the Friedman test indicated significant overall differences, pairwise post hoc comparisons between timepoints were performed using the Wilcoxon signed-rank test. Similarly, paired comparisons between anatomical regions within the same flap—such as distal versus central territories—were conducted using the Wilcoxon signed-rank test, given the paired structure of the data and the absence of normality assumptions.

These temporal and regional analyses were restricted to thermographic variables, as indocyanine green angiography was performed exclusively at baseline (T1).

Diagnostic performance analysis

To further explore the diagnostic performance of thermography, perfusion results were dichotomized into viable and non-viable categories based on predefined criteria. Binary classifications derived from thermography were compared against ICG-A as the reference standard.

Receiver operating characteristic (ROC) analysis was performed using the percentage of non-perfused tissue estimated by thermography as a continuous predictor, with non-viable zones defined according to ICG-A. The area under the curve (AUC) was used as a global measure of discrimination.

An additional ROC analysis was performed using the Aitchison distance between ICG-A and thermography perfusion compositions as a continuous predictor. This approach evaluates whether global compositional discrepancy between techniques can discriminate non-viable zones defined by ICG-A, integrating the relative contribution of well perfused, doubtful, and non-perfused tissue.

VI. Level of statistical significance

All statistical tests were two-tailed. A p-value < 0.05 was considered statistically significant. Given the exploratory nature of the study and the limited sample size, no formal adjustment for multiple comparisons beyond Bonferroni post hoc testing was applied.

Table 4.7. Summary of statistical analyses

Analysis level / objective	Variables analyzed	Statistical test	Purpose
Descriptive analysis	Demographic, surgical, thermographic and ICG-A variables	Descriptive statistics (mean ± SD, min–max, frequencies, percentages)	Characterize the study population and perfusion metrics
Baseline comparison (T1): DIRT vs ICG-A	Global and zonal perfusion percentages (well perfused, non-perfused)	Spearman's rank correlation (ρ)	**Exploratory assessment of association** between thermographic and angiographic perfusion metrics
Agreement analysis (T1)	Global non-perfused surface (%)	Bland–Altman analysis	Evaluate agreement and systematic bias between DIRT and ICG-A
Zonal perfusion distribution	Mean thermographic temperature across zones (1a–4b)	One-way ANOVA with Bonferroni post hoc	Assess spatial temperature gradients within the flap
Perfusion category vs temperature	Mean ROI/cm² temperature by ICG-A perfusion score (0–1–2)	One-way ANOVA with Bonferroni post hoc	Evaluate relationship between angiographic perfusion and temperature
Temporal evolution (T1–T2–T3)	Global and regional thermographic perfusion metrics	Friedman test with Wilcoxon signed-rank post hoc	Assess intraoperative perfusion changes over time
Distal vs central comparison	Distal (1a,4b) vs central (2,3) perfusion metrics	Wilcoxon signed-rank test; Spearman correlation	Evaluate contribution of distal territories to global perfusion behavior

4.11 Ethical Considerations

This study was approved by the Clinical Research Ethics Committee of Hospital de la Santa Creu i Sant Pau (protocol code IIBSP-PER-2019-109). All patients provided written informed consent prior to inclusion. No additional risk was introduced to surgical practice. Data were anonymized and managed in accordance with EU General Data Protection Regulation (GDPR) and Spanish data protection laws.

5

Results

5: Results

5.1 Study population and baseline surgical characteristics

A total of 25 patients undergoing anterolateral thigh (ALT) free flap reconstruction for lower-limb defects were included in the study. All procedures were performed between January 2020 and December 2021. This section describes baseline demographic characteristics, clinical factors potentially affecting distal perfusion or recipient-vessel dissection, indications and anatomical distribution of defects, and baseline surgical characteristics of the ALT flap.

I. Patient demographics

The study population consisted of 22 men (88.0%) and 3 women (12.0%), with a mean age of 56.92 years (standard deviation [SD] 18.37; range 22–87 years). Mean body weight was 80.32 kg (SD 13.73; range 62–110 kg), and mean height was 1.73 m (SD 0.09; range 1.53–1.90 m), resulting in a mean body mass index (BMI) of 27.0 kg/m² (SD 5.2; range approximately 19.7–44.9 kg/m²).

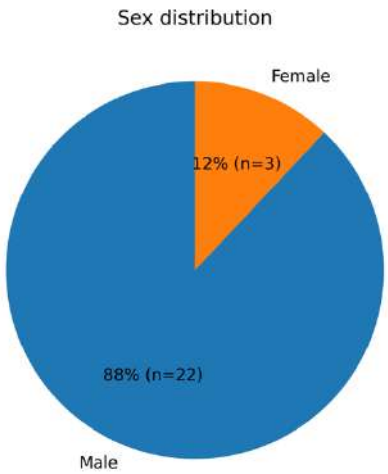


Figure 5.1. *Sex distribution*

These demographic characteristics are summarized in Table 5.1, including measures of central tendency and dispersion, providing an overview of the variability and relative heterogeneity of the study sample.

Table 5.1. Demographic characteristics of the study population (N = 25)

Variable	Mean ± SD	Range	n (%)
Age (years)	56.92 ± 18.37	22–87	
Male			22 (88.0%)
Female			3 (12.0%)
Weight (kg)	80.32 ± 13.73	62–110	
Height (m)	1.73 ± 0.09	1.53–1.90	
BMI (kg/m²)	27.0 ± 5.2	19.7–44.9	

Exploratory correlation analyses were performed to evaluate whether age and body mass index (BMI) were associated with the extent of non-perfused areas at ICG-A T1. Spearman's rank correlation was used due to the limited sample size and non-normal distribution of percentage-based outcomes.

Age was not associated with the percentage of non-perfused area globally or in zones 1a and 4b (all $p > 0.68$). BMI showed a moderate positive correlation with the extent of non-perfused area in zone 1a ($\rho = 0.432$, $p = 0.044$), while correlations with global non-perfused area and zone 4b did not reach statistical significance ($p = 0.149$ and $p = 0.134$, respectively). These findings should be interpreted as exploratory and hypothesis-generating.

II. Clinical factors potentially affecting vascular status and recipient-vessel dissection

Several patient-related factors with potential impact on distal vascularization, microvascular anastomosis, or recipient-vessel dissection were recorded and analyzed (Table 5.2).

Table 5.2. Clinical factors potentially affecting vascularization

Factor	n	%
Active smoking	8	32.0
Non-smoker	17	68.0
Diabetes mellitus	9	36.0
PAD / CLI	4	16.0
Recipient-site revascularization	1	4.0
Previous radiotherapy	4	16.0
Neoadjuvant chemotherapy	2	8.0

Active smoking was present in 8 patients (32.0%), while 17 patients (68.0%) were non-smokers. Diabetes mellitus was diagnosed in 9 patients (36.0%). An exploratory analysis was performed to evaluate whether active smoking or diabetes mellitus were associated with a greater extent of non-perfused areas at ICG-A T1. The percentage of non-perfused flap area was analysed as a continuous variable. Comparisons between groups were performed using the Mann–Whitney U test. No statistically significant differences were observed in the percentage of non-perfused area between smokers and non-smokers (median 8.59% vs 7.00%, p = 0.837), nor between patients with and without diabetes mellitus (median 9.67% vs 6.13%, p = 1.000). These analyses should be interpreted as exploratory due to the limited sample size.

Table 5.3. Association between smoking, diabetes mellitus and extent of non-perfused area at ICG-A T1

Factor	Group	n	Median non-perfused (%)	IQR	p-value
Smoking	**Smoker**	7	8.59	3.88–11.98	0.837
	Non-smoker	15	7.00	4.38–13.07	
Diabetes mellitus	**DM**	8	9.67	6.21–11.09	1.000
	Non-DM	14	6.13	3.76–14.30	

A second exploratory analysis assessed whether smoking or diabetes mellitus were associated with a greater extent of non-perfused areas in high-risk flap regions (zones 1a and 4b) at ICG-A T1. The percentage of non-perfused area was analysed as a continuous variable for each zone separately using the Mann–Whitney U test.

No statistically significant associations were identified between smoking or diabetes mellitus and the extent of non-perfused area in either zone 1a or zone 4b. These findings suggest that, within this cohort, the presence of these clinical factors was not associated with a larger extent of regional non-perfusion at T1.

Table 5.4. Association between clinical factors and non-perfused area in high-risk zones at ICG-A T1

Zone	Factor	Group	n	Median non-perfused (%)	IQR	p-value
1a	**Smoking**	**Smoker**	7	33.33	18.82–51.43	1.000
		Non-smoker	15	29.41	16.82–68.31	
1a	**Diabetes**	**DM**	8	30.56	20.00–70.00	0.606
		Non-DM	14	32.35	4.41–49.71	
4b	**Smoking**	**Smoker**	7	30.00	16.96–57.00	0.396
		Non-smoker	15	50.00	28.64–66.54	
4b	**Diabetes**	**DM**	8	53.47	27.86–77.94	0.537
		Non-DM	14	37.50	22.89–59.38	

Peripheral arterial disease or critical limb ischemia (PAD/CLI) was documented in 4 patients (16.0%). In relation to PAD/CLI, recipient-site revascularization procedures were required in 1 patient, whereas no donor-site revascularization was performed in any case.

Previous radiotherapy involving the recipient area was present in 4 patients (16.0%), and neoadjuvant chemotherapy had been administered in 2 patients (8.0%). These oncologic treatments were considered relevant due to their known effects on tissue fibrosis, vascular fragility, and complexity of recipient-vessel dissection.

Due to the limited number of events observed for these variables (peripheral arterial disease/critical limb ischemia (PAD/CLI), previous radiotherapy, and neoadjuvant chemotherapy), no inferential statistical analysis was performed to assess their association with flap perfusion outcomes. Accordingly, these factors were analysed descriptively in order to characterise the study population and document their prevalence, as any formal assessment of their influence would require a substantially larger cohort.

III. Indications for reconstruction and anatomical distribution of defects

The primary indications for ALT flap reconstruction are detailed in Table 5.5. Defects were most commonly of oncologic origin, accounting for 16 cases (64.0%). Traumatic defects were present in 7 patients (28.0%), while diabetic-related defects accounted for 2 cases (8.0%).

Table 5.5. Indications for surgery distribution

Category	**n**	**%**
Tumoral	16	64.0
Traumatic	7	28.0
Diabetic-related	2	8.0

Regarding anatomical location (Table 5.6), defects were predominantly located in the leg (13 cases, 52.0%) and foot (6 cases, 24.0%). Less frequent locations included the knee (4 cases, 16.0%) and the inguinal region (2 cases, 8.0%). This distribution reflects the predominance of distal lower-limb reconstruction in the present cohort.

Table 5.6. Anatomical location of the defect

Inguinal	2	8.0
Knee	4	16.0
Leg	13	52.0
Foot	6	24.0

IV. ALT flap harvest and baseline surgical characteristics

Baseline surgical characteristics of the ALT flap are summarized in Table 5.7 following the logical sequence of flap elevation and microsurgical reconstruction. Flaps were elevated using different dissection planes according to reconstructive requirements, including subfascial, suprafascial, and superthin techniques (Table 5.8). The type of perforator was classified as musculocutaneous, septocutaneous, or mixed, and the number of perforators included per flap was recorded for each case.

The mean number of perforators included was 1.6 per flap, and the mean pedicle length was 11.2 cm. Mean flap dimensions were 24.2 cm in length and 10.4 cm in width, reflecting the size requirements imposed by distal lower-limb defects. Flap ischemia time, defined as the interval between pedicle division and completion of arterial anastomosis, showed a mean duration of 92.5 minutes (SD 34.2; range 45–180 minutes).

Table 5.7. ALT flap surgical characteristics

Variable	Mean ± SD	Range
Flap length (cm)	24.2 ± 5.0	17–36
Flap width (cm)	10.4 ± 1.7	7–14
Pedicle length (cm)	11.2 ± 2.4	8–17
Number of perforators	1.6 ± 0.6	1–3
Musculocutaneous perforators	14	56.0
Septocutaneous perforators	7	28.0
Mixed perforators	4	16.0
Ischemia time (min)	92.5 ± 34.2	45–180

Table 5.8. ALT flap harvest characteristics

Variable	n	%
Subfascial elevation	17	68.0
Suprafascial elevation	5	20.0
Superthin elevation	3	12.0

The plane of flap elevation (subfascial, suprafascial, and superthin dissection) was recorded as a potential surgical factor influencing flap perfusion. However, due to the very limited number of superthin flaps in the cohort and the resulting imbalance between categories, no inferential statistical analysis was performed to evaluate its association with ICG-A T1 perfusion outcomes. This variable was therefore analysed descriptively only, as any formal comparison would lack sufficient statistical power and could lead to misleading conclusions.

5.2 T1 Indocyanine Green Angiography Perfusion Assessment as Reference Standard

Indocyanine green angiography (ICG-A) performed at **T1 (flap in situ, prior to pedicle division)** was used as the **reference standard** for baseline perfusion assessment of the anterolateral thigh (ALT) flap.

I. Proximal flap perfusion (zones 1a and 1b)

Perfusion results for the **proximal region of the flap**, comprising zones **1a and 1b**, are summarized in **Table 5.9**.

Table 5.9. Proximal zones (1a–1b)

Zone	Perfusion category	Mean (%)
1a	Well perfused	24.38
	Doubtful	34.44
	Non-perfused	41.19
1b	Well perfused	67.40
	Doubtful	27.15
	Non-perfused	5.45

Zone **1a**, corresponding to one of the most distal perfusion territories relative to the central perforator, showed a **low proportion of well-perfused ROI**, with a mean of **24.38%**, accompanied by a substantial proportion of **doubtful areas (34.44%)** and a high percentage of **non-perfused ROI (41.19%)**.

In contrast, zone **1b** demonstrated a markedly improved perfusion profile, with **67.40% of ROI classified as well perfused**, **27.15% as doubtful**, and only **5.45% as non-perfused**, indicating an **intermediate perfusion pattern** between distal and central regions.

II. Central flap perfusion (zones 2 and 3)

Perfusion data for the **central portion of the flap**, corresponding to zones **2 and 3**, are presented in **Table 5.10**.

Table 5.10. Central zones (2–3)

Zone	Perfusion category	Mean (%)
2	Well perfused	92.50
	Doubtful	7.50
	Non-perfused	0.00
3	Well perfused	89.13
	Doubtful	9.24
	Non-perfused	1.64

Zone **2** exhibited the most favorable perfusion profile of the entire flap, with **92.50% of ROI classified as well perfused**, **7.50% as doubtful**, and **no non-perfused areas detected**.

Similarly, zone **3** showed a high proportion of **well-perfused ROI (89.13%)**, with **9.24% of doubtful areas** and a **minimal fraction of non-perfused ROI (1.64%)**.

The close similarity in perfusion distribution between zones 2 and 3 supports their consideration as a **central perfusion unit**, corresponding to the typical location of the dominant perforator within the ALT flap.

III. Distal flap perfusion (zones 4a and 4b)

Results for the **distal region of the flap**, comprising zones **4a and 4b**, are summarized in **Table 5.11**.

Table 5.11. Distal zones (4a–4b)

Zone	Perfusion category	Mean (%)
4a	Well perfused	65.87
	Doubtful	29.13
	Non-perfused	5.00
4b	Well perfused	18.55
	Doubtful	33.90
	Non-perfused	47.54

Zone **4a** displayed an **intermediate perfusion profile**, with **65.87% of ROI classified as well perfused**, **29.13% as doubtful**, and **5.00% as non-perfused**, comparable to the intermediate behavior observed in zone 1b.

Zone **4b**, representing the most distal perfusion territory of the flap, demonstrated the **least favorable perfusion profile**, with only **18.55% of ROI classified as well perfused**, **33.90% as doubtful**, and a predominant proportion of **non-perfused areas (47.54%)**.

IV. Global flap perfusion at T1

A global analysis of perfusion across the entire flap surface is summarized in **Table 5.12**, which reports the **absolute and relative distribution of well-perfused, doubtful, and non-perfused ROI** for the whole flap.

Table 5.12. Global flap perfusion at T1 ICG

Perfusion category	Mean (%)
Well perfused	72.97
Doubtful	18.14
Non-perfused	8.89

At T1, the **mean global perfusion profile** derived from ICG-A analysis demonstrated that **72.97% of the flap surface was classified as well perfused**, while **18.14% corresponded to areas with doubtful perfusion**, and **8.89% of the surface was classified as non-perfused**.

These percentages represent the **observed detection capability of ICG-A in the present cohort** and reflect the integrated contribution of central, intermediate, and distal flap regions under physiological conditions.

V. Inter-patient variability of T1 ICG perfusion percentages

Analysis of inter-patient variability revealed distinct dispersion patterns across flap regions **(Table 5.13)**. **Central zones (zones 2 and 3)** demonstrated not only the highest mean proportion of well-perfused areas but also the **lowest variability**, with standard deviations of approximately **21–23%** and minimal or absent non-perfused areas.

In contrast, **distal zones (zones 1a and 4b)** showed marked variability, with standard deviations exceeding **28–35%** for well-perfused and non-perfused categories, reflecting heterogeneous perfusion behavior across patients. **Intermediate zones (zones 1b and 4a)** exhibited intermediate variability profiles.

These findings indicate that the central portion of the flap displays both **consistently higher perfusion and greater inter-patient stability**, whereas peripheral regions are characterized by increased variability and a higher proportion of compromised perfusion.

Table 5.13. Zonal variability of T1 ICG perfusion percentages (mean ± SD)

Zone	Well perfused (%)	Doubtful (%)	Non-perfused (%)
Zone 1a	24.38 ± 29.44	34.44 ± 33.76	41.19 ± 35.06
Zone 1b	67.40 ± 36.49	27.15 ± 30.61	5.45 ± 13.40
Zone 2	92.50 ± 21.55	7.50 ± 21.55	0.00 ± 0.00
Zone 3	89.13 ± 22.51	9.24 ± 22.11	1.64 ± 5.31
Zone 4a	65.87 ± 33.66	29.13 ± 28.54	5.00 ± 13.14
Zone 4b	18.55 ± 28.97	33.90 ± 25.97	47.54 ± 32.03
Global flap	72.97 ± 20.09	18.14 ± 18.26	8.89 5.42

VI. Observed spatial distribution of perfusion at T1 ICG

Taken together, T1 ICG-A analysis revealed a **consistent central-to-peripheral perfusion gradient** along the proximal–distal axis of the flap. Perfusion was highest in the **central zones (zones 2 and 3)**, intermediate in **zones 1b and 4a**, and lowest in the **most distal zones (zones 1a and 4b)**.

This gradient was observed consistently in both **absolute ROI counts** and **relative zonal percentages**, indicating a true spatial perfusion pattern rather than an effect of zonal surface area.

The **mean global percentage distribution of perfusion categories at T1** was therefore adopted as the **reference perfusion profile** for the study and constituted the **gold standard** against which dynamic infrared thermography was subsequently standardized and evaluated in terms of non-inferiority.

VII. Central versus peripheral perfusion patterns

When zones were conceptually grouped according to their position relative to the dominant perforator, a clear spatial gradient emerged. **Central zones (zones 2 and 3)** showed mean well-perfused areas exceeding **89–92%**, with doubtful perfusion below **10%** and negligible non-perfused surface.

Intermediate zones (zones 1b and 4a) demonstrated a reduction in well-perfused surface to approximately **66–67%**, accompanied by an increase in doubtful areas to around **27–29%**.

In contrast, the **most distal zones (zones 1a and 4b)** exhibited a marked decline in well-perfused surface (**18–24%**) and the highest proportions of non-perfused areas (**41–48%**).

This progressive central-to-peripheral decrease in perfusion was consistently observed across patients and forms the basis for defining the physiological reference perfusion profile at T1.

5.3 Standardization of Dynamic Infrared Thermography Based on the T1 ICG Reference Profile

Dynamic infrared thermography (DIRT) was standardized using the **T1 indocyanine green angiography (ICG-A) perfusion profile** as the reference framework. Given the absence of universally accepted absolute temperature thresholds applicable to intraoperative flap assessment, a **relative, patient-specific approach** was adopted.

Initial exploratory analysis demonstrated that fixed temperature cut-offs (e.g., <25 °C, 25–30 °C, >30 °C), as described in previous experimental or postoperative thermographic studies, were **not applicable** to the present intraoperative setting. Absolute temperature values varied considerably between patients due to individual baseline temperature, operating room conditions, flap thickness, and exposure time, precluding the use of universal thresholds.

For this reason, thermographic data were standardized **de novo**, using the **quantitative perfusion distribution observed with ICG-A at T1** as the physiological reference.

I. Rationale for thermographic standardization

As demonstrated in Section 5.2, T1 ICG-A analysis revealed a reproducible **global perfusion profile** of the ALT flap under physiological conditions, with approximately **73% of the flap surface classified as well perfused**, **18% as doubtful**, and **9% as non-perfused**. This distribution, derived from extensive ROI/cm²-based spatial sampling, was adopted as the **gold standard perfusion profile** for the study.

The objective of thermographic standardization was therefore to define **temperature-based perfusion categories** that would reproduce, as closely as possible, this reference distribution when applied to intraoperative DIRT images, enabling subsequent evaluation of **non-inferiority relative to ICG-A**.

II. Patient-specific temperature normalization

For each patient, thermographic analysis was performed using the same **ROI/cm² grid** applied for ICG-A analysis. From all thermographic ROI sampled within a given patient, the following parameters were calculated:

- The **mean flap temperature ($\bar{T}$)**
- The **standard deviation (SD) of flap temperature**
- Using these parameters, thermographic perfusion categories were defined **relative to the patient's own temperature distribution**, rather than absolute temperature values.

III. Definition of thermographic perfusion categories

Based on the T1 ICG-A reference profile and assuming an approximately normal distribution of temperature values within each flap, thermographic perfusion categories were defined as follows:

Thermographic perfusion categories

Thermographic category	Temperature criterion	Expected proportion (%)
Well perfused	$T \geq (\bar{T} - 1\ SD)$	≈ 68%
Doubtful perfusion	$(\bar{T} - 2\ SD) \leq T < (\bar{T} - 1\ SD)$	≈ 27%
Non-perfused	$T < (\bar{T} - 2\ SD)$	≈ 5%

This classification assigns approximately **68%** of values to the well-perfused category, **27%** to the doubtful category, and **5%** to the non-perfused category under a normal distribution, closely approximating the **global perfusion proportions observed with ICG-A at T1**, while preserving sensitivity to inter-patient variability.

IV. Zonal and global application of standardized thermographic categories

Once defined, thermographic perfusion categories were applied to all ROI/cm² within each patient and subsequently aggregated by **zones and subzones (1a, 1b, 2, 3, 4a, 4b)**, following the same spatial framework used for ICG-A analysis.

This approach allowed:

- Direct **zonal and global comparison** between DIRT and ICG-A at T1,
- Evaluation of thermographic perfusion patterns under different intraoperative conditions (T2 and T3),
- Assessment of **temporal thermographic changes** independent of ICG-A.

V. Methodological implications

By anchoring thermographic interpretation to a **physiologically derived, modality-independent reference profile**, this standardization strategy avoids arbitrary temperature thresholds and enables meaningful comparison between two imaging techniques with fundamentally different physical principles.

Importantly, this approach does not attempt to force thermography to replicate ICG-A at the pixel or ROI level. Instead, it evaluates whether thermography can reproduce **equivalent regional and global perfusion distributions**, consistent with its intended role as a **non-invasive, dye-free intraoperative perfusion assessment tool**.

VI. Global thermographic perfusion profile at T1

After application of the standardized thermographic criteria, T1 DIRT analysis demonstrated a **predominance of well-perfused areas across the flap surface**. At a global level, **82.11%** of thermographic ROI were classified as well perfused, **14.26%** as doubtful, and **4.12%** as non-perfused (**Table 5.14**).

Table 5.14. T1 thermography – global flap perfusion

Perfusion category	Mean (%)
Well perfused	82.11
Doubtful	14.26
Non-perfused	4.12

This global thermographic distribution reflects a **high overall perfusion signal at T1** following standardization and approximates the reference perfusion profile derived from ICG-A, while preserving sensitivity to regional variations.

VII. Zonal thermographic perfusion distribution at T1

When analyzed by anatomical zones, standardized thermography revealed a **clear spatial perfusion gradient** along the proximal–distal axis of the flap (**Tables 5.15–5.17**).

Table 5.15. T1 thermography perfusion in proximal zones (1a–1b)

Zone	Perfusion category	Mean (%)
1a	Well perfused	62.86
	Doubtful	28.91
	Non-perfused	8.23
1b	Well perfused	90.81
	Doubtful	7.22
	Non-perfused	1.96

Table 5.16. T1 thermography perfusion in central zones (2–3)

Zone	**Perfusion category**	**Mean (%)**
2	Well perfused	94.71
	Doubtful	1.79
	Non-perfused	3.49
3	Well perfused	90.36
	Doubtful	7.77
	Non-perfused	1.87

Table 5.17. T1 thermography perfusion in distal zones (4a–4b)

Zone	Perfusion category	Mean (%)
4a	Well perfused	73.44
	Doubtful	23.86
	Non-perfused	2.69
4b	Well perfused	45.75
	Doubtful	43.38
	Non-perfused	10.87

Central zones (zones 2 and 3)

The highest thermographic perfusion values were observed in the central portion of the flap. Zone 2 demonstrated 94.71 % well-perfused ROI, with 1.79 % doubtful and 3.49 % non-perfused areas. Similarly, zone 3 showed 90.36 %well-perfused ROI, 7.77 % doubtful, and 1.87 % non-perfused areas (**Table 5.16**).

Intermediate zones (zones 1b and 4a)

Intermediate zones exhibited a moderate reduction in thermographic perfusion. Zone 1b showed 90.81 % well-perfused ROI, 7.22 % doubtful, and 1.96 % non-perfused areas. Zone 4a demonstrated 73.44 % well-perfused ROI, accompanied by an increase in doubtful areas to 23.86 %, with 2.69 % non-perfused ROI (**Tables 5.15 and 5.17**).

Distal zones (zones 1a and 4b)

The most distal zones demonstrated the lowest thermographic perfusion values. Zone 1a showed 62.86 % well-perfused ROI, 28.91 % doubtful, and 8.23 % non-perfused areas. Zone 4b exhibited the most compromised thermographic profile, with only 45.75 % well-perfused ROI, 43.38 % doubtful, and 10.87 % non-perfused areas (**Tables 5.15 and 5.17**).

VIII. Inter-patient variability of standardized thermography at T1

Inter-patient variability analysis demonstrated that **central zones (zones 2 and 3)** showed the most stable thermographic behavior, with relatively low dispersion in the proportion of well-perfused ROI (zone 2: **94.71 ± 6.33%**; zone 3: **90.36 ± 11.57%**).

In contrast, **distal territories** exhibited markedly higher variability, particularly zone **4b** (**45.75 ± 33.68%** well-perfused; **43.38 ± 28.46%** doubtful), and zone **1a** (**62.86 ± 31.16%** well-perfused). Intermediate zones (1b and 4a) demonstrated intermediate variability profiles. At a global flap level, standardized thermography showed comparatively low dispersion (**82.11 ± 4.36%** well-perfused), indicating consistent overall classification despite regional heterogeneity.

IX. Summary of standardized thermographic behavior at T1

In summary, standardized dynamic infrared thermography at T1 demonstrated a **physiologically coherent spatial perfusion pattern**, characterized by:

- High thermographic perfusion in **central zones**,
- Intermediate perfusion in **zones adjacent to the center**,
- Reduced perfusion in the **most distal flap territories**.

Both the **global distribution** (Table 5.14) and the **zonal gradients**, including inter-patient variability (Table 5.18), were internally consistent and suitable for subsequent **direct comparison with T1 ICG-A**, which is addressed in Section 4.

Table 5.18. T1 thermography – zonal variability (mean ± SD)

Zone	Well perfused (%)	Doubtful (%)	Non-perfused (%)
Zone 1a	62.86 ± 31.16	28.91 ± 24.98	8.23 ± 11.85
Zone 1b	90.81 ± 13.67	7.22 ± 11.78	1.96 ± 4.49
Zone 2	94.71 ± 6.33	1.79 ± 3.64	3.49 ± 4.98
Zone 3	90.36 ± 11.57	7.77 ± 6.40	1.87 ± 7.21
Zone 4a	73.44 ± 24.43	23.86 ± 23.68	2.69 ± 6.17
Zone 4b	45.75 ± 33.68	43.38 ± 28.46	10.87 ± 12.59
Global flap	82.11 ± 4.36	14.26 ± 3.86	4.12 2.48

5.4 T1 comparison between ICG-A and standardized DIRT

At T1, both ICG-A and dynamic infrared thermography (DIRT) were acquired under physiological conditions prior to flap division, representing the key timepoint for evaluating intrinsic spatial perfusion distribution and for testing the performance of thermography against the angiographic reference. Because DIRT was standardized in Section 3 using a patient-specific temperature normalization anchored to the T1 ICG-A reference profile, the present section focuses on **global and zonal agreement at T1** using the ROI/cm² framework, without ROI-to-ROI pairing.

I. Dataset completeness and ROI sampling density for the T1 comparison

Spatial sampling at T1 was based on ROI/cm² grids across the entire flap surface, aggregated by subzones (1a, 1b, 2, 3, 4a, 4b) and at the global flap level. For ICG-A, the number of analyzed ROI ("spots") was available in **22 flaps**, totaling **3,699 ROI**, with a mean of **168.14 ± 36.43 ROI per patient** (range **111–252**). For thermography, "spots" were available in **24 flaps**, totaling **2,633 ROI**, with a mean of **109.71 ± 35.34 ROI per patient** (range **36–184**). A subset of cases lacked complete ICG-A T1 ROI totals (patients 19, 20, and 25 in the current dataset), and one case lacked complete thermographic categorization at T1, therefore **paired ICG-A vs DIRT comparisons were performed on the maximal overlapping set (n = 21)** with complete global percentage distributions in both modalities. Zonal comparisons were performed using the same paired availability per zone when complete data existed.

II. Global perfusion agreement at T1

Using the full ICG-A T1 reference profile (Section 2), the mean global distribution of perfusion categories at T1 was **72.97% well perfused**, **18.14% doubtful**, and **8.89% non-perfused**, defining the angiographic "gold standard" physiological profile for the study. After application of standardized thermographic criteria (Section 3), DIRT demonstrated a global profile at T1 of **82.11% well perfused**, **14.26% doubtful**, and **4.12% non-perfused** (Table 5.18).

In the paired subset (n = 21), DIRT showed a **higher proportion of well-perfused area** than ICG-A at T1 (mean difference **+10.07 ± 22.57 percentage points**, Wilcoxon **p = 0.046**), and a **lower proportion of non-perfused area**(mean difference **–5.17 ± 6.35 percentage points**, Wilcoxon **p = 0.0025**), while doubtful perfusion did not differ significantly at the global level. These results indicate that, at T1, standardized thermography tended to classify a larger fraction of ROI as well perfused and a smaller fraction as non-perfused when compared with the angiographic reference, while preserving a broadly comparable distribution structure consistent with the intended non-inferiority framework.

To visualize the magnitude and direction of global differences, **Figure 5.2** displays the relationship between ICG-A and DIRT for global non-perfused percentage at T1, and **Figure 5.3** provides a Bland–Altman representation of agreement, highlighting systematic bias (DIRT classifying less non-perfused area) and limits of agreement for the non-perfused compartment at T1.

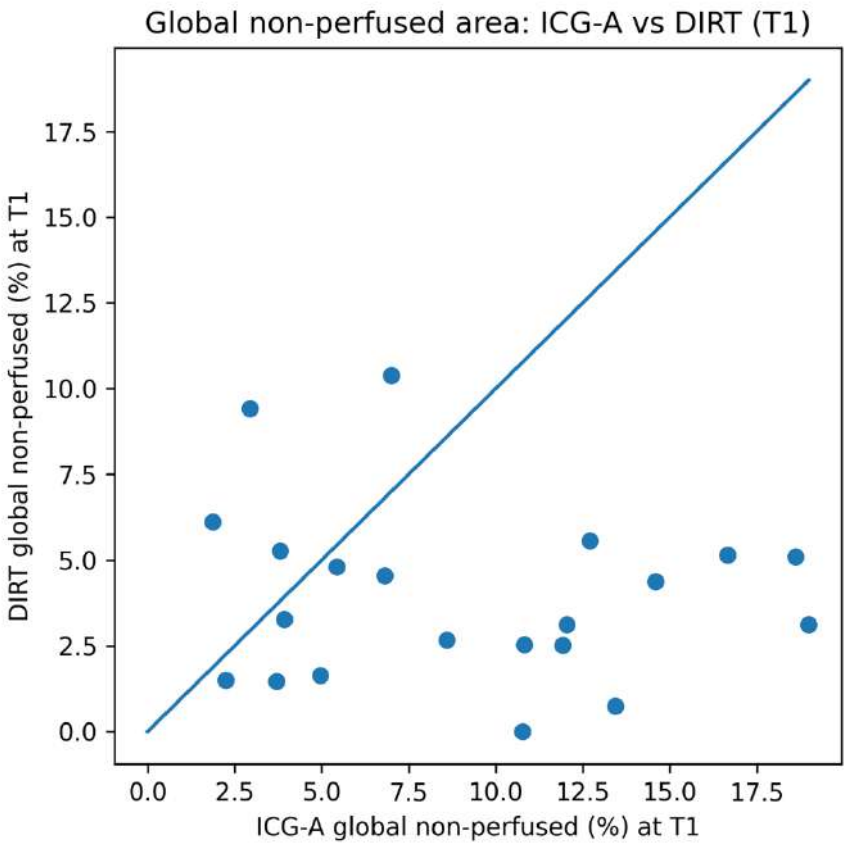


Figure 5.2. *Global non-perfused area at T1: DIRT vs ICG-A*

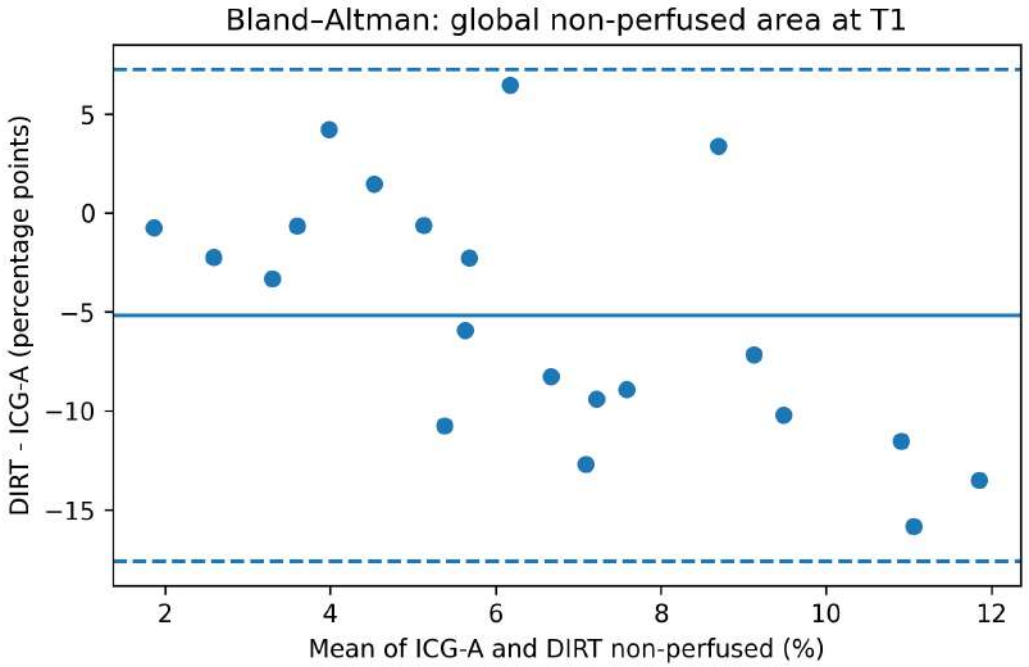


Figure 5.3. *Bland – Altman: Global non-perfused area at T1*

III. Zonal agreement and spatial gradient reproduction at T1

A major objective of the T1 comparison was to determine whether thermography reproduces the **central-to-peripheral perfusion gradient** observed on ICG-A (Section 5.2) when analyzed with identical ROI/cm² zoning.

On ICG-A, zonal mean well-perfused percentages followed the expected gradient: **zones 2 and 3** showed the highest well-perfused surface (**92.50%** and **89.13%**, respectively), intermediate zones **1b and 4a** showed reduced well-perfused surface (**67.40%** and **65.87%**), and the most distal zones **1a and 4b** showed the lowest well-perfused surface (**24.38%**and **18.55%**) with the highest non-perfused proportions (zone **1a: 41.19%**, zone **4b: 47.54%**). This gradient defines a physiologically coherent spatial pattern centered around the perforator territory.

After standardization, thermography reproduced the *direction* of the gradient but with systematic shifts in the category proportions. DIRT showed high well-perfused percentages in the central zones (**zone 2: 94.71%**, **zone 3: 90.36%**) and reduced values

toward the distal territories (**zone 1a: 62.86%**, **zone 4b: 45.75%**), while doubtful and non-perfused categories increased distally (Table 5.15–5.17 and Table 5.18). However, compared with ICG-A, DIRT demonstrated a relative **increase in "well perfused" classification in distal zones** and a corresponding **decrease in "non-perfused" classification**, particularly in the most distal territories (zones 1a and 4b).

In the paired analysis (Table 5.19), the largest modality differences occurred precisely in the distal zones:

- **Zone 1a:** well perfused was higher with DIRT than ICG-A (**+39.10 ± 38.86 pp**, **p = 0.0013**), while non-perfused was lower (**−33.34 ± 36.87 pp**, **p = 0.0005**).
- **Zone 4b:** well perfused was higher with DIRT (**+32.85 ± 41.99 pp**, **p = 0.0040**), while non-perfused was lower (**−37.70 ± 37.03 pp**, **p = 0.0001**).

In contrast, central zones showed smaller differences in well-perfused area between modalities (e.g., zone 2 mean difference **+3.17 ± 24.02 pp**, **p = 0.530**; zone 3 mean difference **+1.03 ± 28.11 pp**, **p = 0.528**), consistent with better apparent agreement where perfusion is robust. A compact visualization of mean well-perfused area by zone for both modalities is provided in **Figure 5.4**, illustrating convergence in zones 2–3 and divergence that increases toward distal territories.

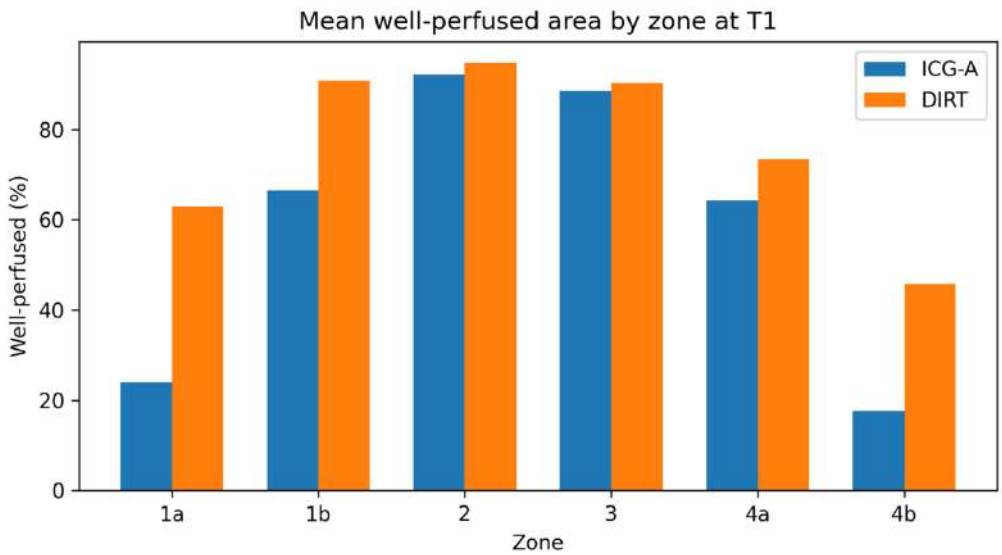


Figure 5.4. *Mean well-perfused area by zone at T1*

IV. Association and correlation metrics between modalities at T1

Beyond category proportions, an ordinal **perfusion index** was derived for each zone and globally by weighting categories as follows: *index = (2 × well-perfused + 1 × doubtful + 0 × non-perfused) / 100*, yielding a 0–2 scale (higher values indicate better perfusion). In the paired global comparison (n = 21), DIRT demonstrated a higher global perfusion index than ICG-A (Wilcoxon **p = 0.010**), consistent with the shift toward "well perfused" classification described above.

Spearman correlation between ICG-A and DIRT global perfusion index at T1 showed a **non-significant association** in the paired dataset (ρ = **–0.323**, p = **0.153**, n = 21), reflecting that thermography—after standardization—captured the overall spatial gradient but did not demonstrate strong rank-order tracking of global perfusion index across individuals in this subset. Zonal Spearman correlations for category percentages were similarly modest overall, with the highest (still non-significant) values observed in the most variable territories (e.g., zone 1a), while central zones tended to show low correlation partly due to restricted range (ceiling effects) in both modalities. These correlation patterns are consistent with the qualitative observation that most between-subject variability is expressed in the distal territories, while central zones remain uniformly well perfused. These findings suggest that, while DIRT captures spatial perfusion patterns within the flap, its global ordinal index does not reliably rank individual flaps in the same order as ICG-A at baseline.

V. Temperature behavior at T1 and its spatial relationship within the flap

Thermographic absolute temperatures at T1 were analyzed in parallel to categorical perfusion mapping to provide an intrinsic physiological description of the thermographic signal prior to modality comparison at later timepoints. Across the 24 evaluable thermography cases, the mean flap temperature at T1 was **27.86 ± 1.45 °C**, with a mean intra-flap temperature SD of **1.54 ± 0.43 °C** (available in 23 cases), and mean minimum and maximum flap temperatures of **23.84 ± 2.04 °C** and **30.75 ± 1.58 °C**, respectively.

A consistent spatial thermal gradient was observed at T1 in the zonal mean temperatures: central zones exhibited higher mean temperatures (**zone 2: 28.64 ± 1.65 °C; zone 3: 28.27 ± 1.66 °C**) compared with distal territories (**zone 1a: 26.91 ± 1.69 °C; zone 4b: 26.29 ± 1.81 °C**). When central (zones 2–3) and distal (zones 1a and 4b) territories were aggregated within-patient, central temperatures remained significantly higher than distal temperatures (paired t-test **$p < 0.001$**), confirming a robust **central-to-peripheral thermal decline** consistent with the expected perfusion gradient at T1.

Together, these temperature findings support that, even before direct modality comparison, thermography provides a physiologically coherent spatial signal across the flap surface at baseline conditions, with higher central temperatures and lower distal temperatures at T1.

VI. Summary of the T1 comparison

At T1, standardized DIRT reproduced a physiologically coherent spatial gradient across ALT flap territories, with the highest perfusion signal centrally and progressive reduction distally. At the global level, DIRT classified a higher proportion of ROI as well perfused and a lower proportion as non-perfused compared with ICG-A (Table 5.18; Figures 5.2–5.3), while preserving meaningful zonal differentiation (Figure 5.4). The largest modality divergences were consistently located in the most distal zones (1a and 4b), whereas central zones showed smaller differences, reflecting greater convergence under robust perfusion conditions. These findings provide the quantitative foundation for the subsequent focused analysis of agreement patterns and performance metrics at T1, and for extending comparisons to T2 and T3 under altered intraoperative hemodynamic conditions.

Table 5.19. T1 agreement between ICG-A and standardized DIRT (paired analysis)

Zone	Category	ICG-A mean ± SD (%)	DIRT mean ± SD (%)	DIRT - ICG-A (pp)	Wilcoxon p
1a	**Well-perfused**	23.95 ± 30.10	63.05 ± 32.50	+39.10 ± 38.86	0.0013
	Non-perfused	41.56 ± 35.89	8.22 ± 11.85	-33.34 ± 36.87	0.0005
1b	**Well-perfused**	66.51 ± 37.14	92.13 ± 13.55	+25.62 ± 41.39	0.0130
	Non-perfused	5.71 ± 13.67	1.16 ± 3.65	-4.56 ± 14.63	0.1159
2	**Well-perfused**	92.14 ± 22.01	95.31 ± 6.47	+3.17 ± 24.02	0.5301
	Non-perfused	0.00 ± 0.00	3.06 ± 5.14	+3.06 ± 5.14	0.0115
3	**Well-perfused**	88.61 ± 22.94	89.64 ± 12.16	+1.03 ± 28.11	0.5277
	Non-perfused	1.72 ± 5.43	2.14 ± 7.69	+0.42 ± 9.81	0.8927
4a	**Well-perfused**	64.24 ± 33.59	71.29 ± 25.44	+7.05 ± 44.43	0.4553
	Non-perfused	5.24 ± 13.41	3.08 ± 6.53	-2.16 ± 11.21	0.6002
4b	**Well-perfused**	17.53 ± 29.28	50.38 ± 33.34	+32.85 ± 41.99	0.0040
	Non-perfused	48.38 ± 32.57	10.68 ± 12.79	-37.70 ± 37.03	0.0001
Global	**Well-perfused**	72.17 ± 20.22	82.24 ± 4.62	+10.07 ± 22.57	0.0460
	Non-perfused	9.13 ± 5.44	3.97 ± 2.60	-5.17 ± 6.35	0.0025

5.5 Temporal evolution of flap perfusion assessed by standardized thermography (T1–T2–T3)

After establishing the standardized thermographic perfusion categories (Section 5.3) and characterizing baseline behavior at T1, the temporal evolution of flap perfusion was analyzed using **dynamic infrared thermography alone** across three predefined intraoperative timepoints: **T1** (baseline, prior to flap division), **T2** (after arterial and single venous anastomosis), and **T3** (after completion of the second venous anastomosis). All analyses were performed using the same ROI/cm² grid and spatial subdivision into zones (1a, 1b, 2, 3, 4a, 4b).

Longitudinal analyses were restricted to cases with complete paired thermographic data at all three timepoints for the respective variables. Across these cases, spatial sampling density remained comparable over time, with no relevant differences in the number of analyzed ROI/cm² between timepoints, ensuring consistency of the temporal comparisons.

I. Global thermographic perfusion changes across timepoints

At the global flap level, standardized thermography demonstrated measurable changes in perfusion category distribution across intraoperative stages (Table 5.20). At **T1**, the flap surface was predominantly classified as well perfused (**81.28 ± 4.80%**), with smaller proportions of doubtful (**14.78 ± 3.98%**) and non-perfused (**4.39 ± 2.86%**) areas. Following arterial and single venous anastomosis (**T2**), the proportion of well-perfused surface remained similar (**80.96 ± 12.91%**), while doubtful perfusion increased (**16.68 ± 11.85%**) and non-perfused areas decreased (**2.52 ± 2.04%**). After completion of the second venous anastomosis (**T3**), well-perfused surface increased to **85.13 ± 3.92%**, with a further reduction in non-perfused areas (**1.73 ± 1.47%**).

Table 5.20. Global thermographic perfusion metrics across intraoperative timepoints (T1–T2–T3)

Metric	T1 (mean ± SD)	T2 (mean ± SD)	T3 (mean ± SD)	Friedman p	Wilcoxon T1 vs T3 p
Well perfused (%)	81.28 ± 4.80	80.96 ± 12.91	85.13 ± 3.92	0.0910	0.00058
Doubtful (%)	14.78 ± 3.98	16.68 ± 11.85	13.01 ± 4.36	0.3679	—
Non-perfused (%)	4.39 ± 2.86	2.52 ± 2.04	1.73 ± 1.47	0.0910	0.0155
Perfusion index (0–2)	1.773 ± 0.091	1.786 ± 0.142	1.833 ± 0.041	0.0152	0.00058

Across the three timepoints, overall differences in the distribution of perfusion categories did not reach statistical significance using Friedman testing; however, **pairwise comparison demonstrated a significant reduction in non-perfused surface between T1 and T3 (Wilcoxon p = 0.0155)**.

To summarize global perfusion changes in a single quantitative metric, a **global thermographic perfusion index** (2 = well perfused, 1 = doubtful, 0 = non-perfused) was calculated. The perfusion index increased progressively from **1.773 ± 0.091 at T1** to **1.786 ± 0.142 at T2** and **1.833 ± 0.041 at T3** (Table 4.20). This increase was statistically significant across timepoints (**Friedman p = 0.0152**) and particularly between **T1 and T3 (Wilcoxon p = 0.00058)**. The temporal evolution of the global perfusion index is illustrated in **Figure 5.5**.

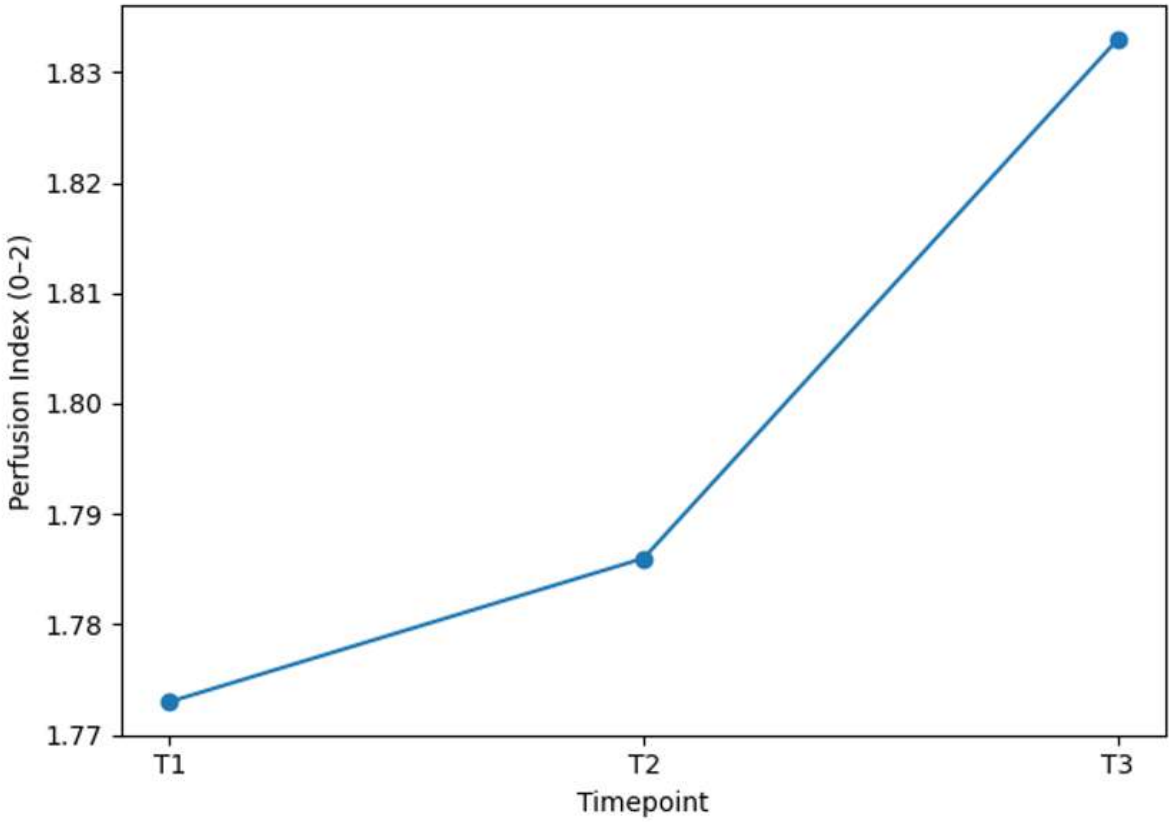


Figure 5.5. *Global thermographic perfusion index across timepoints*

II. Zonal temporal behavior of thermographic perfusion

Zonal analysis revealed heterogeneous temporal behavior across the flap surface, with differences between central, intermediate, and distal territories.

Central zones (zones 2 and 3) remained consistently well perfused throughout the intraoperative sequence. In zone 2, well-perfused proportions were **93.79 ± 6.70% (T1)**, **85.49 ± 18.99% (T2)**, and **94.99 ± 6.28% (T3)**, while zone 3 showed **90.27 ± 13.20%**, **88.87 ± 11.64%**, and **93.11 ± 8.33%** at T1, T2, and T3, respectively. No statistically significant temporal differences were observed in these central territories.

Intermediate zones (zones 1b and 4a) demonstrated greater variability, with numerical reductions in well-perfused surface at T2 and partial recovery at T3, although these changes did not reach statistical significance.

Distal zones (zones 1a and 4b) exhibited the greatest temporal variability and are summarized in **Table 5.21**. In zone 4b, the well-perfused proportion increased from **44.12 ± 33.26% at T1** to **66.28 ± 29.12% at T2** and **63.88 ± 33.27% at T3**, while zone 1a showed comparatively more stable behavior across timepoints. Although Friedman testing did not demonstrate statistically significant differences, the magnitude and direction of change in distal territories indicate that temporal thermographic variability is preferentially expressed in these regions.

Table 5.21. Temporal evolution of thermographic perfusion in distal flap territories (zones 1a and 4b)

Metric (%)	T1 (mean ± SD)	T2 (mean ± SD)	T3 (mean ± SD)	Friedman p
Zone 1a Well perfused	67.96 ± 31.13	69.89 ± 27.56	65.13 ± 29.22	0.2797
Zone 1a Non-perfused	6.32 ± 10.44	4.38 ± 8.96	5.98 ± 9.87	0.3110
Zone 4b Well perfused	44.12 ± 33.26	66.28 ± 29.12	63.88 ± 33.27	0.0970
Zone 4b Non-perfused	9.82 ± 12.34	4.00 ± 10.08	7.00 ± 12.30	0.2215

III. Thermographic temperature dynamics and spatial gradients

Absolute thermographic temperature metrics demonstrated significant temporal and spatial patterns (Table 5.22). Mean flap temperature decreased from **28.01 ± 1.63°C at T1** to **26.41 ± 1.88°C at T2**, followed by partial stabilization at **26.71 ± 1.92°C at T3** (**Friedman p = 0.0042**). Thermal heterogeneity, quantified as the standard deviation of ROI temperatures within the flap, increased at T2 (**1.92 ± 0.64°C**) compared with T1 (**1.58 ± 0.51°C**), and decreased again at T3 (**1.67 ± 0.55°C**), with a significant overall difference (**p = 0.0315**).

Table 5.22. Temporal evolution of thermographic temperature metrics across intraoperative timepoints (T1–T2–T3)

Metric	T1 (mean ± SD)	T2 (mean ± SD)	T3 (mean ± SD)	Friedman p
Mean flap (°C)	28.01 ± 1.63	26.41 ± 1.88	26.71 ± 1.92	0.0042
Thermal heterogeneity (SD, °C)	1.58 ± 0.51	1.92 ± 0.64	1.67 ± 0.55	0.0315
Central zones (°C)	28.45 ± 1.55	26.86 ± 1.97	26.92 ± 2.08	<0.001
Distal zones (°C)	26.60 ± 1.51	25.95 ± 2.11	25.48 ± 2.01	<0.001

A consistent **central-to-distal thermal gradient** was observed at all timepoints. Central zones demonstrated higher temperatures than distal zones at **T1 (28.45 ± 1.55°C vs 26.60 ± 1.51°C)**, **T2 (26.86 ± 1.97°C vs 25.95 ± 2.11°C)**, and **T3 (26.92 ± 2.08°C vs 25.48 ± 2.01°C)**, with all comparisons reaching high statistical significance (**p < 0.001**). The persistence of this gradient across timepoints is illustrated in **Figure 5.6**.

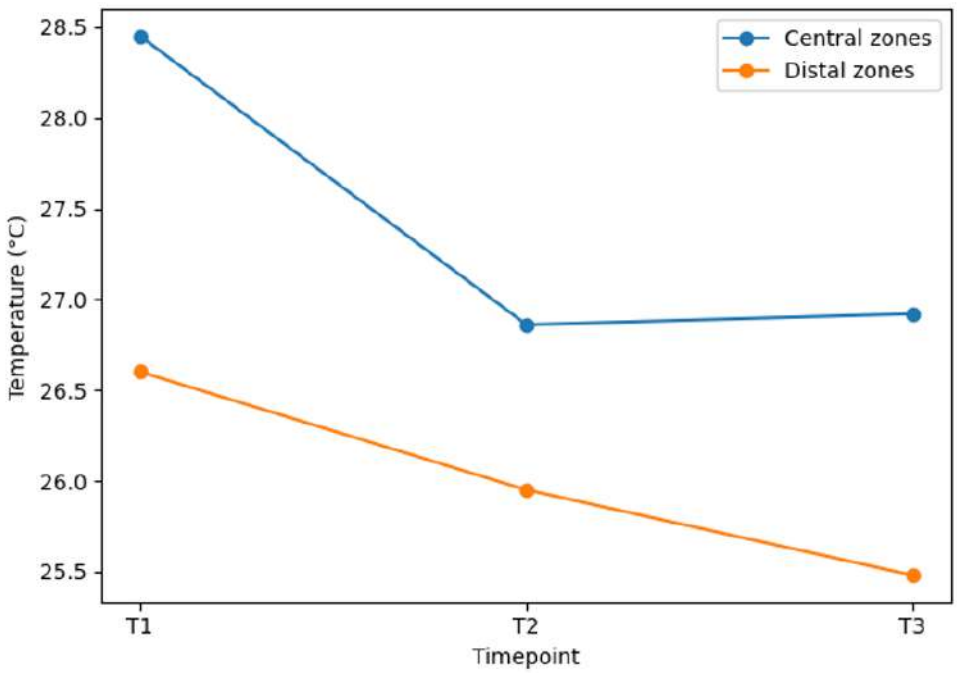


Figure 5.6. *Central vs distal thermographic temperature gradient*

IV. Comparison between baseline and reconstructed physiological states (T1 vs T3)

Because both **T1** (native physiological perfusion) and **T3** (after completion of arterial and dual venous reconstruction) represent relatively stable perfusion states, a direct comparison between these timepoints was performed. At the global level, the perfusion index was significantly higher at T3 than at T1 (**1.833 ± 0.041 vs 1.773 ± 0.091; Wilcoxon p = 0.00058**), accompanied by a significant reduction in non-perfused surface (**1.73 ± 1.47% vs 4.39 ± 2.86%; p = 0.0155**) (Table 5.20). Absolute temperatures remained lower at T3 compared with T1, particularly in distal territories (Table 5.22), while preserving the same central-to-distal gradient. These findings indicate that, although global thermographic perfusion improves from T1 to T3, absolute thermal values do not fully return to baseline levels.

V. Comparison between partial and complete venous outflow (T2 vs T3)

To evaluate the impact of completing venous outflow, thermographic parameters at **T2** (single venous anastomosis) were compared with **T3** (dual venous anastomosis). At the global level, the perfusion index increased numerically from **1.786 ± 0.142 at T2** to **1.833 ± 0.041 at T3**, while the proportion of non-perfused areas decreased from **2.52 ± 2.04%** to **1.73 ± 1.47%** (Table 5.20). Thermal heterogeneity decreased from **1.92 ± 0.64°C at T2** to **1.67 ± 0.55°C at T3** (Table 5.22), indicating increased spatial thermal homogeneity following completion of venous drainage. These changes were most evident in distal territories, where numerical improvements in well-perfused surface were observed (Table 5.21).

VI. Summary of temporal thermographic findings

Standardized dynamic infrared thermography demonstrated the ability to detect **time-dependent, region-specific changes in flap perfusion** across intraoperative stages. Global thermographic perfusion improved significantly from T1 to T3, as reflected by an increase in the perfusion index and a reduction in non-perfused surface. Temporal

variability was preferentially expressed in distal territories, while central zones remained consistently well perfused. Absolute temperature analysis revealed significant temporal changes and a persistent central-to-distal thermal gradient across all timepoints. Together, these findings support the use of thermography as a **dynamic intraoperative tool** capable of capturing both spatial and temporal perfusion patterns independently of angiographic imaging.

5.6 Focused analysis of distal flap territories (zones 1a and 4b)

Given the marked spatial heterogeneity observed in previous analyses, a focused evaluation of the most distal flap territories (zones 1a and 4b) was performed. These regions are anatomically furthest from the dominant perforator and consistently exhibited the lowest perfusion values and the greatest temporal variability across standardized thermographic assessments.

This section specifically addresses the behavior of distal territories using standardized dynamic infrared thermography, integrating zonal comparisons, temporal evolution, and their relationship with global perfusion metrics.

I. Baseline thermographic characteristics of distal territories at T1

At baseline (T1), distal territories demonstrated the most compromised thermographic perfusion profile within the flap. As detailed in Table 5.23 and illustrated in Figure 5.7, distal regions showed significantly lower proportions of well-perfused surface and greater dispersion compared with central territories.

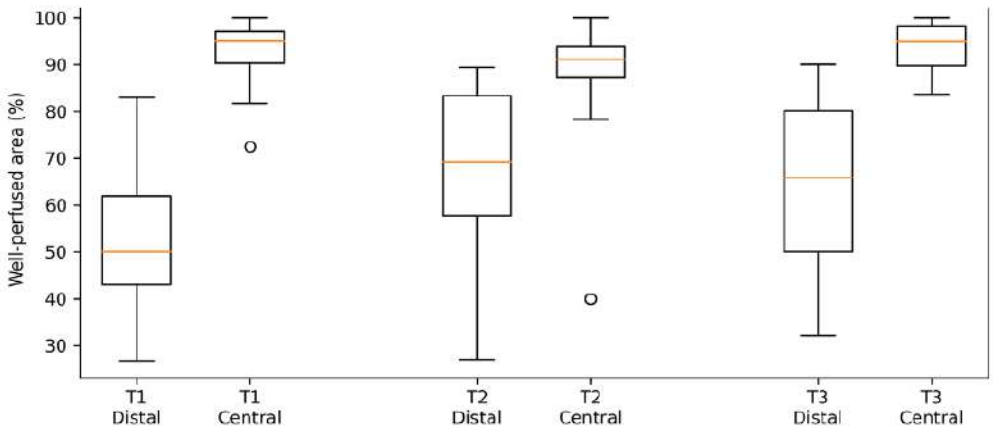


Figure 5.7. *Distal vs Central well-perfused surface across intraoperative timepoints*

Specifically, zone 1a exhibited a mean well-perfused surface of 62.86 ± SD%, with 28.91 ± SD% classified as doubtful and 8.23 ± SD% as non-perfused. Zone 4b demonstrated an even more compromised profile, with only 45.75 ± SD% of the surface classified as well perfused, 43.38 ± SD% as doubtful, and 10.87 ± SD% as non-perfused.

In contrast, central zones (zones 2 and 3) consistently showed well-perfused proportions exceeding 90%, with minimal non-perfused surface. These differences resulted in a clear central-to-peripheral perfusion gradient at baseline, which was visually evident in Figure 5.7 and quantitatively confirmed by paired comparisons (Table 5.23).

Table 5.23. Paired comparison between distal and central territories using standardized thermography

Timepoint	Distal well-perfused (%)	Central well-perfused (%)	Wilcoxon p	Distal non-perfused (%)	Central non-perfused (%)	Wilcoxon p
T1	54.30 ± 16.31	92.54 ± 6.51	0.0000	9.55 ± 6.20	2.68 ± 4.14	0.0010
T2	67.92 ± 17.91	88.37 ± 12.71	0.0001	8.24 ± 7.98	1.96 ± 2.97	0.0074
T3	64.51 ± 18.14	94.05 ± 5.14	0.0002	6.61 ± 8.05	0.12 ± 0.46	0.0109

In addition to categorical perfusion differences, distal territories also exhibited lower absolute thermographic temperatures at T1. Mean distal temperatures were significantly lower than those observed in central regions, confirming the presence of a baseline thermal gradient aligned with the spatial perfusion gradient.

II. Temporal evolution of distal perfusion across intraoperative stages

Across the intraoperative sequence, distal territories demonstrated the greatest degree of temporal variability among all flap regions. Changes in distal perfusion between T1 and T3 were more pronounced than those observed in central territories, albeit with substantial interindividual variability.

As shown in Table 5.24 and summarized graphically in Figure 5.8, distal regions exhibited a greater mean increase in well-perfused surface between T1 and T3 compared with central regions (+8.57 ± 19.78% vs +1.99 ± 5.75%). This increase was accompanied by a reduction in non-perfused surface in distal territories (−1.51 ± 10.09%), whereas changes in central regions were smaller and more homogeneous.

Table 5.24. Magnitude of temporal change (ΔT1–T3) in distal versus central territories using standardized thermography

Metric	Distal Δ (mean ± SD)	Central Δ (mean ± SD)	Wilcoxon p
Δ T1–T3 well-perfused (%)	8.57 ± 19.78	1.99 ± 5.75	0.5791
Δ T1–T3 non-perfused (%)	-1.51 ± 10.09	-3.33 ± 4.56	0.6112

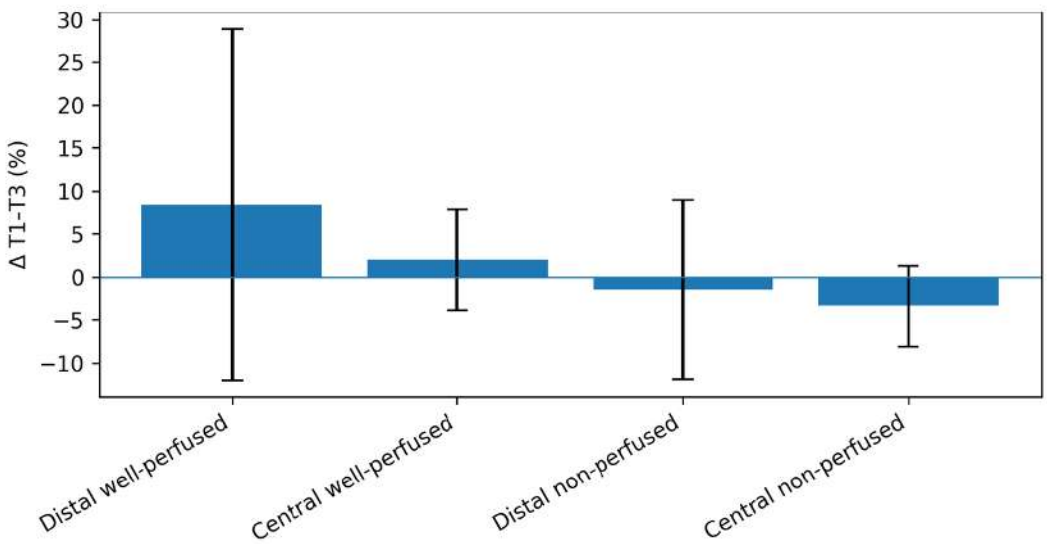


Figure 5.8. *Magnitude of perfusion change between T1 and T3 assessed by standardized thermography*

Despite these numerical differences, paired statistical comparisons did not reach significance, reflecting the wide dispersion of distal responses. This variability contrasts with the relative stability observed in central territories and highlights the sensitivity of distal regions to intraoperative perfusion dynamics.

Temporal analysis across intermediate stages further supported this behavior. Following flap division and partial venous reconnection (T2), distal zones showed the most pronounced fluctuations in both categorical perfusion and temperature metrics, whereas central regions remained largely stable.

III. Distal thermal behavior and intra-flap heterogeneity

Thermographic temperature analysis further emphasized the vulnerability of distal territories. Across all timepoints, distal regions displayed lower absolute temperatures and greater dispersion compared with central zones, contributing disproportionately to intra-flap thermal heterogeneity. On average, distal temperatures remained approximately 1.8–2.0 °C lower than central regions throughout the intraoperative course.

At T2, corresponding to the phase following flap transfer with a single venous anastomosis, distal territories demonstrated the most pronounced temperature decrease. This timepoint coincided with the highest level of physiological stress on the flap and was associated with increased spatial instability of distal perfusion. Specifically, distal zones showed a greater prevalence of doubtful and non-perfused areas, and the highest global thermal heterogeneity observed across timepoints (1.92 ± 0.64 °C), indicating marked spatial variability in heat distribution.

Following completion of the second venous anastomosis (T3), distal temperatures partially stabilized, and overall thermal dispersion decreased (1.67 ± 0.55 °C), reflecting improved spatial homogeneity of the thermographic pattern. Nevertheless, distal temperatures remained consistently lower than those of central regions, and categorical perfusion deficits persisted in a subset of patients, particularly in distal territories, as evidenced by the continued presence of non-perfused and doubtful areas.

IV. Relationship between distal territories and global thermographic behavior

To evaluate the contribution of distal territories to overall flap perfusion, correlations were performed between distal non-perfused surface and global thermographic metrics (Table 5.25). At T1, distal non-perfused surface showed a moderate positive correlation with the global perfusion index, suggesting that baseline global perfusion assessments are partially influenced by distal behavior.

Table 5.25. Correlation between distal non-perfused surface and global thermographic metrics

T1 correlations

Variable	Spearman ρ	p-value
Global perfusion index	0.423	0.0444
Global non-perfused (%)	0.356	0.0954
Global thermal SD	-0.066	0.7634
Mean flap temperature	0.194	0.3758

T3 correlations

Variable	Spearman ρ	p-value
Global perfusion index	-0.167	0.5377
Global non-perfused (%)	0.804	0.0002
Global thermal SD	0.174	0.5184
Mean flap temperature	0.154	0.5692

At T3, a strong positive correlation was observed between distal non-perfused surface and the global non-perfused area of the flap (Spearman ρ = 0.804, p = 0.0002). This relationship is illustrated in Figure 5.9, which demonstrates that increases in distal non-perfused surface are closely associated with higher global non-perfused percentages after completion of venous outflow.

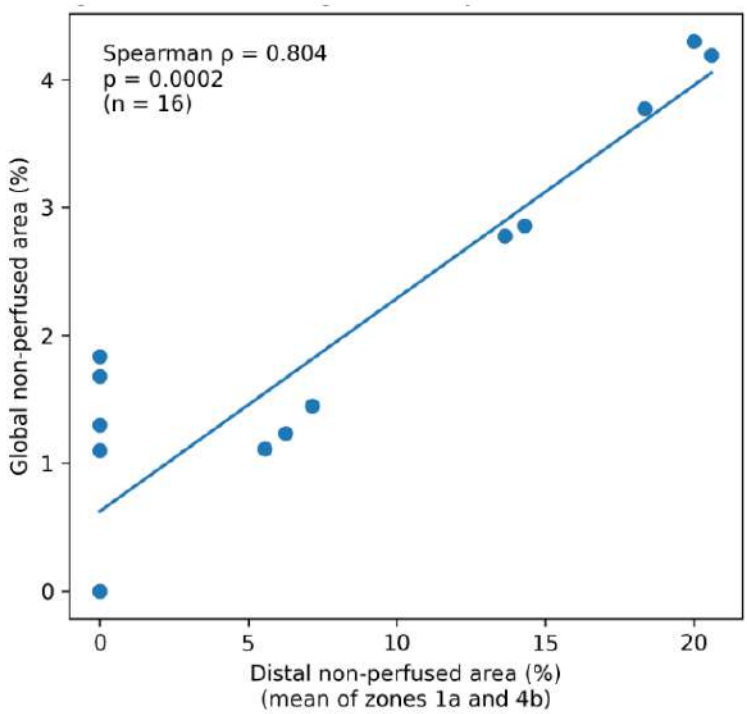


Figure 5.9. *Relationship between distal and global non perfused surface at T3 assessed by standardized thermography*

No significant correlations were observed between distal non-perfused surface and mean flap temperature or global thermal standard deviation, indicating that categorical perfusion deficits in distal territories exert a stronger influence on global perfusion metrics than absolute temperature values alone.

V. Summary of distal territory analysis

In summary, distal flap territories (zones 1a and 4b) represent the regions of greatest perfusion vulnerability and temporal variability within the ALT flap. Standardized thermography consistently identified these zones as having lower baseline perfusion, greater sensitivity to intraoperative changes, and a disproportionate influence on global perfusion metrics. The strong association between distal non-perfusion and global non-perfused surface at T3 underscores the critical role of distal territories in shaping overall perfusion outcomes and supports their prioritization in intraoperative thermographic monitoring.

5.7 Intra-flap thermographic perfusion patterns and zonal temperature distribution (quantitative analysis)

Beyond global perfusion metrics and temporal changes, standardized dynamic infrared thermography enabled a detailed quantitative assessment of the spatial organization of perfusion within the flap. This section analyzes intra-flap thermographic perfusion patterns using zonal percentages and temperature values, focusing on spatial gradients, zonal variability, and reproducibility across patients.

I. Spatial consistency of thermographic perfusion patterns

Across all intraoperative timepoints, thermographic perfusion demonstrated a consistent and structured spatial organization within the flap. Central territories (zones 2 and 3) systematically exhibited the highest proportions of well-perfused surface, while distal territories (zones 1a and 4b) showed lower perfusion values and greater dispersion (Figure 5.7).

At T1, the mean proportion of well-perfused surface exceeded 90% in central zones (94.71% in zone 2 and 90.36% in zone 3), whereas distal zones demonstrated substantially lower values (62.86% in zone 1a and 45.75% in zone 4b). Intermediate zones (1b and 4a) showed transitional perfusion profiles, with well-perfused proportions of 90.81% and 73.44%, respectively. **When zones were grouped for comparative analysis, distal territories showed significantly lower well-perfused surface than central territories across all timepoints (Table 5.23)**.

This spatial hierarchy of perfusion—central > intermediate > distal—was preserved at T2 and T3, with central zones consistently maintaining high well-perfused proportions (>85–90%), while distal zones exhibited wider interindividual variability (Figure 5.7). These findings indicate that standardized thermography captures a stable spatial perfusion pattern within the flap rather than random thermal heterogeneity.

II. Central-to-peripheral perfusion gradients and zonal temperature distribution

Quantitative analysis along the proximal–distal axis revealed a clear central-to-peripheral gradient in both categorical perfusion and absolute temperature values. Mean zonal temperatures were highest in central zones and progressively decreased toward distal territories at all timepoints (Table 5.22).

At T1, mean thermographic temperatures were **28.45 ± 1.55 °C** in central zones compared with **26.60 ± 1.51 °C** in distal zones, confirming a significant baseline thermal gradient. This gradient persisted at T2 and T3, although absolute temperatures varied according to intraoperative stage.

The persistence of parallel gradients in both perfusion categories and absolute temperature values supports the physiological coherence of thermographic spatial mapping and its alignment with the vascular architecture of the ALT flap.

III. Interindividual variability and pattern reproducibility

Despite interindividual variability in absolute perfusion and temperature values, the relative spatial organization of perfusion within the flap was highly reproducible. As summarized in Table 5.23, the standard deviation of well-perfused surface was consistently higher in distal zones than in central zones, reflecting greater variability in distal perfusion behavior.

For example, at T1, the standard deviation of well-perfused surface was **±33.26%** in zone 4b compared with **±7–8%** in central zones, indicating a markedly broader distribution of distal perfusion values across patients. Similar patterns of increased dispersion in distal territories were observed at T2 and T3.

Importantly, even in patients with substantial temporal changes in overall perfusion, the relative ordering of zones according to perfusion status was preserved, with central zones remaining the most consistently perfused regions.

IV. Contribution of zonal behavior to global perfusion metrics

The quantitative influence of zonal behavior on global thermographic metrics was further supported by correlation analysis. At T3, distal non-perfused surface demonstrated a strong positive correlation with the global non-perfused area of the flap (Spearman ρ = 0.804, p = 0.0002; Table 4.25), indicating that increases in distal non-perfusion were closely associated with deterioration of global perfusion status.

In contrast, central zones contributed minimally to global non-perfused percentages, remaining largely stable across patients and timepoints. This relationship is illustrated in Figure 5.9, which demonstrates that distal territories largely determine the global non-perfused burden after completion of venous outflow.

V. Summary of intra-flap spatial thermographic behavior

In summary, standardized dynamic infrared thermography revealed a reproducible and quantitatively defined spatial organization of perfusion within the ALT flap. Central zones consistently demonstrated high and stable perfusion values, whereas distal territories exhibited lower baseline perfusion, greater variability, and a disproportionate influence on global perfusion metrics. These results confirm that thermography provides physiologically meaningful spatial information on intra-flap perfusion and underscore the importance of zonal analysis when interpreting intraoperative thermographic data.

5.8 Compositional concordance between ICG-A and thermography at T1

To further characterize the agreement between indocyanine green angiography (ICG-A) and thermography beyond categorical and percentage-based analyses, a detailed compositional concordance assessment was performed at T1 (baseline, prior to flap division). As perfusion outcomes were expressed as relative proportions of well-perfused, doubtful, and non-perfused tissue summing to 100% within each flap zone, conventional marginal correlations were considered insufficient to fully capture agreement between techniques.

I. Exploratory correlation analysis

As an initial exploratory step, Pearson correlation coefficients were calculated for individual perfusion categories (well perfused, doubtful, and non-perfused) between ICG-A and thermography across flap zones. The resulting correlation matrix is summarized in **Figure 5.10.**

Correlation patterns were heterogeneous and strongly zone dependent. In central regions, correlations were consistently weak to moderate and predominantly negative, with values ranging from **r = −0.21 to −0.09** across zones 2 and 3, none of which reached statistical significance (all **p > 0.30**). In contrast, distal and intermediate zones exhibited greater variability, with both positive and negative correlations observed depending on perfusion category.

The highest correlation coefficient was observed in **zone 4a for the non-perfused category (r = 0.55, p = 0.009)**, indicating a moderate positive association between thermography and ICG-A in this specific territory and category. In other distal regions, correlations were generally weaker and non-significant, including **zone 1a**, where correlation coefficients ranged from **r = 0.08 to 0.40** across categories (all **p > 0.07**).

Overall, these findings indicate that linear associations between modalities are inconsistent and spatially variable, particularly in distal territories, and support the need for compositional approaches to assess concordance between techniques rather than relying on single-category correlation metrics alone.

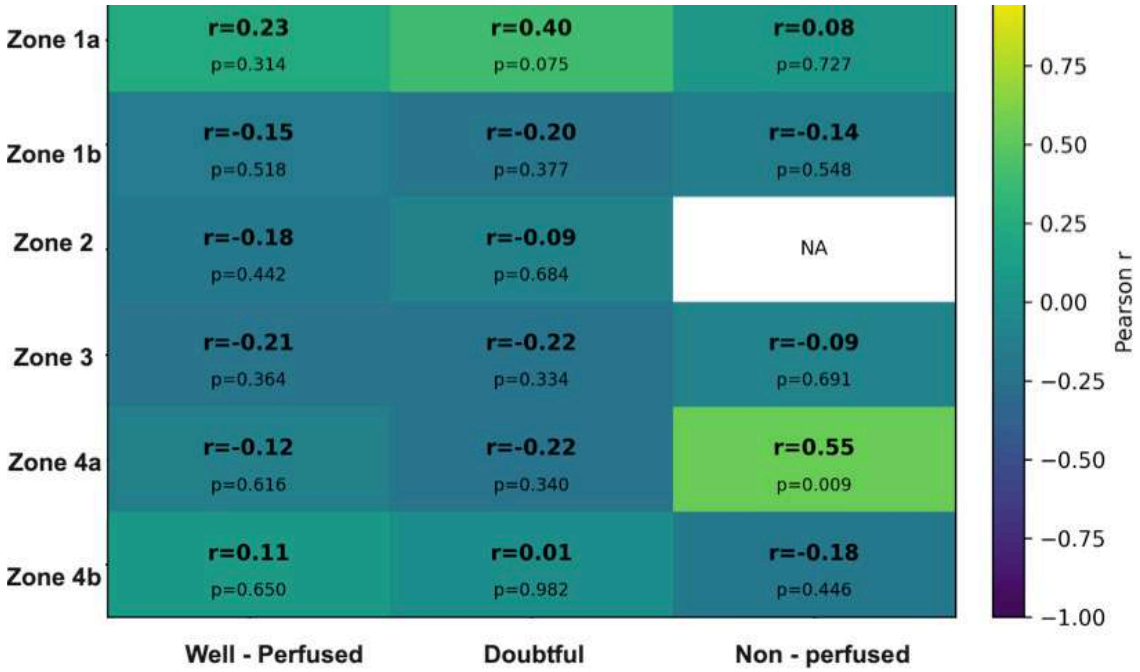


Figure 5.10. *Heat map of Pearson correlations between ICG-A and thermography by flap zone and perfusion category.*

II. Compositional concordance analysis

Formal concordance between ICG-A and thermography was assessed using compositional data analysis methods. Each flap zone was analysed independently (zones 1a, 1b, 2, 3, 4a, and 4b), considering the complete three-part perfusion composition (well-perfused, doubtful, and non-perfused). Concordance was quantified using the Aitchison distance **(Table 5.26)**, which measures the discrepancy between two compositional vectors while accounting for relative redistribution between perfusion categories.

A total of **21 patients** with complete paired data for both modalities across all zones were included in the analysis. Median Aitchison distances demonstrated a clear spatial gradient of concordance across the flap. The **lowest median distances** were observed in central zones, particularly **zone 3 (median 6.84, IQR 7.27)** and **zone 2 (median 7.09, IQR 7.75)**, indicating higher compositional agreement between ICG-A and thermography in these regions.

In contrast, the **greatest compositional discrepancies** were found in distal territories, with the highest median distances in **zone 1a (median 9.37, IQR 2.17)** and **zone 4b (median 9.50, IQR 7.31)**. Intermediate zones (1b and 4a) showed transitional concordance profiles, with median Aitchison distances of **8.01 (IQR 8.47)** and **7.93 (IQR 6.82)**, respectively. This progressive increase in compositional discrepancy from central to distal regions mirrors the spatial variability in perfusion patterns observed in previous analyses.

Table 5.26. Aitchison distance between ICG-A and DIRT by flap zone at T1

Flap zone	Median Aitchison distance	Interquartile range (IQR)
Zone 1a	9.37	2.17
Zone 1b	8.01	8.47
Zone 2	7.09	7.75
Zone 3	6.84	7.27
Zone 4a	7.93	6.82
Zone 4b	9.50	7.31

The distribution of Aitchison distances by flap zone is graphically summarized in the **Figure. 5.11**, illustrating the central-to-distal gradient in compositional concordance.

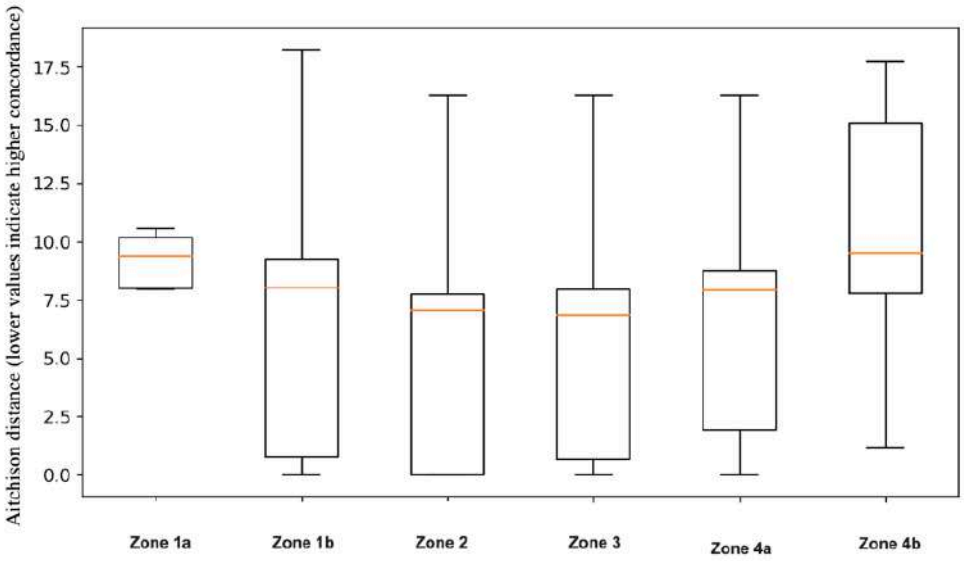


Figure 5.11. Distribution of Aitchison distance between ICG-A and thermography by flap zone at T1

III. Visualization of compositional discrepancies

To facilitate interpretation of compositional discrepancies between indocyanine green angiography (ICG-A) and thermography, ternary plots were generated by anatomical flap region, grouping adjacent subzones. These plots depict the relative distribution of well-perfused, doubtful, and non-perfused tissue at the patient level. In all plots, ICG-A compositions are represented by circular markers and thermographic compositions by triangular markers, with vectors connecting paired observations for each patient.

At the **proximal flap end (zones 1a and 1b)**, ternary plots demonstrated moderate dispersion of perfusion compositions and variable vector lengths between modalities (**Figure 5.12).** Median Aitchison distances in these zones were intermediate to high (zone 1a: **9.37**, zone 1b: **8.01**), reflecting increased compositional discrepancy compared with central regions and heterogeneous redistribution between perfusion categories across patients.

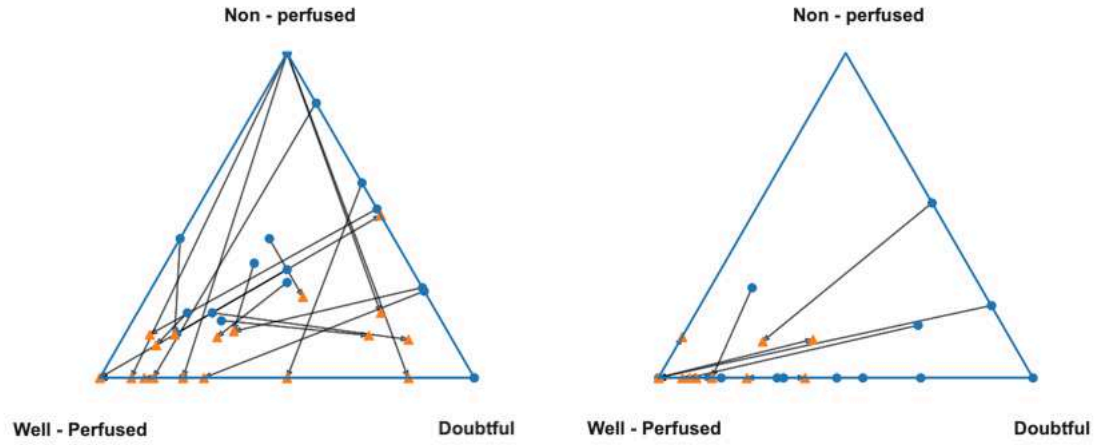


Figure 5.12. *Ternary plots of compositional concordance in proximal flap zones*

In the **central flap region (zones 2 and 3)**, ternary plots showed compact clustering of compositions with limited dispersion and predominantly short, non-directional vectors (**Figure. 5.13)**. These visual patterns are consistent with the lowest median Aitchison distances observed in the study (zone 2: **7.09**, zone 3: **6.84**), indicating high compositional concordance between ICG-A and thermography and minimal redistribution between perfusion categories.

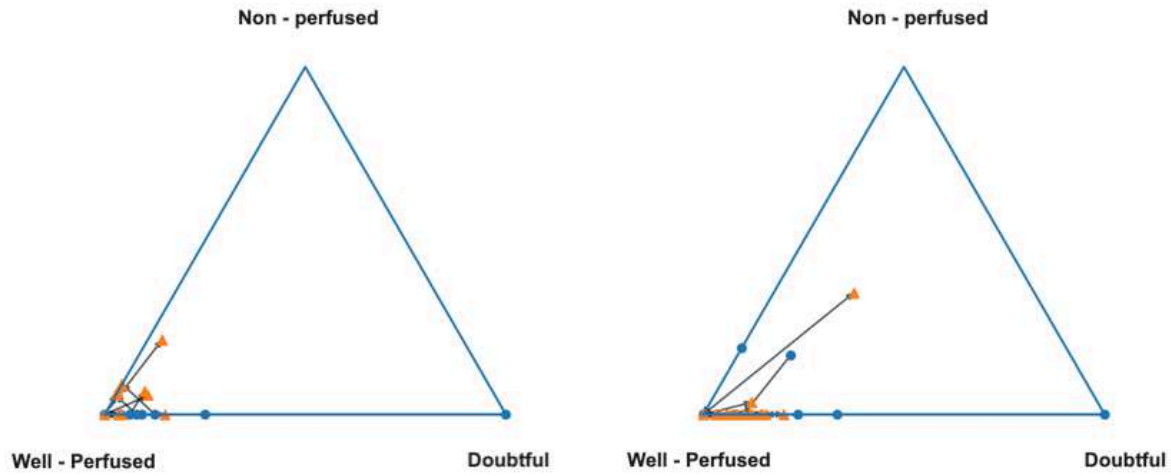


Figure 5.13. Ternary plots of compositional concordance in central flap zones

At the **distal flap end (zones 4a and 4b)**, ternary plots revealed the greatest dispersion of compositions and the longest vectors between modalities (**Figur. 5.14).** These zones corresponded to higher median Aitchison distances (zone 4a: **7.93**, zone 4b: **9.50**) and were characterized by systematic vector orientation toward increased well-perfused classification by thermography relative to ICG-A, reflecting greater compositional discrepancy and heterogeneity in distal territories.

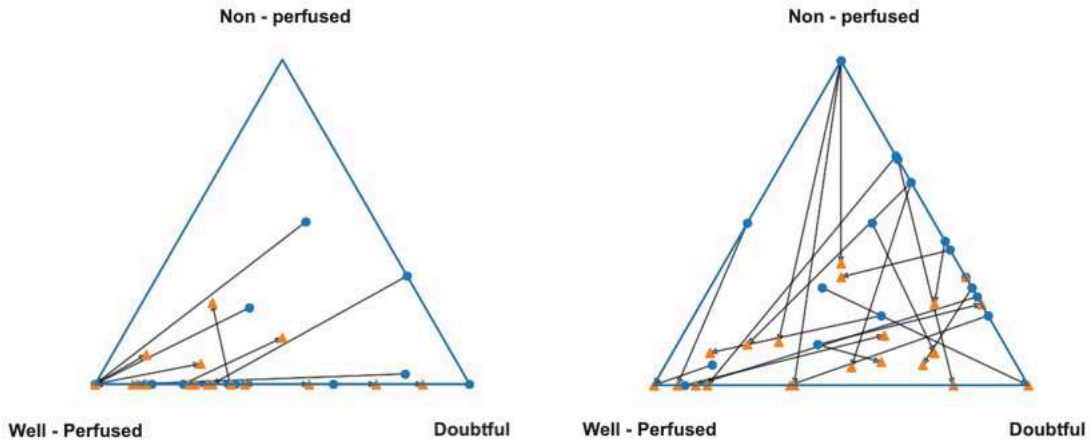


Figure 5.14. *Ternary plots of compositional concordance in distal flap zones*

IV. Proximal versus distal flap ends

To assess whether compositional discrepancies differed between flap ends, Aitchison distances were averaged by patient for the **proximal flap end (zones 1a–1b)** and the **distal flap end (zones 4a–4b)**. Comparative results are summarized in the **Table 5.27.**

Mean Aitchison distance was **8.69 ± 3.12** for proximal territories and **8.72 ± 3.45** for distal territories. No statistically significant difference was observed between proximal and distal flap ends (**p = 0.91**), indicating comparable levels of compositional discrepancy between ICG-A and thermography at both extremities of the flap.

These results suggest that increased disagreement between modalities is a shared characteristic of flap ends rather than being specific to either the proximal or distal extremity.

Table 5.27. Comparison of mean Aitchison distance between proximal and distal flap extremities

Flap region	Mean Aitchison distance	Standard deviation	p value
Proximal flap end (zones 1a–1b)	8.69	3.12	0.91
Distal flap end (zones 4a–4b)	8.72	3.45	

5.9 Diagnostic performance of thermography based on compositional discrepancy

In addition to concordance analysis, the diagnostic performance of thermography was evaluated using indocyanine green angiography (ICG-A) as the reference standard. Zone-level perfusion outcomes were dichotomized into **viable** and **non-viable** categories, yielding a total of **126 paired zone observations**.

The resulting classification performance is summarized in the **Table 5.28**. Thermography correctly identified **107 non-viable zones** (true positives) and **1 viable zone** (true negative). There were **18 false-positive classifications**, while **no false-negative cases** were observed.

Table 5.28. Confusion matrix for thermography using ICG-A as reference standard

	ICG-A non-viable	**ICG-A viable**
Thermography non-viable	107	18
Thermography viable	0	1

Based on these results, thermography demonstrated a **sensitivity of 100%**, a **specificity of 5.3%**, a **positive predictive value of 85.6%**, and a **negative predictive value of 100%**, with an overall diagnostic accuracy of **85.7%**. These findings indicate that zones classified as non-viable by thermography were almost never classified as viable by ICG-A. However, specificity was low, reflecting a tendency of thermography to overestimate perfusion compared with ICG-A, particularly in distal territories.

Receiver operating characteristic (ROC) analysis using the **percentage of non-perfused tissue estimated by thermography** as a continuous predictor is shown in the **Figure 5.15**, yielding modest discriminative performance (**AUC = 0.64**).

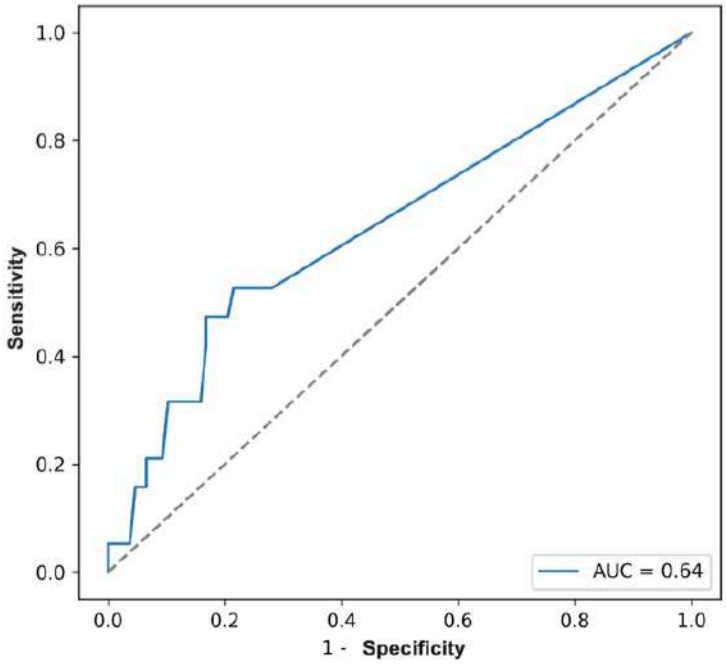


Figure 5.15. *ROC curve for thermography based on percentage of non-perfused area*

In contrast, ROC analysis using the **Aitchison distance between ICG-A and thermography** as a continuous predictor demonstrated improved discrimination (**AUC = 0.77**), as illustrated in the **Figure 5.16**. These results indicate that global compositional discrepancy between modalities provides superior identification of non-viable zones compared with reliance on a single thermographic perfusion category.

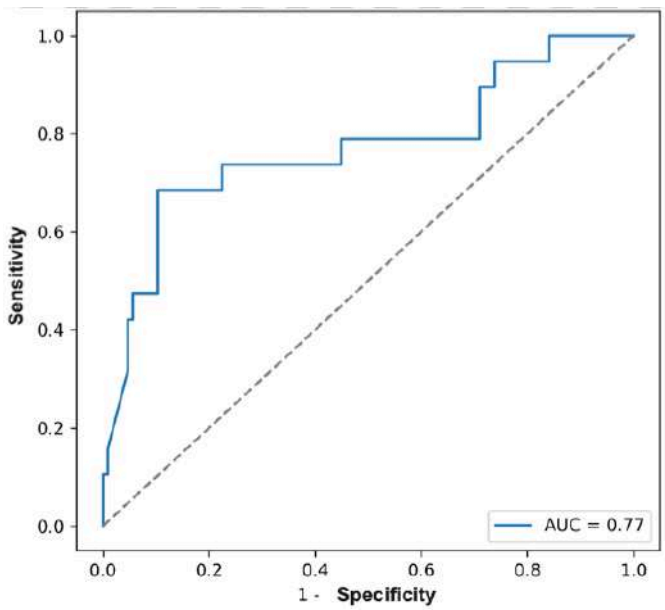


Figure 5.16. *ROC curve for thermography based on Aitchison distance*

Overall, the results demonstrate that thermography captures the global spatial perfusion gradient of the anterolateral thigh flap but shows variable concordance with indocyanine green angiography depending on anatomical region and analytical approach. Quantitative and compositional analyses consistently identified higher agreement in central flap territories and greater discrepancies at flap extremities, particularly in distal zones. While category-based comparisons and linear correlations revealed heterogeneous and zone-dependent associations, compositional analysis provided a more robust framework to characterize redistribution patterns between modalities. Diagnostic performance analyses further highlighted the high sensitivity of thermography for detecting non-viable tissue, albeit at the expense of specificity. Together, these findings define the strengths and limitations of thermography relative to ICG-A and establish the basis for a critical interpretation of their clinical implications.

6

Discussion

6: Discussion

6.1 Summary and global interpretation of the main findings

Lower-limb reconstruction with free tissue transfer remains a cornerstone strategy for limb salvage in complex trauma and oncologic defects, where early coverage, robust vascularity, and reliable wound control are decisive for function and long-term outcome. Classic orthoplastic principles emphasize timing and the biological cost of delayed reconstruction, while contemporary series and systematic reviews confirm that free-flap success is a major determinant of limb preservation and subsequent morbidity.early(1–6) In this context, intraoperative perfusion assessment is clinically relevant not only as a surrogate of immediate flap viability, but also as an actionable parameter guiding decisions such as trimming marginal tissue, revising inset geometry, or optimizing inflow/outflow in borderline situations.

The present study investigated whether standardized dynamic infrared thermography (DIRT) can provide a clinically meaningful evaluation of intraoperative ALT flap perfusion in lower-extremity reconstruction, using indocyanine green angiography (ICG-A) at baseline (T1) as the reference framework. The central message emerging from our results is that thermography offers a consistent, objective, and repeatable characterization of spatial perfusion heterogeneity, but agreement with ICG-A is not uniform across the flap surface. Instead, concordance between modalities is strongly territory-dependent: it is highest in central regions and progressively deteriorates toward flap extremities.

At baseline (T1), central flap zones were predominantly classified as well perfused by both techniques, reflecting expected physiology around the dominant perforator and the relative robustness of adjacent territories. This observation is consistent with established concepts of angiosome/perforasome organization and the progressive reduction of vascular reserve with increasing distance from the source vessels (15–

17,20). From a practical perspective, the “core” of the flap tends to show convergence across modalities because perfusion is abundant, gradients are small, and classification uncertainty is limited. Conversely, distal and proximal ends represent watershed territories where perfusion is more variable and more sensitive to subtle changes in inflow, outflow, tissue handling, and inset geometry (16–20). In lower-limb reconstruction, small marginal deficits at flap ends can have disproportionate clinical consequences, particularly when critical structures (bone, tendon, hardware) are exposed and tolerance for partial breakdown is low.

A second relevant observation is that thermography tended to classify extremity territories as more “well perfused” than ICG-A at baseline, especially in the most vulnerable subzones. This systematic shift suggests that the two modalities are not interchangeable in the territories where decisions are most difficult. The discrepancy is physiologically plausible because ICG-A and DIRT interrogate different signals: ICG-A reflects fluorescence-based intravascular perfusion after tracer injection, whereas thermography reflects surface temperature behavior driven by perfusion-dependent heat transfer and recovery (38,39,47,52–58,63–66). In borderline zones, these signals may diverge due to microvascular recruitment, venous outflow dynamics, ambient conditions, and local heat exchange with underlying tissues.

From the standpoint of real-world intraoperative use, several aspects of ICG-A interpretation deserve emphasis. First, repeated ICG injections may be limited by incomplete washout in some cases, making subsequent control assessments harder to interpret—particularly when transient venous compromise leads to prolonged tracer persistence. Second, ICG-A interpretation is often based on an evolving video sequence (arrival, filling pattern, peak, and washout) rather than on a single static frame. In practice, filling may be delayed, vascular “network” visualization may be poor, and fluorescence may appear diffuse; yet the flap may still be accepted as viable if brightness reaches an apparent peak and no technical cause is identified. This illustrates that commonly used decision cues—arrival time, pattern clarity, and washout—are not uniformly standardized and remain partly experience-driven. Third, distal watershed territories frequently demonstrate delayed filling and intermediate fluorescence. Some

of these areas ultimately behave well, while others do not, highlighting that ICG-A provides a snapshot of perfusion that may not capture subsequent microvascular adaptation, including choke-vessel recruitment. Finally, ICG-A signals can be influenced by systemic and environmental conditions (e.g., vasodilatation with warming), raising the possibility that baseline acquisition conditions may modulate the extent of apparent hypoperfusion in watershed territories. These factors underscore that, while ICG-A is widely used as a reference tool, it is not a perfectly objective ground truth unless acquisition and interpretation are rigorously standardized.

In parallel, the study offered several pragmatic insights regarding thermography. Thermographic assessment is portable and comparatively accessible, which matters because ICG-A platforms are not universally available despite widespread microvascular practice. However, thermography is prone to misinterpretation when users rely on raw color scales: the display is inherently relative (mapped to the hottest and coldest points in the field of view), and inclusion of adjacent warm skin can artificially exaggerate the apparent “coldness” of the flap. This frequently leads observers to equate “blue” with poor perfusion, which may be incorrect when absolute temperature differences are small. Despite these limitations, we observed coherent physiological temperature gradients from central to peripheral territories, supporting that thermography contains meaningful perfusion-related information—consistent with the concept that distal territories contribute disproportionately to intra-flap heterogeneity.(19,64–66)

At the same time, the study highlights that thermography is unlikely to be clinically useful as a standalone tool without improved standardization and software support. Fixed absolute thresholds applied across patients (e.g., universal cut-offs separating perfused from non-perfused tissue) appear unrealistic in the intraoperative setting, given inter-individual variability, differences in systemic perfusion, ambient conditions, flap thickness, and thermal inertia. For clinical translation, a more feasible approach would require real-time, patient-specific standardization (for example, categorization based on each flap’s mean temperature and dispersion), integrated directly into device software to avoid time-consuming manual workflows. Such development would be relevant not

only to routine clinical adoption but also to research reproducibility, enabling consistent categorization without labor-intensive ROI-by-ROI processing.

Finally, important feasibility concerns emerged regarding the dynamic thermography protocol itself. The need for a cooling stimulus and a subsequent recovery interval introduces practical complexity and theoretical risk: transient vasoconstriction, differences in thermoregulatory response, and variability in rewarming kinetics may influence the observed thermal behavior. In free flaps, neural pathways are disrupted, and rewarming depends primarily on convective heat delivered by blood flow and conductive heat exchange with underlying tissues—both of which may vary with flap thickness and inset conditions. These considerations are particularly salient in lower-limb reconstruction, where recipient beds may be relatively cooler and vascular reserve may be compromised compared with trunk reconstruction settings. Taken together, these observations support a nuanced interpretation: thermography can robustly reveal spatial gradients and intra-flap heterogeneity, but its current clinical usability is constrained by workflow and software limitations, and its agreement with ICG-A is most challenged precisely in the watershed territories that matter most surgically.

Overall, the findings suggest that thermography is best viewed as a complementary technology rather than a direct substitute for ICG-A. ICG-A provides a rapid fluorescence-based snapshot of perfusion at a defined moment, whereas thermography—once standardized—may offer repeatable, non-invasive information about spatial gradients and dynamic changes across intraoperative stages. The discordance observed in extremity territories highlights the need for more objective imaging pipelines for both modalities, including quantitative fluorescence metrics for ICG-A and real-time standardized thermal classification for DIRT, ideally validated in larger prospective datasets with clinically meaningful endpoints.

Taken together, these findings support a cautious interpretation of dynamic infrared thermography in the context of lower-limb free flap reconstruction. While standardized thermography reliably captured spatial perfusion gradients and intra-flap heterogeneity, its current performance and workflow constraints do not support its use as a standalone

or replacement modality for indocyanine green angiography in centers where ICG-A is available.

The observed discrepancies between thermography and ICG-A were most pronounced in distal and proximal watershed territories—precisely the regions where intraoperative decisions are most challenging and clinically consequential. In these settings, thermography tended to classify tissue more favorably than ICG-A, suggesting that, in its current form, it may underestimate marginal hypoperfusion or fail to adequately reflect microvascular compromise detectable by fluorescence-based imaging.

Nevertheless, thermography retains potential value as a complementary tool, particularly in environments where ICG-A is unavailable or impractical. Its portability, non-invasiveness, and relative affordability make it attractive from a global and resource-sensitive perspective. However, safe and meaningful clinical adoption would require substantial advances in acquisition protocols, real-time patient-specific standardization, and software-based interpretation support, reducing reliance on subjective color scales and post hoc manual analysis.

Accordingly, dynamic infrared thermography should currently be regarded as an investigational adjunct rather than a definitive intraoperative perfusion assessment modality in lower-limb reconstruction. Its greatest contribution at present lies in highlighting spatial perfusion heterogeneity and prompting further refinement of objective, quantitative imaging strategies—both for thermography itself and for indocyanine green angiography, which also remains subject to interpretative and physiological limitations.

6.2 Agreement between DIRT and ICG-A: what does “agreement” really mean?

In studies comparing imaging modalities for intraoperative perfusion assessment, the concept of “agreement” is frequently oversimplified and often conflated with correlation. While correlation coefficients quantify the strength of association between two variables, they do not necessarily reflect clinical concordance or interchangeability between techniques. This distinction is particularly relevant in flap perfusion assessment, where imaging outputs are not independent scalar measurements but spatially distributed representations of tissue viability.

In the present study, initial analyses demonstrated a moderate-to-strong correlation between global perfusion metrics derived from dynamic infrared thermography and indocyanine green angiography at baseline (T1). Although these findings suggest that both techniques capture related physiological phenomena, correlation alone was insufficient to determine whether thermography could reliably replicate the perfusion information provided by ICG-A, especially at the regional or zonal level.

To address this limitation, agreement was further explored using Bland–Altman analysis for global perfusion parameters. This approach allowed identification of systematic bias between modalities and visualization of the limits within which thermography-derived estimates diverged from ICG-A measurements. While mean differences were acceptable at the whole-flap level, variability increased notably in cases with borderline or heterogeneous perfusion, indicating that global agreement masks relevant regional discrepancies.

More importantly, flap perfusion data are inherently compositional: the proportions of well-perfused, doubtful, and non-perfused tissue within a given zone sum to a constant total. Under these conditions, conventional correlation or difference-based analyses are prone to misinterpretation due to the closure effect, whereby changes in one component necessarily influence the others. This mathematical constraint is rarely acknowledged in surgical perfusion studies but has direct implications for clinical interpretation.

For this reason, compositional data analysis techniques were employed to evaluate agreement between DIRT and ICG-A at the zone and subzone level. By applying centered log-ratio transformation and quantifying discrepancies using the Aitchison distance, the analysis captured global differences in perfusion composition rather than isolated category mismatches. This approach revealed that apparent agreement at the global level often concealed meaningful redistributions between perfusion categories, particularly in flap extremities.

Clinically, this finding is highly relevant. Two imaging techniques may report similar total percentages of “perfused” tissue while disagreeing on whether this tissue is classified as well-perfused, borderline, or frankly non-perfused—a distinction that directly influences intraoperative decision-making. From a reconstructive standpoint, agreement should therefore be understood not as numerical similarity but as consistency in how perfusion risk is spatially and categorically represented.

Taken together, these results underscore that agreement between thermography and ICG-A is context-dependent and scale-sensitive. While acceptable concordance may exist for global assessments, discrepancies emerge when analysis is refined to zones, subzones, and compositional structure. This reinforces the notion that thermography and ICG-A should not be considered interchangeable modalities, but rather tools that capture overlapping yet non-identical dimensions of flap perfusion.

6.3 Spatial heterogeneity of perfusion within the ALT flap

One of the most relevant findings of the present study is the confirmation that perfusion within the anterolateral thigh (ALT) flap is not spatially homogeneous, but instead follows a structured and reproducible pattern of heterogeneity along its longitudinal axis. This observation is consistent with classical angiosome and perforasome theory yet acquires renewed significance when analysed through modern intraoperative imaging modalities such as indocyanine green angiography (ICG-A) and dynamic infrared thermography (DIRT).

In this series, both imaging techniques demonstrated a clear proximal-to-distal gradient in perfusion behavior, with central territories adjacent to the dominant perforator showing more stable and homogeneous perfusion profiles, while flap extremities—both proximal and distal—exhibited greater variability, delayed filling, and increased rates of doubtful or non-perfused areas. Importantly, this heterogeneity was not limited to the distal tip of the flap, which has traditionally been regarded as the most vulnerable region, but was also evident at the proximal extreme, particularly in thin or suprafascial ALT dissections.

This bilateral vulnerability of flap extremities supports the concept that both proximal and distal ends function as watershed territories within the ALT flap. While distal hypoperfusion has been extensively described in the literature, proximal ischemic behavior has gained increasing relevance in contemporary perforator-based flap surgery, where aggressive thinning and suprafascial dissection may disrupt choke vessel networks and reduce collateral inflow. In this context, perfusion becomes increasingly dependent on microvascular recruitment rather than direct arterial supply, rendering these regions more susceptible to transient or sustained hypoperfusion.

The spatial heterogeneity observed in this study also provides a physiological explanation for the discrepancies identified between DIRT and ICG-A. Central zones demonstrated higher concordance between modalities, with smaller compositional distances and more consistent perfusion classification. In contrast, peripheral zones—particularly subzones 1a and 4b—showed greater divergence, reflecting the dynamic

and transitional nature of perfusion in these territories. These discrepancies do not necessarily indicate failure of one modality, but rather underscore the limitations of single-timepoint assessments in regions governed by delayed choke vessel opening and venous outflow adaptation.

From a clinical perspective, these findings challenge the adequacy of global or flap-level perfusion metrics as the sole basis for intraoperative decision-making. A flap that appears globally well perfused may still harbor small peripheral territories at risk of partial necrosis, which are clinically significant in lower-limb reconstruction where exposed structures, narrow flap geometry, and limited redundancy magnify the impact of even minor tissue loss. The present results support a shift toward zonal and subzonal analysis, particularly when evaluating thin ALT flaps intended for distal lower-extremity defects.

Furthermore, the observed spatial heterogeneity highlights a fundamental limitation shared by both DIRT and ICG-A: both techniques capture perfusion at a specific moment in time, without accounting for the delayed recruitment of choke vessels or the temporal evolution of microcirculatory adaptation. Intraoperative imaging therefore represents a snapshot rather than a prediction of long-term perfusion stability. This limitation is particularly relevant in watershed territories, where initial hypoperfusion may resolve—or persist—depending on patient-specific vascular responsiveness, systemic hemodynamics, and postoperative conditions.

The present study reinforces the notion that perfusion assessment in ALT flaps should be interpreted as a spatially structured phenomenon rather than a binary or uniform process. Recognizing and respecting this heterogeneity allows for a more nuanced interpretation of imaging findings and provides a rational framework for understanding why agreement between modalities is highest in central zones and progressively deteriorates toward the flap extremities. Ultimately, this spatial perspective is essential for integrating intraoperative perfusion imaging into meaningful, patient-specific surgical decision-making.

6.4 Temporal intraoperative changes and the role of venous drainage (T1–T2–T3)

A distinctive feature of this study is its longitudinal intraoperative design, allowing assessment of perfusion dynamics across three key surgical timepoints: before flap division (T1), after arterial inflow and single venous drainage (T2), and after completion of dual venous outflow (T3). This temporal framework provides valuable insight into the evolving physiology of free flap perfusion and highlights fundamental differences between arterial inflow, venous drainage, and their respective imaging correlates.

At baseline (T1), perfusion assessment reflects the native vascular environment of the flap, with intact choke vessel networks and physiological venous drainage. In this setting, ICG-A primarily depicts arterial inflow patterns and early microvascular filling, while thermography reflects steady-state cutaneous heat distribution under stable perfusion conditions. Although heterogeneity is already evident at this stage—particularly in peripheral territories—both modalities tend to show relatively coherent perfusion maps.

Following flap transfer and completion of the arterial anastomosis with a single venous outflow (T2), the perfusion landscape changes substantially. This phase represents a critical physiological transition in which arterial inflow may be technically adequate, yet venous drainage capacity remains borderline or insufficient. Clinically, this is often the stage at which surgeons encounter ambiguous findings: delayed filling, diffuse fluorescence without a clear vascular pattern, or patchy washout on ICG-A, despite a patent arterial anastomosis.

In this context, thermography demonstrated a particular sensitivity to changes related to venous congestion. Areas with impaired venous outflow frequently exhibited delayed or reduced thermal recovery, increased thermal heterogeneity, or paradoxical temperature behavior that could not be explained by arterial insufficiency alone. This observation reinforces the concept that venous congestion is not equivalent to arterial hypoperfusion and should not be interpreted as such. Whereas ICG-A primarily visualizes inflow and early capillary filling, thermography captures the downstream consequences

of impaired venous clearance, including altered convective heat transport and stagnation of warm blood within the microcirculation.

The addition of a second venous anastomosis (T3) resulted in further redistribution of perfusion patterns, often with improvement in thermal homogeneity and stabilization of previously borderline territories. Importantly, these changes were not always linear or immediate. In several cases, thermal recovery lagged behind the technical completion of venous drainage, reflecting the time-dependent nature of microvascular adaptation and the progressive recruitment of venous and choke vessel pathways. This non-linearity underscores a critical limitation of static intraoperative imaging: perfusion is a dynamic process, and both DIRT and ICG-A provide snapshots rather than continuous physiological trajectories.

An additional methodological consideration should be acknowledged when interpreting the thermographic changes observed between T2 and T3. Although the improvement in perfusion patterns detected after the completion of the second venous anastomosis may suggest a beneficial effect of increased venous outflow, the present study design does not allow a causal relationship to be definitively established. No comparison group with a single venous anastomosis was included, and therefore the thermographic changes observed between these timepoints could also reflect the physiological adaptation of the flap during the early period following revascularization. Future studies incorporating comparative designs would be required to determine the specific contribution of a second venous anastomosis to flap perfusion dynamics.

The temporal dissociation between arterial inflow, venous drainage, and thermal normalization helps explain some of the discrepancies observed between imaging modalities at different timepoints. While ICG-A may show satisfactory fluorescence shortly after anastomosis, thermography may still reveal persistent thermal deficits, particularly in peripheral or watershed zones. Rather than representing a false-positive finding, this likely reflects delayed venous equilibration or microcirculatory congestion that has not yet resolved at the time of imaging.

These findings emphasize the central role of venous drainage in determining flap perfusion stability and highlight the limitations of interpreting perfusion exclusively through arterial-centric paradigms. Venous congestion, particularly when transient or partial, may not manifest as classical non-perfusion on ICG-A but can significantly influence tissue oxygenation, heat dissipation, and ultimately flap viability. Thermography, by capturing these downstream physiological effects, may therefore provide complementary information that is not accessible through fluorescence angiography alone.

Finally, the non-linear and time-dependent behavior of thermal changes observed in this study reinforces the need for caution when extrapolating intraoperative imaging findings to long-term outcomes. Neither modality can predict with certainty whether delayed choke vessel opening will occur or whether borderline territories will ultimately survive. However, the combined temporal analysis across T1, T2, and T3 offers a richer physiological context, allowing surgeons to interpret perfusion findings not as isolated events but as evolving processes shaped by inflow, outflow, and microvascular adaptation.

6.5 Subjectivity of ICG-A and the need for objective fluorescence quantification

Although indocyanine green angiography (ICG-A) is widely regarded as the current reference technique for intraoperative perfusion assessment, its interpretation in clinical practice remains largely qualitative and operator-dependent. In most reconstructive settings, including the present study, perfusion is ultimately classified visually into ordinal categories (e.g., well perfused, doubtful, non-perfused), based on the surgeon's interpretation of fluorescence intensity, filling pattern, and washout behavior.

This visual, experience-based assessment introduces an inherent degree of subjectivity. Interobserver variability has been previously acknowledged in the literature, particularly in borderline territories showing delayed or heterogeneous fluorescence. Even for experienced surgeons, the distinction between slow arterial inflow, venous congestion, and physiologically delayed filling remains challenging, especially when fluorescence appears diffuse rather than following a clearly recognizable vascular network.

An additional limitation of ICG-A relates to contrast kinetics. In some cases, incomplete washout of indocyanine green after an initial injection may complicate the interpretation of subsequent angiographic assessments performed during the same procedure. This phenomenon is particularly relevant when intraoperative conditions change, such as after revision of the pedicle or completion of an additional venous anastomosis. Residual fluorescence may persist despite improved venous drainage, making it difficult to objectively determine whether observed signal represents true reperfusion or contrast retention from prior injections.

Furthermore, ICG-A findings are influenced by systemic and environmental factors that are not always standardized. Several studies have shown that patient temperature and degree of vasodilation can significantly affect fluorescence patterns, with prewarming associated with a reduction in apparent hypoperfused or watershed zones. This raises the possibility that some areas classified as non-perfused under standard intraoperative conditions might demonstrate improved fluorescence under optimized thermal or

hemodynamic states. Consequently, ICG-A should be interpreted as a snapshot of perfusion under specific physiological conditions, rather than as an absolute predictor of tissue fate.

Another conceptual limitation is that ICG-A primarily reflects intravascular flow at a given moment and does not provide direct information about the future behavior of choke vessels or delayed microvascular recruitment. As a result, distal territories that appear poorly perfused intraoperatively may later recover, while others may progress to partial necrosis despite initially acceptable fluorescence. This temporal uncertainty further complicates the use of rigid visual thresholds to guide definitive intraoperative decisions.

Taken together, these considerations challenge the notion of ICG-A as a fully objective "gold standard." Rather, it should be regarded as a highly sensitive but interpretation-dependent reference technique. This perspective does not diminish its clinical value but underscores the need for more standardized and quantitative approaches to fluorescence analysis. Objective measurement of fluorescence intensity, time-to-peak signal, and washout kinetics—ideally integrated into user-independent software—could substantially improve reproducibility and comparability across patients, centers, and studies.

In this context, the present work highlights the importance of exploring complementary imaging modalities and analytical frameworks that move beyond purely visual classification. The limitations identified in ICG-A interpretation provide a strong methodological rationale for investigating standardized, quantitative tools—such as compositional analysis and thermographic normalization—to better characterize perfusion heterogeneity and uncertainty in complex reconstructive scenarios.

6.6 Strengths and weaknesses of dynamic infrared thermography

Dynamic infrared thermography (DIRT) offers a fundamentally different approach to intraoperative perfusion assessment compared with fluorescence-based techniques. Rather than visualizing intravascular contrast passage, DIRT captures temperature changes at the skin surface as an indirect marker of blood flow and heat delivery. This conceptual difference underlies both its potential strengths and its current limitations.

Strengths of dynamic infrared thermography

One of the principal advantages of DIRT is its **non-invasive nature**. The technique does not require intravenous contrast administration, thereby avoiding the rare but well-documented risks associated with indocyanine green injection, including allergic reactions and dose-related limitations. This allows repeated assessments without cumulative exposure, making DIRT particularly attractive for iterative intraoperative evaluation.

DIRT is also **technically portable and relatively accessible**. Compared with ICG-A systems, thermographic cameras are smaller, less expensive, and easier to integrate into different operative environments. This characteristic has important implications for global surgical practice, as many centers performing complex microsurgical reconstruction do not have access to fluorescence angiography systems. In such settings, DIRT may represent a feasible adjunct or screening tool rather than a definitive replacement.

Another strength lies in the **physiological coherence of spatial thermal gradients**. In this study, thermography consistently demonstrated higher temperatures in central flap regions and progressively lower temperatures toward flap extremities, mirroring well-established principles of perforasome anatomy and distal watershed vulnerability. This concordance suggests that thermography is sensitive to real perfusion-related phenomena rather than random thermal noise.

DIRT also provides **continuous information over time**, rather than a single contrast-dependent snapshot. In principle, dynamic thermal recovery after a cold challenge could offer insight into perfusion responsiveness and vascular reserve. Although this potential was not fully exploited in the present study, it represents a conceptual advantage over static imaging modalities.

Finally, thermography has **educational and exploratory value**. The visualization of thermal gradients can facilitate understanding of flap physiology, particularly for trainees, and may help identify gross perfusion abnormalities or unexpected regional behavior during flap elevation and inset.

Limitations and weaknesses of dynamic infrared thermography

Despite these advantages, several important limitations constrain the current clinical applicability of DIRT.

A major concern is the **requirement for thermal stimulation**, typically involving flap cooling followed by rewarming. Although this maneuver is necessary to generate dynamic contrast, it introduces a potential confounding factor: cold-induced vasoconstriction. In thin or highly dissected perforator flaps, especially in distal lower-limb reconstructions, even transient vasospasm may alter perfusion in a manner that is not purely diagnostic but iatrogenic. Furthermore, interindividual variability in thermoregulatory response means that identical cooling protocols may produce markedly different recovery patterns across patients.

The **interpretation of thermographic images is technically demanding**. Current commercial software relies heavily on relative color scales, which are automatically adjusted to the temperature range within the field of view. As a result, cooler regions may appear pathologic simply because warmer adjacent tissues are included in the frame, even when absolute temperature differences are small and clinically irrelevant. This creates a high risk of misinterpretation by observers unfamiliar with the underlying physics of thermal scaling.

Related to this, DIRT currently lacks **standardized, patient-specific quantitative thresholds**. Absolute temperature cutoffs reported in the literature vary widely and are unlikely to be universally applicable, given interpatient differences in baseline temperature, flap thickness, environmental conditions, and systemic hemodynamics. In this study, meaningful interpretation required normalization of temperatures relative to the flap-specific mean and dispersion, a process that is not currently automated in clinical devices and limits real-time applicability.

DIRT also captures only a **surface thermal phenomenon**, providing no direct information about deeper microvascular flow or venous drainage patterns. Areas may appear warm due to conductive heat transfer from underlying tissues rather than true perfusion, particularly in thinner flaps placed over well-perfused recipient beds. Conversely, viable but poorly insulated regions may appear falsely cold. This limitation complicates the interpretation of small distal territories, which are often the most clinically relevant in ALT flaps.

Another important limitation is that thermography, even when described as “dynamic,” ultimately yields a **static endpoint measurement** in most practical implementations. The present study relied on thermographic images acquired after a defined recovery period, without full temporal analysis of the rewarming curve. As such, the technique does not capture the dynamic evolution of choke vessel recruitment or delayed perfusion improvement, phenomena that are known to influence flap survival but unfold over longer time scales.

Finally, the **clinical predictive value of DIRT remains limited**. While thermography can identify broad perfusion gradients and highlight vulnerable territories, it does not reliably discriminate which small distal regions will ultimately progress to necrosis, particularly in thin ALT flaps where failures often involve only a few square centimeters. In its current form, DIRT should therefore be regarded as an adjunctive tool rather than a standalone decision-making modality.

Overall assessment

Taken together, dynamic infrared thermography represents a promising but immature technology for intraoperative perfusion assessment. Its strengths lie in accessibility, non-invasiveness, and physiologically plausible spatial information, whereas its limitations stem from technical complexity, lack of standardization, and constrained predictive precision. In the present study, these characteristics help explain both the partial concordance with ICG-A and the systematic discrepancies observed in distal flap territories.

6.7 Methodological limitations of the study

Several methodological limitations of the present study should be acknowledged when interpreting the results.

First, the sample size was relatively limited. Although adequate for an exploratory and method-comparison study and consistent with previously published series in intraoperative perfusion assessment, the number of included flaps restricts the statistical power for detecting small effects and limits the generalizability of the findings. As a consequence, some analyses—particularly subgroup and zonal comparisons—should be interpreted as hypothesis-generating rather than definitive.

Second, this was a single-center study, reflecting the surgical technique, intraoperative workflow, and imaging protocols of one institution. While this ensured high internal consistency and standardized acquisition conditions, it may introduce center-specific bias and limits extrapolation to different surgical environments, patient populations, or institutional practices.

Third, indocyanine green angiography was performed exclusively at baseline (T1) and served as the reference standard for perfusion assessment. Consequently, direct angiographic comparison with thermography at later intraoperative stages (T2 and T3) was not available. This design choice reflects common clinical practice and safety considerations but restricts the ability to directly validate thermographic findings against ICG-A after venous outflow modifications.

Fourth, ICG-A perfusion classification was based on a visual ordinal scale (0–1–2), which is inherently subjective and susceptible to interobserver variability. Although classification was performed by experienced surgeons and followed predefined criteria, the lack of quantitative fluorescence intensity measurements represents a limitation and may have influenced zone-level categorization, particularly in borderline territories.

Fifth, no systematic correlation with postoperative clinical outcomes (e.g., partial flap necrosis, delayed wound healing, or need for revision surgery) was performed. As a result, the study focuses on intraoperative perfusion assessment and inter-modality agreement rather than on predictive validity for long-term flap viability.

Sixth, thermographic analysis required controlled cooling and rewarming phases, introducing potential physiological variability related to patient-specific thermoregulation, flap thickness, and environmental factors. Although acquisition conditions were standardized as much as possible, residual variability cannot be completely excluded.

Finally, image analysis relied on manual or semi-manual workflows, including ROI placement and zone delineation. While this approach ensured anatomical accuracy, it is time-consuming and may limit real-time clinical applicability. Automated or semi-automated image processing tools could improve efficiency and reproducibility in future studies.

Taken together, these limitations do not invalidate the findings but define the scope within which the results should be interpreted. Importantly, they also highlight key areas for methodological refinement and future research, many of which are addressed in the following sections.

6.8 What we would do differently if the study were repeated

If this study were to be repeated, several methodological and conceptual refinements would be implemented to strengthen its clinical relevance, robustness, and translational potential.

First, a larger and multicenter cohort would be prioritized. Expanding the sample size across different institutions would increase statistical power, reduce center-specific bias, and allow exploration of inter-institutional variability in surgical technique, patient characteristics, and perfusion behavior. A multicenter design would also facilitate validation of the observed spatial and temporal perfusion patterns across diverse clinical settings.

Second, quantitative indocyanine green angiography would be incorporated instead of, or in addition to, visual ordinal classification. Objective fluorescence intensity measurements—ideally standardized for injection protocol, camera distance, exposure, and timing—would reduce subjectivity and interobserver variability. Quantitative ICG metrics could enable true ROI-level comparison with thermographic data and allow more rigorous modeling of perfusion gradients and thresholds.

Third, dynamic thermographic analysis would be expanded beyond static post-rewarming images. Rather than relying solely on final temperature snapshots, future studies should analyze the full temporal recovery curve following thermal challenge, including rewarming velocity, time-to-peak temperature, and spatial propagation of thermal recovery. These dynamic parameters may better reflect underlying vascular physiology and help distinguish perfusion-driven rewarming from passive heat transfer from surrounding tissues.

Fourth, flap thickness and composition should be systematically recorded and integrated into the analysis. Given the known influence of subcutaneous fat and flap thinning on thermal behavior, incorporating flap thickness measurements—obtained

intraoperatively or from preoperative imaging—would allow adjustment for this important confounder and improve interpretation of thermographic findings.

Fifth, automated or semi-automated image analysis tools should be developed and implemented. Software capable of automatically calculating flap-specific mean temperature, standard deviation, and standardized perfusion categories in real time would greatly enhance clinical feasibility. Ideally, thermographic systems should generate perfusion maps based on patient-specific normalization rather than fixed absolute temperature thresholds.

Sixth, postoperative clinical outcomes should be formally correlated with intraoperative imaging findings. Linking intraoperative perfusion metrics to objective endpoints such as partial flap necrosis, wound complications, or need for revision surgery would allow assessment of predictive validity and clinical utility beyond intraoperative concordance.

Finally, future studies should explore advanced analytical approaches, including machine learning and artificial intelligence. Pattern recognition algorithms trained on combined thermographic, angiographic, and clinical data may help identify complex perfusion signatures that are not apparent through conventional statistical analysis and could support real-time decision-making in the operating room.

In summary, while the present study provides a structured and reproducible framework for comparing dynamic infrared thermography and indocyanine green angiography, future iterations should move toward greater objectivity, automation, and clinical integration. These refinements would help transform thermography from an exploratory research tool into a more practical and reliable adjunct for intraoperative perfusion assessment.

6.9 Clinical implications

The findings of this study have several practical implications for intraoperative decision-making in lower-limb reconstruction using anterolateral thigh flaps, while also delineating clear directions for future clinical application and research.

From a clinical standpoint, dynamic infrared thermography should not be interpreted as a replacement for indocyanine green angiography in centers where ICG-A is readily available. Rather, its value lies in its potential role as a complementary or screening tool, particularly in settings where access to fluorescence angiography is limited or unavailable. In such contexts, thermography—when interpreted with appropriate physiological understanding—may provide useful information regarding global perfusion behavior and spatial gradients within the flap.

One of the most relevant clinical contributions of thermography is its ability to visualize perfusion as a continuous spatial phenomenon rather than as a binary or categorical outcome. The identification of consistent central-to-distal thermal gradients reflects underlying vascular physiology and aligns with established concepts of perforasomes and watershed territories. This makes thermography particularly valuable for educational purposes, helping surgeons—especially those in training—understand perfusion dynamics beyond visual inspection alone.

However, the present results also underscore the limitations of thermography in guiding fine-grained intraoperative decisions. The difficulty in reliably discriminating small, clinically critical areas of hypoperfusion at the level of a few square centimeters limits its utility for deciding precise flap trimming or resection margins in lower-limb reconstruction, where distal tissue loss may have significant functional consequences. This reinforces the need for caution when interpreting thermographic images, especially when relying on absolute temperature values or color scales generated by non-specialized software.

A pragmatic future clinical model would therefore involve a stepwise or algorithmic approach to intraoperative perfusion assessment. Thermography could be used as an initial, rapid screening method to identify global perfusion asymmetries or suspicious territories. In cases where thermographic findings are equivocal or suggest compromised perfusion, targeted confirmation with ICG-A could then be performed. Such an approach would optimize resource utilization while preserving diagnostic accuracy.

6.10 Final synthesis

This thesis explored the role of dynamic infrared thermography as a complementary tool to indocyanine green angiography for intraoperative assessment of perfusion in anterolateral thigh flaps used for lower-limb reconstruction. Rather than focusing on a single metric or categorical outcome, the study approached flap perfusion as a spatial, dynamic, and inherently heterogeneous phenomenon.

The results demonstrate that thermography captures physiologically coherent perfusion gradients across the flap, particularly along the proximal–distal axis, and reflects changes associated with intraoperative events such as flap transfer and completion of venous drainage. However, thermography systematically differed from ICG-A in the classification of perfusion categories, especially in distal and watershed territories, where thermography tended to overestimate well-perfused surface. These discrepancies were not random but spatially structured, reinforcing the concept that “agreement” between modalities cannot be reduced to single-category correlations or binary classifications.

By applying compositional data analysis, this work provides a novel framework for understanding how perfusion categories redistribute across zones when assessed with different imaging techniques. The use of Aitchison distance allowed quantification of global and regional disagreement while preserving the multicomponent nature of perfusion data. This approach revealed that disagreement between thermography and ICG-A is greatest in flap extremities, a finding that aligns with known vascular physiology and perforasome behavior.

Importantly, this thesis also highlights the limitations of considering ICG-A as an unquestionable reference standard. The visual and semi-quantitative nature of ICG interpretation, its sensitivity to systemic and environmental conditions, and its inability to account for delayed microvascular adaptation underscore the need for cautious interpretation of intraoperative fluorescence findings. In this context, thermography should not be viewed as a replacement for ICG-A, but rather as a complementary modality that offers distinct physiological information.

From a clinical perspective, the findings support a pragmatic and hierarchical approach to intraoperative perfusion assessment. Thermography may serve as a rapid, non-invasive method to identify global perfusion asymmetries or suspicious territories, while ICG-A remains valuable for confirmatory assessment in high-risk or ambiguous cases. Such an approach may be particularly relevant in settings with limited access to advanced imaging technologies.

Ultimately, the principal contribution of this work lies not in establishing definitive thresholds or predictive rules, but in advancing a conceptual and methodological framework for studying flap perfusion using multimodal imaging. By emphasizing spatial analysis, compositional concordance, and physiological interpretation, this thesis lays the groundwork for future research aimed at objective, reproducible, and clinically meaningful perfusion assessment. The integration of advanced image analysis, dynamic testing paradigms, and outcome-based validation will be essential steps toward translating these insights into routine reconstructive practice.

6.11 Achievement of the Study Objectives

The present study was designed to address four specific objectives related to the intraoperative evaluation of anterolateral thigh (ALT) flap perfusion using dynamic infrared thermography (DIRT) and indocyanine green angiography (ICG-A). The discussion of the results allows an assessment of the extent to which each of these objectives was achieved and what conclusions can reasonably be drawn from the findings.

Objective 1: Correlation between DIRT and ICG-A after flap elevation

The first objective of this study was to evaluate the correlation between DIRT and ICG-A in the assessment of flap perfusion after flap elevation. The results demonstrated that both techniques consistently identified the region surrounding the dominant perforator as the most reliably perfused area of the flap. This central perfusion pattern was reproducibly detected using both imaging modalities, suggesting that thermographic patterns are capable of reflecting the underlying vascular territories of perforator-based flaps.

However, relevant discrepancies were observed in peripheral areas of the flap. Compared with ICG angiography, thermography showed a more limited capacity to discriminate small areas of relative hypoperfusion. In particular, the temperature variations detected across the flap surface were often subtle and spatially heterogeneous, making it difficult to reliably identify areas smaller than approximately 1 cm^2 that could potentially be at risk of compromised perfusion. This limitation is likely related to the spatial resolution of thermographic imaging and to the indirect nature of temperature-based perfusion assessment.

Therefore, while the results support the ability of DIRT to identify global spatial perfusion patterns, they also suggest that thermography may be less precise than ICG angiography for detecting small areas of impaired perfusion. Consequently, the first objective can be considered achieved in terms of demonstrating a general correlation of perfusion

patterns between both techniques, although the limitations of thermography in detecting small areas of potential risk must be acknowledged.

Objective 2: Thermographic behaviour of the flap over time

The second objective of the study was to analyse the thermographic behaviour of the flap following transfer over time. Sequential thermographic assessments performed at the defined intraoperative time points (T1, T2 and T3) demonstrated that the thermal distribution of the flap is dynamic and evolves after revascularization. These findings suggest that flap perfusion is not a static phenomenon but rather reflects a process of microcirculatory adaptation during the early intraoperative period.

DIRT proved particularly useful in illustrating these dynamic changes, allowing visualization of progressive thermal redistribution across the flap surface following vascular anastomosis. This temporal behaviour may reflect physiological mechanisms such as microvascular recruitment, changes in venous outflow conditions, or redistribution of blood flow within the perforator territory.

At the same time, it is important to recognize that thermographic measurements are highly sensitive to external and technical factors. Surface temperature may be influenced by ambient temperature, operating room conditions, tissue exposure time, camera calibration, and other environmental variables. As a result, thermography may present a higher degree of variability compared with techniques that directly visualize vascular flow. These factors should be taken into account when interpreting thermographic findings and represent an inherent limitation of the method.

Nevertheless, the present study successfully characterized the temporal thermographic behaviour of ALT free flaps during intraoperative revascularization. Therefore, the second objective of the study can be considered achieved.

Objective 3: Thermographic changes after completion of a second venous anastomosis

The third objective of the study was to evaluate the thermographic changes associated with the completion of a second venous anastomosis. In several cases, the

thermographic images obtained after the second venous anastomosis showed a more homogeneous distribution of temperature across the flap surface when compared with the patterns observed immediately after the initial revascularization.

These findings may suggest that additional venous drainage could influence the thermal behaviour of the flap and potentially improve perfusion dynamics. However, the present study design does not allow a causal relationship to be established between the completion of the second venous anastomosis and the observed thermographic changes. Because no comparison group with a single venous anastomosis was included, it is equally plausible that the changes observed between T2 and T3 represent the natural physiological adaptation of the flap during the first minutes after revascularization.

For this reason, the results of the present study should be interpreted as descriptive observations rather than definitive evidence of the specific effect of a second venous anastomosis. Nevertheless, these findings raise the possibility that thermography may be particularly sensitive to changes related to venous drainage and venous congestion, an aspect that deserves further investigation. Future studies specifically designed to evaluate venous outflow conditions may help clarify whether DIRT could provide clinically relevant information regarding venous physiology in free flaps.

Accordingly, the third objective of the study was partially achieved: the study was able to describe thermographic changes associated with this surgical step, but it cannot definitively determine their underlying cause.

Objective 4: Relationship between thermographic distribution and ICG-A perfusion categories

The fourth objective was to explore the relationship between thermographic distribution and the perfusion categories identified by ICG angiography. The results demonstrated that both techniques generally agreed in identifying the best-perfused regions of the flap, particularly in areas adjacent to the dominant perforator. This

agreement supports the concept that thermographic imaging can reflect the global distribution of perfusion within the flap.

However, the correlation between thermographic findings and ICG-A perfusion categories was less consistent in peripheral or borderline areas. These discrepancies likely reflect the intrinsic differences between both technologies. While ICG angiography directly visualizes vascular perfusion through fluorescence imaging, thermography evaluates perfusion indirectly through changes in surface temperature following a thermal stimulus.

DIRT assessment requires the application of a cooling stimulus to generate a detectable rewarming pattern. Although this maneuver allows visualization of perfusion dynamics, it may also contribute to variability in peripheral regions of the flap. After cooling, the rewarming process depends on local perfusion but also on heat diffusion through surrounding tissues and environmental conditions. As a result, the time required for peripheral areas to recover their baseline temperature may be longer and more heterogeneous than in well-perfused central regions. In the present study, thermographic acquisition was performed within a standardized intraoperative timeframe; however, it is possible that longer observation periods might allow peripheral regions to gradually rewarm, potentially reducing some of the variability observed in these areas.

In contrast, ICG angiography relies on the intravascular distribution of the fluorescent dye, which reaches perfused tissues regardless of surface temperature. This fundamental difference between the two techniques may explain why ICG-A was able to delineate peripheral perfusion territories more clearly than thermography under the same conditions.

Furthermore, the cooling stimulus required for DIRT represents a practical limitation of the technique. Excessive cooling could theoretically induce vasospasm or alter microvascular behaviour in delicate reconstructive settings. For these reasons, while the fourth objective was achieved in demonstrating a general relationship between

thermographic patterns and ICG-A perfusion categories, the limitations inherent to temperature-based perfusion assessment must be carefully considered when interpreting these results.

Overall interpretation

Taken together, the findings of this thesis indicate that dynamic infrared thermography is capable of detecting spatial patterns of perfusion in ALT free flaps and of illustrating the dynamic behaviour of flap perfusion during the intraoperative period. The technique demonstrated a reasonable agreement with ICG angiography in identifying the dominant perforator territory and the general gradient of perfusion across the flap.

At the same time, the results highlight several important limitations of thermography as an intraoperative perfusion assessment tool. Compared with ICG angiography, DIRT appears less precise in identifying small areas of compromised perfusion, particularly when temperature differences are subtle and spatially heterogeneous. In addition, thermographic measurements are highly dependent on environmental conditions and technical factors, which may introduce variability in the interpretation of results.

For these reasons, the findings of the present study do not support the use of thermography as a direct replacement for ICG angiography in clinical decision-making. Rather, DIRT should be understood as a complementary technique that may provide additional physiological insight into flap perfusion dynamics.

In particular, the potential sensitivity of thermography to changes related to venous drainage suggests that this technology could contribute to a better understanding of venous physiology in perforator flaps. However, this hypothesis cannot be confirmed within the framework of the present study and should be explored in future research specifically designed to investigate this aspect.

Future studies incorporating improved thermographic equipment, higher spatial resolution, longer observation times for thermal recovery, and experimental designs focused on venous physiology may further clarify the potential clinical role of dynamic infrared thermography in microsurgical reconstruction.

7

Conclusions

7: Conclusions

1. **Dynamic infrared thermography (DIRT) demonstrated a consistent spatial and physiological relationship with intraoperative flap perfusion in anterolateral thigh (ALT) flaps**, showing temperature gradients that followed expected perforator-based vascular territories from central to peripheral regions. These findings support DIRT as a technique capable of capturing meaningful perfusion-related information at both regional and zonal levels.

2. **Agreement between DIRT and indocyanine green angiography (ICG-A) was moderate and zone-dependent**, particularly at baseline (T1), with higher concordance in central territories and greater discrepancy in peripheral watershed zones. This indicates that "agreement" between techniques should not be interpreted as equivalence, but rather as complementary perspectives on different physiological aspects of flap perfusion.

3. **Temporal intraoperative changes after venous anastomosis highlighted fundamental differences between arterial inflow and venous outflow phenomena**, with thermography showing sensitivity to dynamic changes related to venous drainage that were not always clearly distinguishable using ICG-A alone. These findings emphasize that venous congestion and arterial hypoperfusion represent distinct pathophysiological entities that cannot be fully characterized by a single imaging modality.

4. **Despite its practical advantages, DIRT cannot currently replace ICG-A in centers where fluorescence angiography is available**, due to limitations related to temperature dependency, technical complexity, and lack of standardized software-based interpretation. However, DIRT may serve as a valuable complementary or screening tool—particularly in resource-limited settings—provided that its physiological constraints are understood and that future developments enable automated, patient-specific thermal standardization.

8

Future lines

8: Future lines

Beyond its current clinical application, this work highlights several future research directions that may substantially expand the role of thermography in reconstructive microsurgery.

First, future studies should move beyond static temperature measurements and explore high-resolution, pixel-by-pixel analysis of thermographic dynamics, particularly during controlled thermal challenges. Rather than focusing solely on absolute temperature values, the velocity and spatial propagation of thermal recovery may provide more physiologically meaningful indicators of tissue perfusion. Dynamic recovery curves at the pixel level could help distinguish regions that rewarm predominantly through active blood flow from those that equilibrate via conduction from surrounding tissues.

Second, alternative stimulation paradigms should be investigated to improve feasibility and reduce the theoretical risks associated with external cooling. One promising concept would be a “thermal bolus” perfusion test, consisting of transient perfusion of the flap circulation with warm saline through the vascular pedicle (e.g., via a catheterized arterial limb or controlled intraluminal irrigation under standardized conditions). This could potentially generate an immediate and quantifiable thermographic signal without requiring surface cooling, allowing assessment of intravascular heat delivery and distribution across the flap. If validated, such a protocol might enable rapid intraoperative thermographic testing that is more compatible with clinical workflows.

Third, the development of multimodal imaging platforms deserves further exploration. Hybrid systems combining infrared thermography and near-infrared fluorescence imaging—through synchronized acquisition or real-time image fusion—could enable direct spatial comparison between thermal and fluorescence signals. Overlaying thermographic and ICG-A data within a unified software environment may enhance interpretation, reduce subjectivity, and facilitate region-specific correlation analyses.

Fourth, advances in image processing and artificial intelligence are likely to play a central role. Automated algorithms trained on large datasets could identify subtle thermal gradients, recovery kinetics, or spatial signatures not easily recognized by human observers. Such tools could support objective classification at ROI or pixel level and improve reproducibility.

Finally, to establish predictive validity, future studies should incorporate outcome-based validation strategies. Because in humans intraoperative decisions frequently lead to resection of territories considered non-viable by ICG-A, direct comparison between imaging predictions and subsequent necrosis is inherently limited. Therefore, animal models may provide a more appropriate platform to evaluate the true capacity of thermography (alone or combined with ICG-A) to discriminate tissue destined for necrosis, allowing controlled preservation of borderline territories and systematic follow-up.

In summary, the future of thermography in reconstructive microsurgery lies not in replicating existing techniques, but in developing physiology-driven dynamic metrics, improved stimulation protocols, and integrated multimodal analysis pipelines. With appropriate technological refinement and validation, thermography could evolve from an exploratory adjunct into a more clinically actionable component of intraoperative perfusion assessment.

9

Bibliography

9: Bibliography

1. Early Microsurgical Reconstruction of Complex Trauma for Extremities (Godina, 1986).
2. Gustilo RB, Anderson JT. Prevention of infection in the treatment of one thousand and twenty-five open fractures of long bones: retrospective and prospective analyses. JBJS [Internet]. 1976;58(4). Available from: https://journals.lww.com/jbjsjournal/fulltext/1976/58040/prevention_of_infection_in_the_treatment_of_one.4.aspx
3. Yazar S, Lin CH, Wei FC. One-stage reconstruction of composite bone and soft-tissue defects in traumatic lower extremities. Plast Reconstr Surg. 2004;114(6):1457–66. doi:10.1097/01.PRS.0000138811.88807.65 PubMed PMID: 15509933.
4. Bigdeli AK, Gazyakan E, Schmidt VJ, Bauer C, Germann G, Radu CA, et al. Long-Term Outcome after Successful Lower Extremity Free Flap Salvage. J Reconstr Microsurg. 2019;35(4):263–9. doi:10.1055/s-0038-1675146 PubMed PMID: 30326522.
5. Serra PL, Boriani F, Khan U, Atzeni M, Figus A. Rate of Free Flap Failure and Return to the Operating Room in Lower Limb Reconstruction: A Systematic Review. Journal of Clinical Medicine. Multidisciplinary Digital Publishing Institute (MDPI); 2024. doi:10.3390/jcm13154295
6. Culliford IV AT, Spector J, Blank A, Karp NS, Kasabian A, Levine JP. The fate of lower extremities with failed free flaps: A single institution's experience over 25 years. Ann Plast Surg. 2007 Jul;59(1):18–21. doi:10.1097/01.sap.0000262740.34106.1b PubMed PMID: 17589253.
7. Sushruta, Bhishagratna KKL. An English Translation of the Sushruta Samhita. Calcutta, India: K.K. Bhishagratna; 1918.
8. Curtorum Chirurgia (Tagliacozi, 1597).
9. Fang F, Chung KC. An Evolutionary Perspective on the History of Flap Reconstruction in the Upper Extremity. 2014. doi:10.1016/j.hcl.2013.12.001
10. Gillies H. PRACTICAL USES OF THE TUBED PEDICLE FLAP. Report.
11. Contribution of the Axial and Perforator Vasculature to Circulation in Flaps (Fujino, 1967).
12. Experimental myocutaneous studies (Mccraw, 1977).
13. Song Y guang, Chen G zhang, Song Y liang. The free thigh flap: a new free flap concept based on the septocutaneous artery. Br J Plast Surg. 1984;37(2):149–59. doi:10.1016/0007-1226(84)90002-X PubMed PMID: 6713155.
14. Koshima I, Soeda S. Inferior epigastric artery skin flaps without rectus abdominis muscle Cm? 1. Joumol ofPlastic Surgery. 1989. Report.
15. Taylor GI, Palmer JH. The vascular territories (angiosomes) of the body: experimental study and clinical applications. Vol. 40. 1987. Report.
16. Taylor GI, Corlett RJ, Dhar SC, Ashton MW. The anatomical (angiosome) and clinical territories of cutaneous perforating arteries: Development of the concept

and designing safe flaps. Plast Reconstr Surg. 2011 Apr;127(4):1447–59. doi:10.1097/PRS.0b013e318208d21b PubMed PMID: 21460653.
17. Saint-Cyr M, Wong C, Mark Schaverien M, Ali Mojallal M, Rohrich RJ. The Perforasome Theory: Vascular Anatomy and Clinical Implications. Report.
18. The delay phenomenon (Dhar, Taylor, 1999).
19. Chubb DP, Taylor GI, Ashton MW. True and "choke" anastomoses between perforator angiosomes: Part ii. dynamic thermographic identification. Plast Reconstr Surg. 2013 Dec;132(6):1457–64. doi:10.1097/01.prs.0000434407.73390.82 PubMed PMID: 24281576.
20. Taylor GI, Corlett RJ, Ashton MW. The functional angiosome: Clinical implications of the anatomical concept. Plast Reconstr Surg. 2017;140(4):721–33. doi:10.1097/PRS.0000000000003694 PubMed PMID: 28953725.
21. Koshima I, Fukuda H, Utunomiyaand R, Soeda S. The anterolateral thigh flap; variations in its vascular pedicle. British Journal of Plastic Surgery. 1989. Report.
22. Anatomical variations and technical problems of tha ALT (Kimata, 1998).
23. Wei FC. https://www.microsurgeon.org/anterolateralthigh. 2026. Anterolateral Thigh Flap.
24. Ali RS, Bluebond-Langner R, Rodriguez ED, Cheng MH. The versatility of the anterolateral thigh flap. Plastic and Reconstructive Surgery. 2009. doi:10.1097/PRS.0b013e3181bcf05c PubMed PMID: 19952707.
25. Adani R, Tarallo L, Marcoccio I, Cipriani R, Gelati C, Innocenti M. Hand reconstruction using the thin anterolateral thigh flap. Plast Reconstr Surg. 2005 Aug;116(2):467–73. doi:10.1097/01.prs.0000173059.73982.50 PubMed PMID: 16079675.
26. Zeng A, Qiao Q, Zhao R, Song K, Long X. Anterolateral thigh flap-based reconstruction for oncologic vulvar defects. Plast Reconstr Surg. 2011 May;127(5):1939–45. doi:10.1097/PRS.0b013e31820e9223 PubMed PMID: 21532422.
27. Hong JP. Reconstruction of the diabetic foot using the anterolateral thigh perforator flap. Plastic and Reconstructive Surgery. 2006. p. 1599–608. doi:10.1097/01.prs.0000207057.16292.8f PubMed PMID: 16641732.
28. Hsu CC, Lin Y Te, Lin CH, Lin CH, Wei FC. Immediate emergency free anterolateral thigh flap transfer for the mutilated upper extremity. Plast Reconstr Surg. 2009 Jun;123(6):1739–47. doi:10.1097/PRS.0b013e3181a65b00 PubMed PMID: 19483573.
29. Hong JP, Shin HW, Kim JJ, Wei FC, Chung YK. The use of anterolateral thigh perforator flaps in chronic osteomyelitis of the lower extremity. Plast Reconstr Surg. 2005 Jan;115(1):142–8. doi:10.1097/01.PRS.0000138750.54859.AC PubMed PMID: 15622244.
30. Park JE, Rodriguez ED, Bluebond-Langer R, Bochicchio G, Christy MR, Bochicchio K, et al. The anterolateral thigh flap is highly effective for reconstruction of complex lower extremity trauma. Journal of Trauma - Injury, Infection and Critical Care. 2007 Jan;62(1):162–5. doi:10.1097/01.ta.0000250599.84033.1f PubMed PMID: 17215749.
31. Mureau MAM, Posch NAS, Meeuwis CA, Hofer SOP. Anterolateral thigh flap reconstruction of large external facial skin defects: A follow-up study on functional and aesthetic recipient- and donor-site outcome. Plast Reconstr Surg.

2005 Apr;115(4):1077–86. doi:10.1097/01.PRS.0000156153.17258.CE PubMed PMID: 15793449.
32. Have we found the ideal flap - 672 ALT (Wei, 2002).
33. Duan A. Evaluating the clinical efficacy of the anterolateral thigh flap in lower limb reconstruction surgeries: a systematic review and meta-analysis. Am J Transl Res. 2024;16(7):3326–37. doi:10.62347/hfve6316
34. Wen J, Zhou Z, Boey J, Yu L, Marei AE, Meng F, et al. Clinical evaluation of orthoplastic limb salvage protocol using anterolateral femoral free flap and kickstand fixation: A retrospective case-control study. Foot. Churchill Livingstone; 2025. doi:10.1016/j.foot.2025.102176 PubMed PMID: 40541043.
35. Bennice J, Puig Dubois J, Gallucci GL, De Carli P, Boretto JG. Versatilidad del colgajo libre anterolateral de muslo en la reconstrucción de defectos de cobertura en los miembros superiores e inferiores. [Versatility of the anterolateral thigh free flap in upper and lower extremities defects coverage reconstruction.]. Revista de la Asociación Argentina de Ortopedia y Traumatología. 2018 Aug 19;83(3):167–78. doi:10.15417/issn.1852-7434.2018.83.3.812
36. Min K, Hong JP, Suh HP. Risk Factors for Partial Flap Loss in a Free Flap: A 12-Year Retrospective Study of Anterolateral Thigh Free Flaps in 303 Lower Extremity Cases. Plast Reconstr Surg. 2022 Nov 1;150(5):1071E-1081E. doi:10.1097/PRS.0000000000009646 PubMed PMID: 36067478.
37. Jallali N, Ridha H, Butler PE. Postoperative monitoring of free flaps in UK plastic surgery units. Microsurgery. 2005;25(6):469–72. doi:10.1002/micr.20148 PubMed PMID: 16134095.
38. Hope-Ross M, Yannuzzi LA, Gragoudas ES, Guyer DR, Slakter JS, Sorenson JA, et al. Adverse Reactions due to Indocyanine Green. Ophthalmology. 1994;101(3):529–33. doi:10.1016/S0161-6420(94)31303-0 PubMed PMID: 8127574.
39. Lu CH, Hsiao JK. Indocyanine green: An old drug with novel applications. Tzu Chi Medical Journal. Wolters Kluwer Medknow Publications; 2021. p. 317–22. doi:10.4103/tcmj.tcmj_216_20
40. Flower RW. Injection technique for indocyanine green and sodium fluorescein dye angiography of the eye. Report.
41. Flower RW, Hochheimer BF. A clinical technique and apparatus for simultaneous angiography of the separate retinal and choroidal circulations. Report.
42. ICG for flaps (Still, 1999).
43. ICG for axial flap (Eren, 1995).
44. ICG in rats flap model (Rubben, 1994).
45. Krishnan KG, Schackert G, Steinmeier R. The role of near-infrared angiography in the assessment of post-operative venous congestion in random pattern, pedicled island and free flaps. Br J Plast Surg. 2005 Apr;58(3):330–8. doi:10.1016/j.bjps.2004.10.003 PubMed PMID: 15780227.
46. Surface Quantification of Injected Fluoresecein as a Predictor of Flap Viability (Graham, 1982) .
47. Holm C, Mayr M, Höfter E, Becker A, Pfeiffer UJ, Mühlbauer W. Intraoperative evaluation of skin-flap viability using laser-induced fluorescence of indocyanine

green. Br J Plast Surg. 2002;55(8):635–44. doi:10.1054/bjps.2002.3969 PubMed PMID: 12550116.
48. The superior cosmetic results of nipple-sparing mastectomies (NSM) account for the [Internet]. doi:10.3978/j.issn.2227-684X.2015.04.15
49. Pruimboom T, Schols RM, Van Kuijk SMJ, Van Der Hulst RRWJ, Qiu SS. Indocyanine green angiography for preventing postoperative mastectomy skin flap necrosis in immediate breast reconstruction. Cochrane Database of Systematic Reviews. 2019 Mar 14;2019(3). doi:10.1002/14651858.CD013280
50. Munabi NCO, Olorunnipa OB, Goltsman D, Rohde CH, Ascherman JA. The ability of intra-operative perfusion mapping with laser-assisted indocyanine green angiography to predict mastectomy flap necrosis in breast reconstruction: A prospective trial. Journal of Plastic, Reconstructive and Aesthetic Surgery. 2014;67(4):449–55. doi:10.1016/j.bjps.2013.12.040 PubMed PMID: 24507962.
51. Sood M, Glat P. Potential of the SPY intraoperative perfusion assessment system to reduce ischemic complications in immediate postmastectomy breast reconstruction. Ann Surg Innov Res. 2013 Jul 23;7(1). doi:10.1186/1750-1164-7-9
52. Matsui A, Lee BT, Winer JH, Laurence RG, Frangioni J V. Quantitative assessment of perfusion and vascular compromise in perforator flaps using a near-infrared fluorescence-guided imaging system. Plast Reconstr Surg. 2009 Aug;124(2):451–60. doi:10.1097/PRS.0b013e3181adcf7d PubMed PMID: 19644259.
53. Gurtner GC, Jones GE, Neligan PC, Newman MI, Phillips BT, Sacks JM, et al. Intraoperative laser angiography using the SPY system: Review of the literature and recommendations for use. Annals of Surgical Innovation and Research. 2013. doi:10.1186/1750-1164-7-1
54. Goncalves LN, van den Hoven P, van Schaik J, Leeuwenburgh L, Hendricks CHF, Verduijn PS, et al. Perfusion parameters in near-infrared fluorescence imaging with indocyanine green: A systematic review of the literature. Life. MDPI AG; 2021. doi:10.3390/life11050433
55. Lee BT, Matsui A, Hutteman M, Lin SJ, Winer JH, Laurence RG, et al. Intraoperative near-infrared fluorescence imaging in perforator flap reconstruction: Current research and early clinical experience. Journal of Reconstructive Microsurgery. 2010. p. 59–65. doi:10.1055/s-0029-1244805 PubMed PMID: 20027541.
56. Cornelissen AJM, van Mulken TJM, Graupner C, Qiu SS, Keuter XHA, van der Hulst RRWJ, et al. Near-infrared fluorescence image-guidance in plastic surgery: A systematic review. European Journal of Plastic Surgery. Springer Verlag; 2018. p. 269–78. doi:10.1007/s00238-018-1404-5
57. Mothes H, Dönicke T, Friedel R, Simon M, Markgraf E, Bach O. Indocyanine-green fluorescence video angiography used clinically to evaluate tissue perfusion in microsurgery. Journal of Trauma - Injury, Infection and Critical Care. 2004 Nov;57(5):1018–24. doi:10.1097/01.TA.0000123041.47008.70 PubMed PMID: 15580026.
58. Holm C, Tegeler J, Mayr M, Becker A, Pfeiffer UJ, Mühlbauer W. Monitoring free flaps using laser-induced fluorescence of indocyanine green: A preliminary experience. Microsurgery. 2002;22(7):278–87. doi:10.1002/micr.10052 PubMed PMID: 12404345.

59. Obana A, Miki T, Hayashi K, Takeda M, Kawamura A, Mutoh T, et al. Survey of complications of indocyanine green angiography in Japan. Am J Ophthalmol. 1994;118(6):749–53. doi:10.1016/S0002-9394(14)72554-1 PubMed PMID: 7977601.
60. Smit JM, Negenborn VL, Jansen SM, Jaspers MEH, de Vries R, Heymans MW, et al. Intraoperative evaluation of perfusion in free flap surgery: A systematic review and meta-analysis. Microsurgery. John Wiley and Sons Inc.; 2018. p. 804–18. doi:10.1002/micr.30320 PubMed PMID: 29577423.
61. Choudhary S, Khanna S, Mantri R, Arora P. Role of Indocyanine Green Angiography in Free Flap Surgery: A Comparative Outcome Analysis of a Single-Center Large Series of 877 Consecutive Free Flaps. Indian Journal of Plastic Surgery. 2023 Jun;56(03):208–17. doi:10.1055/s-0043-57270
62. DIRT for quantifying dermal perfusion - potential and limitations (Wilson, 1989) .
63. De Weerd L, Miland ÅO, Mercer JB. Perfusion dynamics of free DIEP and SIEA flaps during the first postoperative week monitored with dynamic infrared thermography. Ann Plast Surg. 2009 Jan;62(1):42–7. doi:10.1097/SAP.0b013e3181776374 PubMed PMID: 19131718.
64. De Weerd L, Mercer JB, Weum S. Dynamic Infrared Thermography. Clinics in Plastic Surgery. 2011. p. 277–92. doi:10.1016/j.cps.2011.03.013 PubMed PMID: 21620152.
65. De Weerd L, Mercer JB, Setså LB. Intraoperative dynamic infrared thermography and free-flap surgery. Ann Plast Surg. 2006 Sep;57(3):279–84. doi:10.1097/01.sap.0000218579.17185.c9 PubMed PMID: 16929195.
66. Thiessen FEF, Tondu T, Vermeersch N, Cloostermans B, Lundahl R, Ribbens B, et al. Dynamic infrared thermography (DIRT) in Deep Inferior Epigastric Perforator (DIEP) flap breast reconstruction: Standardization of the measurement set-up. Gland Surgery. AME Publishing Company; 2019. p. 799–805. doi:10.21037/gs.2019.12.09
67. Hallock GG. Smartphone Thermal Imaging Can Enable the Safer Use of Propeller Flaps. Semin Plast Surg. 2020 Aug 1;34(3):161–4. doi:10.1055/s-0040-1714291
68. DIRT and AR ALT (Cifuentes, 2017) .
69. DIRT + Doppler for perforator ALT (Zhu, 2023) .
70. Sjøberg T, Mercer JB, Weum S, De Weerd L. The Value of Dynamic Infrared Thermography in Pedicled Thoracodorsal Artery Perforator Flap Surgery. Plast Reconstr Surg Glob Open. 2020. doi:10.1097/GOX.0000000000002799
71. Müller-Seubert W, Ostermaier P, Horch RE, Distel L, Frey B, Cai A, et al. Intra-and Early Postoperative Evaluation of Malperfused Areas in an Irradiated Random Pattern Skin Flap Model Using Indocyanine Green Angiography and Near-Infrared Reflectance-Based Imaging and Infrared Thermography. J Pers Med. 2022 Feb 1;12(2). doi:10.3390/jpm12020237
72. Lu Y, Sun N, Wu P, Zhou G, Peng L, Tang J. The application of infrared thermography technology in flap: A perspective from bibliometric and visual analysis. Int Wound J. 2023 Dec 1;20(10):4308–27. doi:10.1111/iwj.14333 PubMed PMID: 37551726.
73. Francis JE, Roggli R, Love TJ, Robinson CP. Thermography as a Means of Blood Perfusion Measurement [Internet]. 1979. Report. Available from: http://biomechanical.asmedigitalcollection.asme.org/

74. Weum S, Mercer JB, de Weerd L. Evaluation of dynamic infrared thermography as an alternative to CT angiography for perforator mapping in breast reconstruction: A clinical study. BMC Med Imaging. 2016 Jul 15;16(1). doi:10.1186/s12880-016-0144-x PubMed PMID: 27421763.
75. John HE, Niumsawatt V, Rozen WM, Whitaker IS. Clinical applications of dynamic infrared thermography in plastic surgery: A systematic review. Gland Surg. 2016 Apr 1;5(2):122–32. doi:10.3978/j.issn.2227-684X.2015.11.07 PubMed PMID: 27047781.
76. Kawai K, Imanishi N, Nakajima H, Aiso S, Kakibuchi M, Hosokawa K. Vascular anatomy of the anterolateral thigh flap. Plast Reconstr Surg. 2004 Oct;114(5):1108–17. doi:10.1097/01.PRS.0000135332.97062.7F PubMed PMID: 15457020.
77. Saint-Cyr M, Schaverien M, Wong C, Nagarkar P, Arbique G, Brown S, et al. The extended anterolateral thigh flap: Anatomical basis and clinical experience. Plast Reconstr Surg. 2009 Apr;123(4):1245–55. doi:10.1097/PRS.0b013e31819e2718 PubMed PMID: 19337093.
78. Lee YC, Chen WC, Chou TM, Shieh SJ. Anatomical variability of the anterolateral thigh flap perforators: Vascular anatomy and its clinical implications. Plast Reconstr Surg. 2015 Apr 1;135(4):1097–107. doi:10.1097/PRS.0000000000001103 PubMed PMID: 25502859.
79. Nojima K, Brown SA, Acikel C, Arbique G, Ozturk S, Chao J, et al. Defining vascular supply and territory of thinned perforator flaps: Part I. Anterolateral thigh perforator flap. Plast Reconstr Surg. 2005 Jul;116(1):182–93. doi:10.1097/01.PRS.0000170801.78135.00 PubMed PMID: 15988266.
80. Taylor GI, Chubb DP, Ashton MW. True and “choke” anastomoses between perforator angiosomes: Part i. anatomical location. Plast Reconstr Surg. 2013 Dec;132(6):1447–56. doi:10.1097/PRS.0b013e3182a80638 PubMed PMID: 24281575.
81. Björck M, Earnshaw JJ, Acosta S, Gonçalves FB, Cochennec F, Debus SE, et al. Editor’s Choice – European Society for Vascular Surgery (ESVS) 2020 Clinical Practice Guidelines on the Management of Acute Limb Ischaemia. European Journal of Vascular and Endovascular Surgery. 2020 Feb 1;59(2):173–218. doi:10.1016/j.ejvs.2019.09.006 PubMed PMID: 31899099.
82. Conte MS, Bradbury AW, Kolh P, White J V., Dick F, Fitridge R, et al. Global Vascular Guidelines on the Management of Chronic Limb-Threatening Ischemia. European Journal of Vascular and Endovascular Surgery. 2019 Jul 1;58(1):S1-S109.e33. doi:10.1016/j.ejvs.2019.05.006 PubMed PMID: 31182334.